# PROGRESS TOWARD A COLON TARGETING NANOPARTICLE BASED DRUG DELIVERY SYSTEM

A Dissertation

by

XIAO YU

Submitted to the Office of Graduate Studies of
Texas A&M University
in partial fulfillment of the requirements for the degree of

DOCTOR OF PHILOSOPHY

May 2012

Major Subject: Chemical Engineering

Progress toward a Colon Targeting

Nanoparticle Based Drug Delivery System

# PROGRESS TOWARD A COLON TARGETING NANOPARTICLE BASED DRUG DELIVERY SYSTEM

A Dissertation

by

XIAO YU

Submitted to the Office of Graduate Studies of
Texas A&M University
in partial fulfillment of the requirements for the degree of

DOCTOR OF PHILOSOPHY

Approved by:

| | |
|---|---|
| Chair of Committee, | Michael Pishko |
| Committee Members, | Jaime Grunlan |
| | Hae-Kwon Jeong |
| | Victor Ugaz |
| Head of Department, | Charles Glover |

May 2012

Major Subject: Chemical Engineering

# ABSTRACT

Progress toward a Colon Targeting

Nanoparticle Based Drug Delivery System. (May 2012)

Xiao Yu, B.S., Tianjin University;

M.Med., Zhejiang University

Chair of Advisory Committee: Dr. Michael Pishko

Hydrophobic drug paclitaxel nanoparticles (PAX NPs) and pH sensitive hydrogels were prepared in this study to build a colon targeting nanoparticle based drug delivery system for oral administration.

Negative charged PAX NPs at the size of 110 ± 10 nm were fabricated, characterized and then encapsulated in synthetic / biomacromolecule shell chitosan, dextran-sulfate using a layer by layer (LbL) self-assembly technique. Surface modifications were performed by covalently conjugating with poly (ethylene glycol) ($H_2N$-PEG-carboxymethyl, Mw 3400) and fluorescence labeled wheat germ agglutinin (F-WGA), so as to build a biocompatible and targeted drug delivery system. Extended release of drug paclitaxel can be realized by adding more polyelectrolyte layers in the shell. High cell viability with PEG conjugated and high binding capacities of WGA modified nanoparticles with Caco-2 cells were observed. Preliminary study on stability of the nanoparticles in suspension at different pH was also performed.

Two dextran based pH sensitive and enzyme degradable hydrogels: dextran maleic acid (Dex-MA), and glycidyl methacrylated dextran (Dex-GMA) were synthesized for oral delivery of nanoparticles. Hydrogels of both kinds were stable in simulated gastric fluid, but were prone to swelling and degradation in the presence or absence of enzyme dextranase in simulated intestinal fluid. The release profiles of nanoparticles could be tuned from 5 hr to 24 hr periods of time with more than 85% of

the nanoparticle released in the simulated intestinal fluid. The release of PAX NPs was completed with longer time periods (45 hr-120 hr). Two possible release mechanisms were discussed for Dex-MA and Dex-GMA-co-AA hydrogels respectively: degradation controlled, and diffusion controlled.

These biodegradable hydrogels, which can release nanoparticles depending on pH changes, together with the biocompatible and targeted nanoparticles, may be suitable as a potential colon targeting system for oral delivery of drug nanoparticles.

## ACKNOWLEDGEMENTS

I would like to thank my committee chair, Dr. Pishko, and my committee members, Dr. Ugaz, Dr. Jeong, Dr. Grunlan, for their guidance and support throughout the course of this research.

Thanks also go to my friends, colleagues and the department faculty and staff for making my time at Texas A&M University a great experience. With the great supports from Dr. Hahn, Dr. Shantz, Dr. Ugaz, Dr. Cheng and Dr. Kao, I obtained so much convenience on using the instruments. I also want to extend my gratitude to the staff in the material characterization facility (MCF). They not only provided very well-maintained equipments, but also offered valuable advice on preparation and observation of the samples.

Finally, thank my family for their encouragement all the time.

# NOMENCLATURE

| | |
|---|---|
| CS/DEX-PEG | Chitosan/dextran conjugated with PEG |
| Dex-MA | Dextran maleic acid |
| Dex-GMA | Glycidyl methacrylated dextran |
| EDC | 1-Ethyl-3-(3-dimethylaminopropyl) carbodiimide |
| F-NPs | Fluorescent nanoparticles |
| F-WGA | Fluorescence labeled wheat germ agglutinin |
| LbL | Layer by layer |
| L.E. /E.E. | Loading efficiency / encapsulation efficiency |
| PAH | Poly (allylamine) hydrochloride |
| PAX NPs | Paclitaxel nanoparticles |
| PE | Polyelectrolyte |
| PEG | Poly (ethylene glycol) ($NH_2$-PEG-carboxymethyl) |
| PEM | Polyelectrolyte multilayer |
| PSSCMA | Poly (4-styrenesulfonic acid-co-maleic acid) sodium salt |
| PS NPs | Polystyrene nanoparticles |
| PVA | Poly (vinyl alcohol) |
| SGF | Simulated gastric fluid |
| SIF | Simulated intestinal fluid |
| S-NHS | Sulfo N-hydroxysulfosuccinimide |
| SR | Swelling ratio |

# TABLE OF CONTENTS

# LIST OF FIGURES

FIGURE Page

FIGURE Page

# LIST OF TABLES

# 1. INTRODUCTION

## 1.1 Motivation

Normal cell cycle consists of an ordered set of events, resulting in the production of two daughter cells. Cancer, known as medical neoplasm, is a broad group of various diseases, all involving unregulated cell growth. Cancer cells have defects in regulatory circuits that govern normal cell proliferation and homeostasis, which causes cells dividing and growing uncontrollably, forming malignant tumors, and invading nearby parts of the body.[1] Observations of human cancers and animal models argue that tumor development proceeds via a process formally analogous to Darwinian evolution, in which a succession of genetic changes, each conferring one or another type of growth advantage, leads to the progressive conversion of normal human cells into cancer cells.[2] This year, cancer is projected to become the leading cause of death worldwide. Colon and rectum cancer, also known as colorectal cancer or large bowel cancer, was the third leading cause of cancer-related death in 2011.[3]

Effective treatments of cancer include surgical removal, chemotherapy, radiotherapy, immunotherapy, and their combinations.[4] Presently, the challenge of an effective anti-cancer treatment in the pharmaceutical industry has been more about the development of creative formulations, which are capable of providing access to the desired tissue, while maintaining prolonged therapeutic effects.[5] For chemotherapy, delivery of the anticancer drugs to the desired site (drug targeting) and release of them in a prolonged profile (controlled release) will play a major role in the future.

Oral drug delivery is the most popular route to treat all kinds of diseases. It has the advantages over current cancer chemotherapy. It is convenient and has higher

---

This dissertation follows the style of *ACS Journal Biomacromolecules*.

patient compliance, especially for patients with advanced or metastatic cancer.[6] Challenges that exist in oral drug delivery include: low bioavailability (hydrophobic drug) and acidic environment in human stomach (disruption of the delivery vehicle).[4] However, with the development of nanotechnology and environmental stimuli smart materials, possible solutions and new improved chemotherapy may be provided.

Paclitaxel (PAX, Figure 1) is one of the best anti-tumor drugs found from nature in the past decades. It is the first member of texane class and has unique ability to stabilize microtubule function, thus inducing cell death.[7] Paclitaxel is water insoluble, and chemical solvents such as ethanol, Tween 80, and castor oil (Cremophor EL) are used in currently approved formulations. The commercially formulated paclitaxel is a mixture of Cremophor EL and dehydrated ethanol under the trademark 'TAXOL' (Bristol-Myers Squibb Co., NJ, USA). However, this formulation caused side effects including hypersensitivity reaction, thinned or brittle hair, pain in the joints of the arms or legs, fever, cough, which were associated with the Cremophor EL used. To avoid these solvent side effects, Cremophor EL-reduce or free formulations such as albumin-bound nanoparticles, trademark 'Abraxane' (American Bioscience, Inc., CA, USA), mucoadhesive lipid dosage, lyophilized polymeric micelles (Genexol-PM, Samyang Co. Seoul, Korea) have been developed.[8, 9, 10]

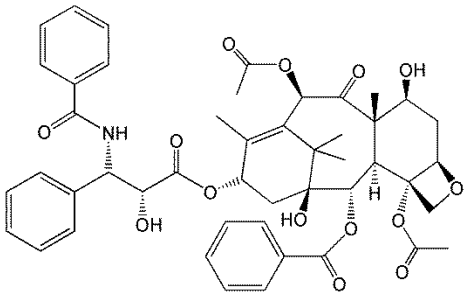


**Figure 1.** Chemical structure of paclitaxel; reproduced and cited.

In this study, a novel lectin-mediated nanoparticle drug delivery system were fabricated, and polysaccharide-based delivery devices were designed and prepared, which can potentially target the human colon and maximize the therapeutic impact on

the pathologic cells. Poly (ethylene glycol) (PEG) and lectin F-WGA will be chemisorbed to the surface of the nanoshell, promoting biocompatibility and tumor specificity of the drug delivery system.

## 1.2 Specific aims and based hypothesis

### 1.2.1 Fabrication, encapsulation and surface modifications of paclitaxel based core-shell structured nanoparticles

This anti-tumor drug delivery system consists of a drug based core encapsulated by polyelectrolyte layers including synthetic polymers Poly (4-styrenesulfonic acid-co-maleic acid) sodium salt/Poly (allylamine) hydrochloride (PSSCMA/PAH), and biomacromolecules chitosan/dextran. The solid paclitaxel drug cores will be fabricated by a solvent-evaporation emulsification method. The core-shell structured nanospheres will be formed by the layer by layer (LbL) self-assembly technique and specific sites on the surfaces will be provided to enhance biocompatibility and cell targeting.

### 1.2.2 Synthesis and characterization of new biocompatible and pH sensitive hydrogels for colon targeting drug delivery

Synthesize biocompatible and pH sensitive dextran based hydrogels that can potentially deliver the nanoparticles to the human colon and degrade in the presence of the enzyme dextranase. These hydrogels can respond to the environmental pH changes. Enzymes produced by the micro flora in human colon can degrade the backbone of the hydrogels and then release the nanoparticles trapped inside. Hydrogels will be characterized based on the precursors' degree of substitution, the hydrogel swelling ratios in different pH buffers (i.e. SIF vs. SGF), and ratios between two monomers, *etc*.

### 1.2.3 *In vitro* nanoparticle and paclitaxel release studies

F-NPs and PAX NPs will be loaded into different dextran based hydrogels. The release profiles can be determined by measuring the fluorescent level or drug

concentration versus time. Tunable release can be obtained by adjusting the hydrogel compositions and layer number of the self-assembly.

### 1.2.4 *In vitro* study with Caco-2 cells

This aims to test the efficiency of this drug delivery system. Nanoparticles will be encapsulated and modified before being incubated with Caco-2 cells to study the binding and uptake capability of the nanoparticles. Suspended Caco-2 cells will be used to study the biocompatibility of these dextran based hydrogels.

The above proposed research aims are based on the following hypothesis: LbL self-assembled nanoparticles will be successfully fabricated due to the electrostatic interaction between cationic and anionic polyelectrolytes; the hydrogel will effectively protect the nanoparticles in the stomach, degrade and release them in the colon; controlled release of the drug can be achieved by tuning the non-degradable composition in the hydrogels, the number of polyelectrolyte layers and their layer thickness; particle surface modifications can minimize opsonization and target specifically to Caco-2 cells.

# 2. LITERATURE REVIEW

## 2.1 Nanoparticle based drug delivery system

### 2.1.1 Layer by layer (LbL) self-assembly

As material science has been developed into an interdisciplinary field, organic, polymeric and even biological components, besides classic metals and inorganic compounds, have been integrated in the new material development for a variety of applications.[11]

LbL self-assembly is such a technique that oppositely charged polymers can be deposited on solid surfaces at ambient conditions. (Figure 2) It provides a convenient and simple approach to fabricate multilayered polymer films at the nanoscale.[12] It was popularized in 1992 by Decher and has been demonstrated as a general and reproducible technique to build up multi-component and functional nano-scale thin films on solid substrates.[13,11] Sequential addition of the anionic and cationic polyelectrolytes is characterized by a stepwise increase of the adsorbed amount and layer thickness. It is also confirmed by the alternating positive and negative values from the zeta potential measurements.[14] X-ray photoelectron spectroscopy (XPS) can further provide details of the surface chemistry of the polyelectrolyte multilayer.

Electrostatic interaction between oppositely charged macromolecules is the main driving force of forming these nano thin films. For electrostatic interactions a certain number of ionic bonds between the layer and the substrate or between each adjacent layer are required for adherence.[11] Stability of the multilayer of polyelectrolytes has been studied and several factors were considered to have pronounced effects: polymer charge, charge density, ionic strength, buffer pH (also influences polymer charge), and polymer type.[13] Stable polyelectrolyte thin films can be formed when both polymers are highly charged and the ionic strength is low.[14] The pH of the buffer would affect the degree of dissociation, charge state and conformation of the weak polyelectrolyte in the solution, e.g. chitosan. Nanoscale structure of these layers can therefore be tuned based

on pH changes.[13] It was found that thicker polyelectrolyte layers PAH/PAA were obtained when the pH value of the PAA solution was close to its pKa at 4.5. Ionic strength in the deposition and washing solutions also increased the thickness of PAA/PAH coatings.[15]

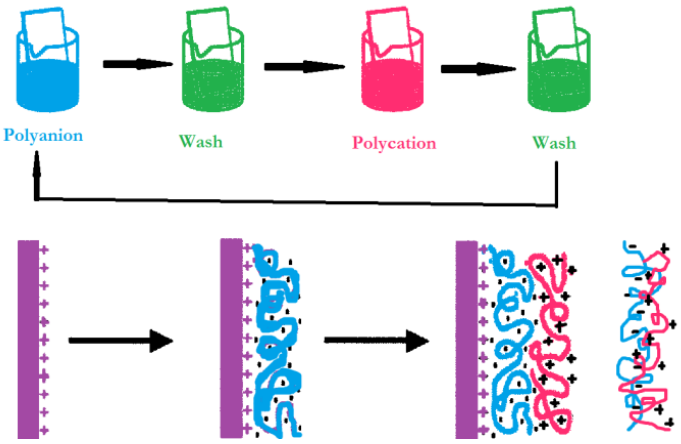


**Figure 2.** Schematic of the LbL procedure.

Besides the electrostatic interactions, other secondary interactions, such as hydrogen bonding, hydrophobic interaction and van der Waals force, also exist.[16] Interactions between polyions had been considered in determining the selectivity of three basic polyamines, which depended on degree of ionization as caused by the pH in the solution, as well as the number of hydrogen bonding units, in the polyacid or on the surface.[16] At low pH, the secondary interaction of polyacid polymer appeared to be particular important with heightened hydrogen bonding formation and maximized potential hydrophobic interaction.[16] Both synthetic polymers and biomacromolecules have been successfully used for the deposition of multilayered polyelectrolytes.[13, 15] With the increased application of LbL self-assembly technique in the biomedical field, biomacromolecules have gained more and more attention. Biopolymers are a class of polymers produced by living organisms. Starch, proteins, peptides and DNA all belong to biopolymers. Biologically derived polysaccharide is one kind of the biopolymers and can be negatively or positively charged in solution under certain pH value, therefore they

can be used as polyelectrolytes for the LbL self-assembly. Due to their origin from nature, they are normally non-toxic, biocompatible and biodegradable.

Chitosan (CS) is a natural polysaccharide usually obtained from chitin, and presently it is extensively used in pharmaceutical, cosmetics, and food industries.[17] Figure 3 (left) shows its structure. It has primary amines in the repeating units, with an intrinsic pKa varying from 6.46 to 7.32.[13] Chitosan is a weak polycation, and usually insoluble above its pKa. After protonation of the amine group below its pKa, it becomes soluble and positively charged.[18] Therefore it can act as a weak polycation in the diluted acid solution. Weak polyelectrolytes have a rich range of electrostatic and secondary interactions arising from their structures and degree of ionization. Fine control of building the polyelectrolyte layers may be realized by manipulating these interactions through proper solution conditions and polyelectrolyte structures.[16] Changing the charge density and ionic strength in the solution can change the conformation of chitosan chains.[19] The pH dependent thickness behavior of sequentially adsorbing this chitosan layer may be observed. Dramatically different polymer adsorption behavior was found as one systematically increases the charge density of a weak polyelectrolyte; thickness could change from 8 nm to 0.4 nm over a very narrow pH range.[20] Various medical applications of chitosan as a polyelectrolyte layer in nanostructured thin films had been identified, such as sensing and biosensing.[21] It can serve as a matrix for immobilization of biomolecules in the LbL films, helping preserve the bioactivity of biomolecules for long periods of time even in dry, solid films. Its biocompatibility properties may also facilitate the application for tissue engineering.[21]

Dextran sulfate (Dex) in sodium salt form is a strong polyanion, soluble and stable in water with a broad range of pH values (Figure 3 right). It contains approximately 17% sulfur which is equivalent to approximately 2.3 sulfate groups per glucosyl residue. Due to the repulsion of the negatively charged sulfate groups, the dextran sulfate polymer will be fully extended in low ionic strength solutions. As salt (increase of ionic strength) was added in the LbL assembly procedure, a thicker layer could be obtained with intact characteristics of each layer.[22] The biodegradability of

these biomacromolecule thin films is a very important requirement for them to be used in biomedical fields. Enzyme hydrolysis of the chitosan and dextran LbL assembly had been quantitatively studied and it was found the construction of an LbL assembly facilitated rapid hydrolysis when the polymer substrate exhibited electrostatic repulsion against the enzyme. Controlled release of therapeutics can be therefore performed by adjusting the enzyme hydrolysis rate.[22] LbL assembly of chitosan and dextran-sulfate polyelectrolytes could also have alternate anti- vs. pro-coagulant activity of human whole blood at the 1 M of NaCl buffer concentration.[23] Another dextran based weak polyelectrolyte, carboxymethyl dextran sodium salt (CM-dextran), can also be used in this LbL self-assembly procedure. It can provide specific surface sites for functional modifications when adsorbed as the outmost layer. The pKa of this weak polyanion is at 6.1; similar to chitosan, the pH of the solution needs to be adjusted for better encapsulation.

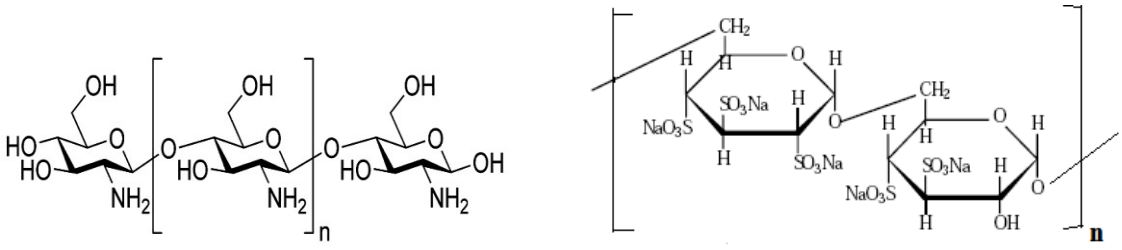


**Figure 3.** Chemical structures of chitosan (left) and dextran-sulfate sodium salt (right) [18].

### 2.1.2 PEG conjugation onto drug nanoparticles

Poly (ethylene glycol) (PEG) has been intensively studied recently in drug delivery, especially in the development of nanoparticle based formulation. Peptides and proteins can be encapsulated within the nanoparticles to increase their potential therapeutic effect.[24] It was found that hydrophilic surfaces of the PLA-PEG conjugated nanoparticles could lead to extended nasal delivery of active antigen, and more efficient transport through rat nasal mucosa.[24] Without PEG surface modifications, nanoparticles

can be quickly opsonized and cleared by the macrophages. So the PEG conjugation was developed as the first strategy to increase nanoparticles' circulating time by avoiding non-specific protein adhesion on the particles' surfaces in blood upon administration.[25] Moreover, the particle surface can be modified while still maintaining its main biological functions, such as enzyme activity or receptor recognition.[26] It can also shield particles from the uptake by the reticuloendothelial system (RES), preventing recognition and degradation by proteolytic enzymes. The PEG conjugation increased the apparent size of the polypeptide, thus reducing the renal filtration and altering biodistribution.[27]

### 2.1.3 Conjugation of fluorescent labeled wheat germ agglutinin (F-WGA)

Transformed or cancerous cells often express different amount of glycans compared with their normal counterparts, thus providing a possible solution to deliver the drug particles specifically to tumor cells.[28] Lectin is a sugar-binding protein that can recognize and bind to sugar complexes due to its high specificity for the chemical structure of the glycans. It has been proved that nanoparticles conjugated with lectin F-WGA will allow efficiently targeting to cancer cells. Recently it has been demonstrated *in vitro* that it may be possible to exploit the increased WGA binding capacity exhibited by Caco-2 cells compared to that of non-cancerous human colonocytes for tumor-specific drug delivery in colon cancer chemotherapy.[29] The toxicity study of WGA conjugated nanoparticles was also investigated and it was demonstrated *in vivo* to be a safe carrier system for intranasal delivery of therapeutic agents to the brain.[30]

### 2.1.4 Paclitaxel nanoparticle based formulation

Paclitaxel is one of the best anti-cancer drugs found from nature and has been approved by the FDA for the treatment of breast cancer, ovarian cancer and non-small-cell lung cancer.[31] Commercially available paclitaxel formulations require the use of nonionic surfactant polyoxyethylated castor oil, i.e. Cremophor EL® and ethanol, because of its poor aqueous solubility and oral bioavailability.[32] However, the Cremophor EL can cause serious side effects including hypersensitivity reactions,

neurotoxicity, nephrotoxicity and hypotensive vasodilation.[33] Therefore, novel Cremophor EL free formulations have been developed recently.

Nanoparticle albumin-bound paclitaxel (nab™-paclitaxel) is a solvent-free paclitaxel formulation, which can be prepared by high-pressure homogenization of paclitaxel in the presence of albumin into a nanoparticle suspension.[31] Paclitaxel nanoparticles (PAX NPs) at the size of 130 nm have several advantages over the Cremophor EL-paclitaxel: no need for premedication for the hypersensitivity reactions, shorter infusion time and elimination of Cremophor EL impact, etc.[31-32] Phase I and pharmacokinetic study of this formulation had been performed.[32] No acute hypersensitivity reactions were observed for all nineteen patients during the infusion period, and the maximum tolerated dose (MTD) was determined to be 300 mg/m$^2$. These results supported further Phase II trials to finally determine the drug's ant-tumor activity.[32]

Another novel nanoparticle based system, consisting of chitosan and glyceryl monooleate (GMO), was also developed for sustained paclitaxel delivery.[33] Polycationic nanoparticles (400 to 700 nm) were fabricated by the multiple emulsion solvent evaporation methods and showed a hydrophobic inner-core with a hydrophilic coating. This novel formulation exhibited a fourfold increase on cellular uptake and a 1000-fold reduction in the IC50 (half maximum inhibitory concentration) of paclitaxel.[33]

A polymer cross-linking method was used to engineer paclitaxel-loaded hyaluronan nanoparticles for local delivery of the drug for cancer therapy.[34] *In vivo* administration of the drug–loaded nanoparticles via direct intratumoral injection in female rats showed effective inhibition of tumor growth in all treated rats. One case of complete remission of the tumor nodule and two cases of persistent reduction of tumor size had also been observed on subsequent days.[34]

The latest paclitaxel nanoparticle formulation PGG-PAX is based on poly-(ɤ-glutamylglutamine) (PGG) and paclitaxel (PAX) being linked via ester bonds.[35] Very small nanoparticls were formed spontaneously in plasma. Three different tumor models were used in the study and the PGG-PAX formulation produced greater inhibition of

tumor growth than Abraxane (the albumin-bound paclitaxel nanoparticle based formulation) among all the models when mice were given single equitoxic doses of the drug.[35]

## 2.2 Oral and colon targeting drug delivery

### 2.2.1 Colon targeting oral drug delivery

Challenges that exist in oral drug delivery of paclitaxel include: low bioavailability due to the hydrophobic property of the drug itself, first metabolism process, acidic environment in human stomach, and possible leakage of the dosage when passing through the small intestine.[4] However, combining nanotechnology and smart hydrogels, novel nanoparticle formulations together with site specific delivery vehicles show great potential in promoting new chemotherapy and provide possible solutions to these problems.

Colon drug delivery has lots of advantages: near neutral pH environment, less enzyme activity and longer residence time, which could improve the drug bioavailability, reduce side effects and facilitate the site specific targeting .[36]

Colon drug delivery can be realized by encapsulating active compounds or nanoparticles within proper delivery vehicles, which can help the therapeutics survive the severe environment in the human stomach, going through the small intestine within the residence time, and finally reach the colon and then degrade in the colon in the presence of specific enzymes. These hydrogels, also called smart materials, function because of a stimuli-responsive mechanism. Smart materials can change their structures reversibly in response to external change including pH, temperature, light, and concentration of chemical substances.[37]

Physiological pH of human gastrointestinal tract (GIT) increases progressively from the stomach (pH 1-2), to small intestine (pH 6-7) at the site of digestion and to 7-8 in the distal ileum.[38] Due to these physiological characteristics, a controlled drug delivery system could be designed to potentially regulate the drug release through external pH changes. Moreover, the intestinal micro flora are characterized by a complex

and relatively stable community of microorganisms, some of which are responsible for a wide variety of metabolic processes, such as degradation of polysaccharides.[38] Colon targeting drug delivery vehicles, pH sensitive hydrogels, combining properties of responding to physiological pH changes and enzyme induced decomposition in the human colon, may be potential good candidates for oral administration of nanoparticles. (Figure 4) Factors that may affect the enzymatic degradation include temperature, buffer pH, sugar type and the structure of the hydrogel network.[39]

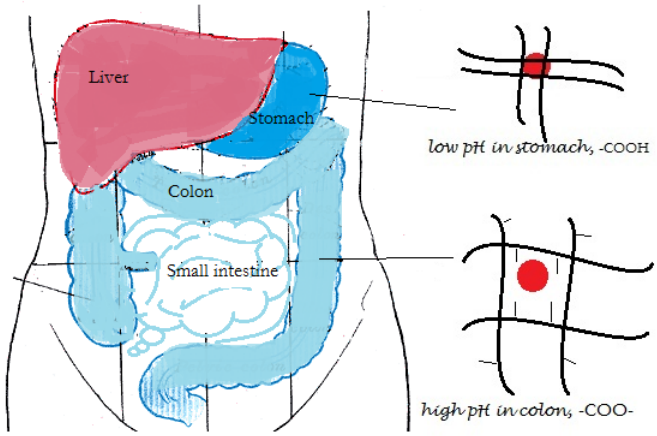


**Figure 4.** Colon targeting drug delivery for oral administration, reproduced with modification.[40]

### 2.2.2 Polysaccharide based pH sensitive and biodegradable hydrogels

The use of biodegradable polymers holds great promise among the different approaches to achieve colon targeting drug delivery. Natural polymers, e.g. polysaccharides, have great appeal as they are comprised of polymers with a large number of derivable groups, a wide range of molecular weights, varying chemical compositions, low toxicity and specific biodegradability.[41]

Dextrans are a class of polysaccharides with a linear polymer backbone with mainly 1, 6-α-d-glucopyranosidic linkages. They are obtained from bacterial cultures of Leuconostoc mesenteroides NRRL B-512.[42] To form a functional hydrogel, different

chemical modifications have been performed to synthesize suitable precursors.[43,44] Methacrylated dextran is one of the most popular photo-reactive derivatives that can be copolymerized to form pH sensitive hydrogels.[45] At high derivation degree in methacrylic groups (20 mol %), the photocrosslinking can take place in aqueous solution in the absence of photoinitiators.[46] Dextran-maleic acid is another precursor that can be synthesized by reacting dextran with maleic anhydride in the presence of a catalyst (Figure 5).[44] It can be photocrosslinked with a well-known temperature sensitive precursor NIPAAm to form hybrid hydrogels that exhibit duo environmental responsive properties.[47] Besides dextran, inulin is also a good natural polysaccharide that has been derived with methacrylic anhydride (MA), which forms inulin based hydrogel under UV irradiation without using photoinitiators.[48] A further modified hydrogel inulin-MA-SA (succinic anhydride) is synthesized, exhibiting pH sensitive property and improved acid-resisting ability.[48]

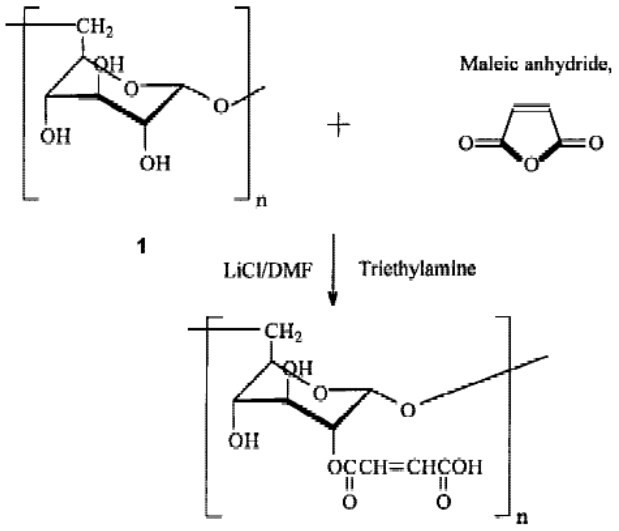


**Figure 5.** Preparation of precursor dextran-maleic acid. Reproduced.[44]

All the polysaccharide based hydrogels can be degraded by enzyme polysaccharidases, like glycosidase, which are released by the human colonic microflora.[41] Degradation rates of these hydrogels can be adjusted through changing the

degree of substitution when synthesizing the precursor, the cross-linking density during the UV irradiation, and copolymer component compositions, etc.

### 2.3 *In vitro* drug release models

*In vitro* dissolution study has been well recognized as an important element in the drug development. It is defined as the rate of mass transfer from a solid surface into the dissolution medium. Drug dissolution and release kinetics are influenced by drug solubility, drug polymorphic form, particles size, and crystallinity.[49]

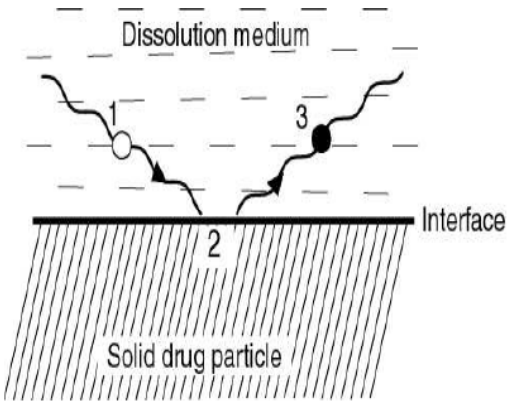


**Figure 6.** Drug dissolution from the solid surface to medium. Reproduced.[49]

In this study, anti-cancer drug paclitaxel will be trapped into nanoparticles; nanoparticles will be encapsulated by multi-layers of polyelectrolyte thin films. Hydrogels will be synthesized and used as a vehicle to possibly deliver these surface modified nanoparticles through oral route. The study of the drug release mechanisms from different kinds of delivery systems can promote a better understanding of what happened; important goals such as controlling the therapeutics' concentration over time and predicting a release profile can be realized. Based on the drug delivery system prepared, two main releases can be expected: the drug molecules' release from the nanoparticles and the nanoparticles' release from the hydrogels.

For low water soluble drugs, the self-erosion of the matrix is usually the dominant release mechanism. Different assumptions / models have been proposed to

describe the drug release mechanism from solid particles to the bulk medium. Diffusion layer model assumes that the reaction at the solid/liquid interface is instantaneous forming a saturated solution in the static liquid film adjacent to the solid surface. The interfacial barrier model proposes that there is a high activation free energy barrier that has to be overcome before the solid can dissolve. A third model called Danckwert's model is to assume that the new packets of solvent reach the interface by eddy diffusion randomly.[49]

**Table 1. Summary of *in-vitro* drug release characterization mathematics models [49]**

| Model | Formula | Comments |
|---|---|---|
| Zero order | $M=M_0+K_0t$ | Ideal model |
| First order | $dM/dt=k(Ms-Mt)$ | Log(cumulative%) drug vs. time |
| Higuchi | $Mt=k_H(t)^{0.5}$ | Release based on diffusion |
| Korsmeyer-Peppas | $\frac{Mt}{M\infty} = kt^n$ | n indicates release mechanism |

Table 1 summarized several mathematic models that describe *in vitro* drug releases. Zero order release kinetics is referred as the process of constant drug release from a drug delivery device and it is considered as the ideal way of drug releasing from vehicles. First order release is to describe the rate changes of drug which depends first orderly on the concentration gradients.[49] Higuchi model is another popular model that describes the release of a drug from an insoluble matrix as the square root of a time-dependent process based on Fickian diffusion.

For drug release from a polymeric system, the Korsmeyer-Peppas model can be used and actually expand the application of the Higuchi model to characterize different diffusion mechanisms. This model was described as fitting the first 60% of the drug release data in the exponential equation $\frac{Mt}{M\infty} = kt^n$.[50] The n value is used to classify different release mechanisms for cylindrical shaped matrices.[49] Influence of the device geometry on the release mechanism, showing that for pure Fickian release, the exponent n has a limiting value of 0.43 for spheres.[51] A value of n in the range from 0.43 to 1.00

indicated non-Fickian transport. When it takes a value of 1, the drug release is independent of time, suggesting zero order release kinetics, known as case II transport. Other n values and their corresponding release mechanisms were listed in Table 2. The choice of the appropriate mathematical model, when elucidating drug release mechanism, strongly depends on the desired or required predictive ability and accuracy of the model.[51]

**Table 2. Exponent n of the power law and drug release mechanism from the polymeric controlled release system [51]**

| Exponent n | | | Release mechanisms |
|---|---|---|---|
| Thin film | Cylinder | Sphere | |
| 0.5 | 0.45 | 0.43 | Fickian diffusion |
| 0.5 – 1.0 | 0.45 – 0.89 | 0.43 – 0.85 | Anomalous transport |
| 1.0 | 0.89 | 0.85 | Case II transport |

# 3. FABRICATION AND SURFACE MODIFICATION OF PAX NPs*

Paclitaxel nanoparticles (PAX NPs) were fabricated at the size around 100 nm by the modified emulsification evaporation method. Both synthetic polyelectrolyte and biomacromolecules dextran and chitosan were assembled onto polystyrene / PAX NPs using the LbL self-assembly technique. Surface modifications were then performed onto nanoparticles' outmost layer by conjugating with poly (ethylene glycol) and wheat germ agglutinin, so as to build a biocompatible and targeting drug delivery system.[18]

## 3.1 Introduction

Efficacy of most therapeutic drugs treating cancer requires sufficient amount and specific targeting to tumor cells. With the application of nanotechnology, drugs can be prepared in the form of nanoparticles with particular size, promoting passive accumulation of active molecules to pathological areas.[52, 53]

Different kinds of polyelectrolyte nanofilms have been used for the LbL self-assembly procedure, including charged metal, dyes, nanoparticles, proteins, DNA and virus. Today it has become a standard method with applications ranging from optical, electrochemical materials, biomedical devices and drug delivery systems.[54] Using the layer-by-layer assembly method, the hydrophobic property of the drug can be temporarily covered by synthetic or biological polyelectrolytes.[55] Through simply selecting proper outermost layers, biocompatible and targeted functional groups can be further modified onto the nanoparticles' surfaces.

---

*Parts of this section are reproduced with the permission of (Yu, X.; Pishko, M. V., *Biomacromolecules* **2011,** *12* (9), 3205-3212.). Copyright (2011) American Chemical Society.

### 3.2 Materials and Methods

Poly (allylamine) hydrochloride (PAH, Mw~70 000 g/mol), Poly(4-styrenesulfonic acid-*co*-maleic acid) sodium salt (PSSCMA, Mw~20,000 g/mol), chitosan (low molecular weight), dextran-sulfate (average Mw > 500,000), poly (vinyl alcohol) (PVA, Mw 9000-12,000 g/mol and Mw 22,000 g/mol), sodium alginate (from brown algae, low viscosity) were purchased from Sigma-Aldrich, USA. Semisynthetic paclitaxel (from *Taxus* sp.), ≥ 97% was purchased from Sigma, USA. $NH_2$-poly (ethylene glycol) - carboxymethyl, Mw~ 3400, was purchased from Laysan Bio, Inc. USA. Fluorescence labeled wheat germ agglutinin (F-WGA) was purchased from Sigma, USA. EDC (ECDI; 1-ethyl-3-(3-dimethylaminopropyl) carbodiimide, HCl), and s-NHS (sulfo N- hydroxysulfosuccinimide) were purchased from Fisher scientific, USA. Ultrapure water used for all experiments was obtained from a Millipore system with a specific resistance 18 MΩ/cm. Polyelectrolyte solutions were prepared in a 30 mM KCl solution or 0.15 M NaCl. Phosphate-buffered saline solution (PBS, pH 7.4) consisted of 1.1 mM potassium phosphate monobasic, 3 mM sodium phosphate dibasic heptahydrate, and 0.15 M NaCl.

**Preparation and characterization of paclitaxel nanoparticles.** Solvent emulsification evaporation method has widely been used to encapsulate hydrophobic drugs in polymeric matrices.[56] PAX NPs were prepared by a modified method without adding polymers into the organic phase.[57] The procedure of preparing these nanoparticles can be described as: 2% w/v PVA and 1% w/v sodium alginate were dissolved in ultrapure water and then emulsified at a constant speed using a homogenizer with twice volume paclitaxel/acetone solution under low heat. After emulsifying for 2 hours, the collected drug nanoparticles were centrifuged, suspended and washed by PBS at pH 7.4. All particles were stored at 4 ºC for further use.

Loading efficiency (L.E.) was calculated according to the mass change before and after the emulsification procedure. The encapsulation efficiency (E.E.) was calculated based on the mass ratio between the entrapped and the initial fed paclitaxel during the preparation process (1). 60 μL of well-sonicated PAX NPs were centrifuged

down and dissolved in 1 mL mobile phase acetonitrile/$H_2O$ (7/3, v/v) by sonication. Samples were then filtered for HPLC analysis.

$$\text{PAX NPs E.E. \%} = \frac{\text{Mass of Paclitaxel encapsulated in PAX NPs}}{\text{Mass of initially fed Paclitaxel (1 mg/mL)}} \quad (1)$$

**Particle size distribution.** Particle size distribution of ultracentrifuge and filtered particles was analyzed by Brookhaven ZetaPALS instrument with the dynamic light scattering (DLS) software and confirmed with results from SEM. Refractive index of the solution for all samples was set to 1.46.

**Layer by layer (LbL) assembly.** LbL assembly is a technique that can be used to build multi-component polymer films in nanometer size onto solid substrates with controlled thickness and layer number.[11] Alternating polyelectrolyte layers at the concentration of 20 mg/mL for PAH/PSSCMA (in 30 mM KCl), or 2 mg/mL for CS/DEX were adsorbed onto solid drug nanoparticles until a desired layer number was obtained. CS/DEX were prepared in 0.15 M NaCl; pH of the CS solution was adjusted to 4.0, incubation time 20 min, and followed by ultracentrifugation at 11,000 rpm/20 min. (PAH/PSSCMA stands for a bilayer of PAH and PSSCMA; CS/DEX stands for a bilayer of chitosan and dextran adsorbed on particles).

**PEG and F-WGA surface modifications.** After a desired number of polyelectrolyte layers were assembled onto PAX NPs, PEG and F-WGA were conjugated onto the particles by a standard carbodiimide chemical reaction.[58] 40 mg/mL of EDC was used as the carbodiimide and 4 mg/mL of s-NHS was added to activate and form a more stable intermediate first. Samples were shaken for 20 min at a speed of 500 rpm, and then a twice-washing step was followed with 0.15 M NaCl. 10 mg of NH2-PEG-CM / F-WGA was added to start the reaction for 20 hr at a speed of 500 rpm. Samples were washed three times after the reaction stopped.

**Surface characterization.** X-ray photoelectron spectroscopy (XPS) analysis was performed using a Kratos Axis Ultra imaging XPS instrument to detect the variations in chemical composition and the oxidation state on particles' surfaces. The X-ray source was a monochromatic aluminum (1486.6 eV). Survey and high resolution spectra were

collected at a takeoff angle of 90° with respect to the sample plane. 40 μL sample solution was dropped on small glass pieces and dried under ambient condition overnight. Charge neutralization was used. All spectra were referenced for C-C in the carbon 1s peak at 285 eV. Survey spectra were collected from 1200 to 0 eV with pass energy 160 eV, and high resolution spectra (C 1s, O 1s, N 1s, and S 2p) were collected with pass energy 40 eV.

**Field emission-scanning electron microscopy (FE-SEM).** JEOL JSM-7500F field emission scanning electron microscopy was used for particle imaging. All samples were prepared by dropping well sonicated and suspended drug nanoparticles onto a TEM copper grid, dried under ambient conditions and stored in a vacuum oven at room temperature for a day before imaging.

## 3.3 Results

### 3.3.1 Fabrication and characterization of PAX NPs

3.3.1.1 Optimization of particles' size and surface charges

Most methods preparing nanoparticles involve a two-step reaction, preparation of an emulsified system and formation of nanoparticles. This second step is achieved either by the precipitation or the gelation of a polymer or by polymerization of monomers. Generally, the principle of second step gives its name to the method. Some other methods do not require the preparation of an emulsion prior to obtaining of the nanoparticles. They are based on the precipitation of spontaneous dispersed polymers or self-assembly of macromolecules to form nanogel or polyelectrolyte complex.[59] Here we used a modified solvent emulsification evaporation method to prepare PAX NPs.

PVA at two different molecular weights was used as the surfactant to study its effects on size and charge of the nanoparticles. (Table 3) These particles' negative charge was possibly caused by the adsorption of sodium alginate. It is known that the emulsifier tends to bind to the nanoparticles surface through hydrophobic interactions, while the hydrophilic chains protrude into the surrounding medium, thus the negative

surface charges are present on the nanoparticles.[60] Results of ζ-potential suggested organic/aqueous (O/W) phase ratio did not significantly affect particle's ζ-potential. Final experimental condition to prepare PAX NPs was optimized to be: organic/aqueous phase ratio 2:1, PVA 9,000-10,000 g/mol. This condition resulted in the formation of solid drug nanoparticles at the average size of 110 nm, with a narrow size distribution and relative high ζ-potential of -40 ± 3.0 mV. These results confirmed that by varying experimental conditions, such as organic/aqueous phase ratio or organic phase composition, control of PAX NPs' size and surface charge may be realized.[60]

Size, morphology and surface charge of PAX NPs were characterized. Particle size determined by SEM was around 100 nm. The PAX NPs prepared by this method were within the tumor pore cutoff size 380-780 nm and negatively charged.[61] The average L.E. for PAX NPs during the preparation process was 97.5%. Size distribution by SEM was obtained through counting the particle number at a specific size and then combining results of different areas from the SEM images. Figure 7 shows the data obtained by DLS, it resulted in 60 nm bigger of the average size as compared to the SEM results. This was possibly due to the different states of the particles, i.e. samples for SEM imaging were dried in a vacuum oven, while particles for DLS were well dispersed in an aqueous solution with the hydrodynamic diameter measured.

**Table 3. Optimized conditions for preparing PAX solid core nanoparticles**

| Experiment Number [a] | O/W (v/v) | PVA M.W. (g/mol) | Size (nm) (SEM images) | ζ-potential (mV) |
|---|---|---|---|---|
| 1 | 1:1 | 9,000-10,000 | 64 ± 20 | -52 ± 3.0 |
| 2 | 2:1 | 22,000 | 71 ± 10 | -21 ± 6.4 |
| 3 | 2:1 | 9,000-10,000 | 113 ± 14 | -42 ± 2.6 |
| 4 | 3:1 | 9,000-10,000 | 147 ± 28 | -42 ± 2.1 |

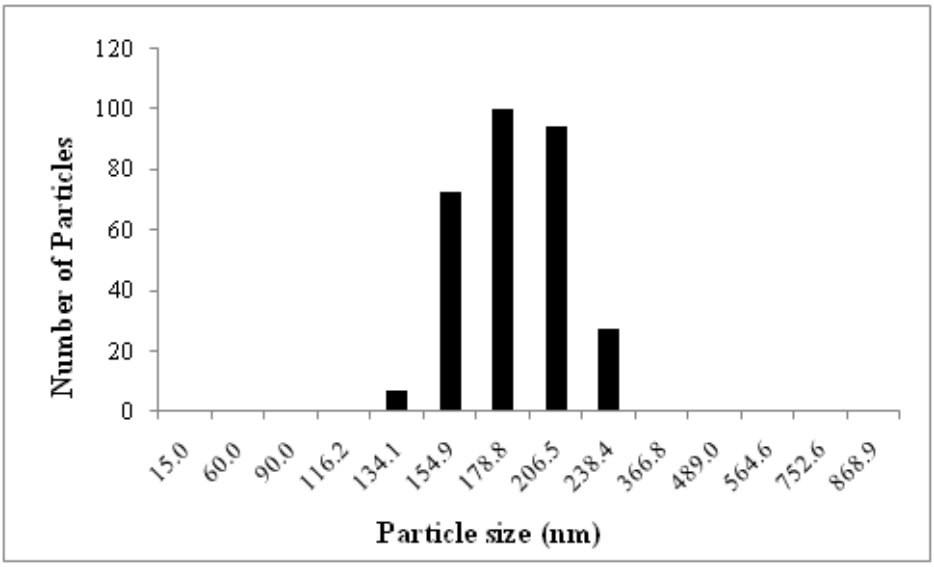


**Figure 7.** Size distribution of PAX NPs by DLS. [a]

[a] Experiments were performed with the homogenization speed at 6000 rpm and organic phase composition at 2 mg paclitaxel/ 50 mL acetone. 2% w/v of PVA was dissolved in the aqueous phase.

3.3.1.2 Encapsulation efficiency and stability of PAX NPs in different pH of the aqueous solutions

PAX NPs were characterized by size and zeta potential as shown in Table 4. pH of the aqueous solution changes the charge state of alginate, thus it may influence the emulsification process and formation of PAX NPs.

The pKa of alginate is 3.36-3.65 at 25 ºC. When the pH in the aqueous was adjusted below 3, alginate was precipitated as semi-transparent gels. When the pH changed to 3.6, after the emulsification and centrifugation, white precipitates were observed, which were difficult to dissolve in water. Transparent gels were formed during the washing of PAX NPs at this pH value. At pH 5 and 7.3, PAX NPs were well prepared with no gels formed. As the alginate chain would keep a greater part of ionized carboxyl groups at pH 5, more stable particle suspensions could be expected. Encapsulation efficiency was also higher when the aqueous pH was adjusted to 5.

Stability of PAX NPs in SGF/SIF/water (SGF: simulated gastric fluid; SIF: simulated intestinal fluid) was investigated. Measurement of zeta potential is one simple way to study the stability of a particle suspension. Charges of PAX NPs in water were caused by the carboxyl groups in alginate, which was adsorbed on the drug particles during the emulsification. The pH of the medium had a significant influence on particles' surface charges. In SGF (pH 1.2), low charge on particle surfaces may induce instability and particle aggregation, as shown by zeta potential at -1 mV in KCl at pH 1.2. The PAX NPs were stable in SIF and water, showing zeta potential around -40 or -50 mV. (Table 5) Encapsulation efficiency did not change much between the medium SGF or SIF and the control (water).

**Table 4. Effect of pH in the aqueous solution on PAX NPs' encapsulation efficiency**

| pH of aqueous solution | Particle size (DLS, nm) | ζ-potential* (mV) | Encapsulation Efficiency (E.E.) % |
|---|---|---|---|
| 7.3 | 186 | -39 ± 4.0 | 33 ± 1.6 |
| 5 | 132 | -50 ± 2.7 | 43 ± 2.0 |
| 3.6 | 139 | -31 ± 3.6 | 29 ± 7.1 |
| 2 | N/A | N/A | N/A |

*Zeta potential was measured in 1mM KCl at pH 5.6, room temperature.
E.E. % was determined by [(measured PAX mass) / (initially fed PAX mass)] ×100 (n = 3 for each experiment at given pH of aqueous solution).

**Table 5. Preliminary study on PAX NPs' stability in SGF vs. SIF**

| Measurement | Control (water, pH 5.6) | SGF | SIF |
|---|---|---|---|
| Zeta potential* Before incubation | -50 ± 2.7 | -28 ± 2.2 | -39 ± 1.1 |
| Zeta Potential After incubation | -39 ± 3.8 | -16 ± 3.7 | -50 ± 4.2 |
| Stability after incubation† | 1 | 0.99 | 1.13 |

† Stability was calculated by [paclitaxel concentration in PAX NPs incubated in SGF or SIF/ paclitaxel concentration in PAX NPs incubated in water]. Stability study was done in SGF/SIF/water in a shaking water bath for 2 hr at 37 ºC.
* Zeta potential was measured in 1mM KCl at pH 5.6, room temperature.
^ SGF: simulated gastric fluid; SIF: simulated intestinal fluid.

### 3.3.2 LbL self-assembly with synthetic polymers and biomacromolecules

Core-shell PAX NPs were fabricated *via* the LbL assembly technique. Solid PAX NPs with negative charge were used as the core and encapsulated by both synthetic and biocompatible polyelectrolytes (PEs). Z-potential of the sample was then measured (Figure 8). Synthetic polymers PAH/PSSCMA were well studied and the adsorption of these PEs alternatively onto PAX NPs suggested the feasibility of fabricating core-shell structured nanoparticles using the LbL technique.[57] The outermost layer of these particles was set to be PSSCMA in order to provide the carboxylic acid group for surface modifications.

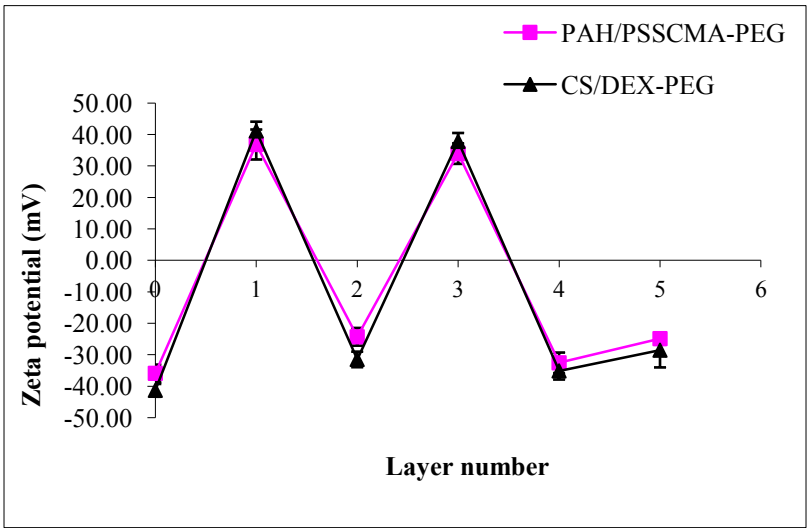


**Figure 8.** Zeta potential of LbL polyelectrolyte assembled PAX NPs.

Multilayer thin film in nanometer size was adsorbed onto solid drug nanoparticles mainly due to the electrostatic interaction between oppositely charged PEs.[62-63] The nanoshell thickness built in this way could range from several to hundred nanometers by varying the layer number and layer thickness.[64] Therefore, nanoscale

control on nanoparticles' surface could be realized through tuning layer number and thickness. The effects of the solution's ionic strength and pH on polyelectrolyte multilayer thickness had been studied, and it was found that the thickness would increase from less than 2 nm to 4 nm per bilayer by changing the solution's pH. Using moderate ionic strength of buffer solutions could get access to wider ranges of layer thickness.[13] Besides the dominant electrostatic interaction between the PE layers, secondary interactions such as hydrogen bonding, van der Waals force, and hydrophobic force also exist. The effect of the solution's pH on selective adsorption of PEs was investigated and showed that hydrogen bonding interaction of PAA became important at a low pH value, while electrostatic interactions became predominant at a high pH value. [16]

From the chemical structures of PE pairs PAH/PSSCMA, CS/DEX, each PE layer has its own characteristic element. Cationic polymers PAH and CS have the element nitrogen; anionic polymers PSSCMA and DEX have the characteristic element sulfur. This fact provided us another way to confirm if the LbL assembly was successful. Figure 8 shows the high resolution N 1s XPS spectra during adsorption of synthetic polymers PAH/PSSCMA. High resolution XPS spectra could provide us additional information about surface sensitivity, since the atomic charge state could be resolved more detailed at a lower energy.[62] Binding energy at 401 eV for N 1s represents protonated amine, which exists in PAH. From Figure 8, nitrogen intensity increased after adding PAH layer and decreased after adding PSSCMA layer. The initial N 1s peak failed to show up in the PAX NPs. This may be possible due to the fact that the paclitaxel is water insoluble and tends to stay inside of the nanoparticles, rather than on the surface of the nanoparticles when they were formed.[4] High resolution S 2p XPS spectra also showed the increase of the peak intensity corresponding to the adsorbed PSSCMA layer.

Relative atomic mass compositions could be obtained according to relative peak area integrated from XPS spectra. The atomic mass compositions of S and N changed in response with the adsorption of each PE layer, CS or DEX (Figure 10). Carbon and oxygen were two main elements existing on particle surfaces; N and S were two

characteristic elements presented on adsorbed PE layers. Alternating mass composition change of N and S suggested the successful adsorption of each PE layer.

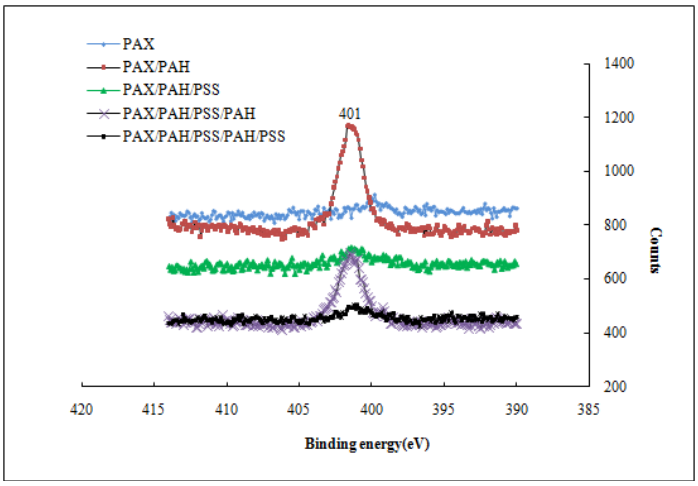


**Figure 9.** High resolution N 1s XPS spectra of PAH/PSSCMA LbL assembled onto PAX NPs. (XPS samples were prepared by dropping 20 µL of well dispersed particle solutions onto glass chips and dried at ambient conditions overnight. XPS spectra were obtained after encapsulating each P.E. layer.)

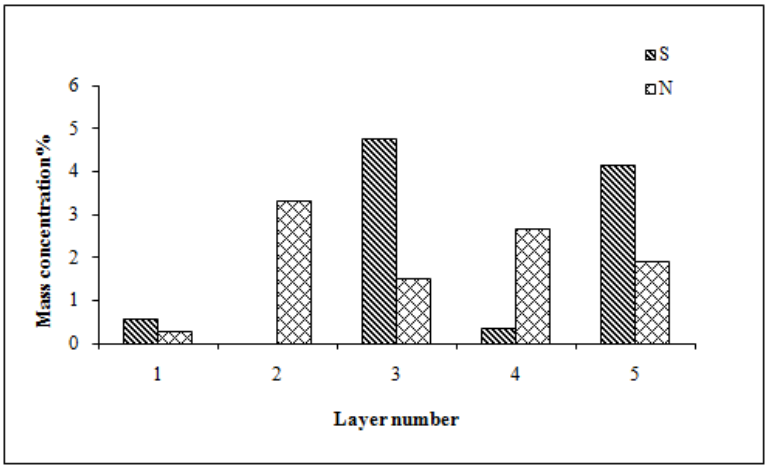


**Figure 10.** Atomic N and S mass composition change corresponding to alternative CS/DEX layer adsorbed onto PAX-NP. (1-bare PAX NPs; 2/4-add CS layer; 3/5-add DEX layer).

### 3.3.3 Surface modifications of core-shell nanoparticles

3.3.3.1 Conjugation of Poly (ethylene glycol)

After the polyelectrolyte layers were assembled onto nanoparticles, PEG ($H_2N$-PEG-CM, MW 3400) was conjugated to create a hydrophilic and biocompatible surface by a standard carbodiimide chemical reaction.[58] High resolution C 1s, N 1s, S 2p XPS spectra were obtained and atomic state changes before and after the PEG chemisorptions were studied. In high resolution C 1s XPS spectra, there were two peaks presented before and after the PEG conjugation. Binding energy at 285 eV was referred as the C-C bond. There was a shoulder peak at 286.1 eV representing C-O or C-N bonds.[65] After the PEG conjugation, an amide bond was formed and thus increased the intensity of the shoulder peak at 286.1 eV and decreased the intensity of the C-C peak at 285 eV, indicating the successful chemisorptions of PEG (Figure 11 a, b).

High resolution N 1s XPS spectra showed there were two N 1s peaks at different binding energies (401 and 399 eV) before and after the PEG conjugation; this related to two different states of nitrogen.[62] The percentage of relative peak area for the secondary amine at 399 eV increased from 48.5 % to 72.9 % after the PEG conjugation, which was due to the newly formed amide bond. After PEG conjugation with the outermost layer PSSCMA, high resolution S 2p XPS spectra showed the sulfur peak disappeared, suggesting that the outermost PSSCMA layer was fully covered by PEG.

In order to conjugate CS/DEX encapsulated nanoparticles with PEG, the outermost layer of the nano-assembly was set to be PSSCMA. The carboxyl group in PSSCMA could react with the free amine group of $H_2N$-PEG-CM, forming an amide bond. Figure 11-b showed the high resolution C 1s XPS peak spectra before and after the PEG conjugation. Similar to previous results, there was an obvious increase of intensity in C-N shoulder peak at the binding energy 286.3 eV, and the intensity of C-C bond at the binding energy 285 eV decreased after the PEG conjugation.

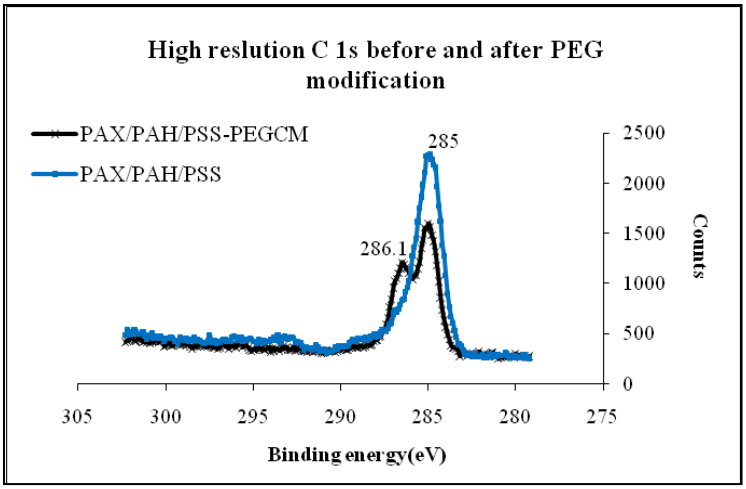


a) Synthetic polyelectrolyte PAH/PSSCMA

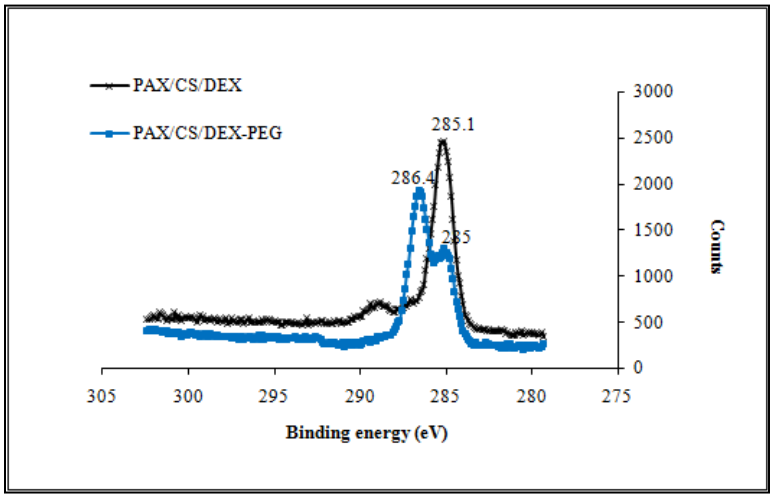


b) Bio-polyelectrolyte CS/DEX

**Figure 11.** High resolution C 1s XPS spectra of LbL assembled PAX NPs before and after PEG conjugation (both samples were encapsulated with 3 bilayers PEs). Binding energy at 285 eV represented carbon bond, and binding energy at 286-287 eV attributed to C-N or C-O bond.

The predominant N 1s XPS peak switched from binding energy at 401 eV (free amine) to the peak at 399 eV (secondary amine) after the PEG modification (Table 6). No enhancement on N 1s peak intensity was observed after the conjugation, possibly because the amine group is not present in PEG repeat units. The PEG conjugation

shielded the last layer of DEX (containing sulfate groups), so the high resolution sulfur peak disappeared after conjugating with PEG (Figure 12).

**Table 6. High resolution N 1s XPS spectra analysis**

| | B.E.(eV) | Area | Area% |
|---|---|---|---|
| Before conjugation | 399 | 0 | 0 |
| | 401 | 323 | 100 |
| After conjugation | 399 | 255 | 80 |
| | 401 | 63 | 20 |

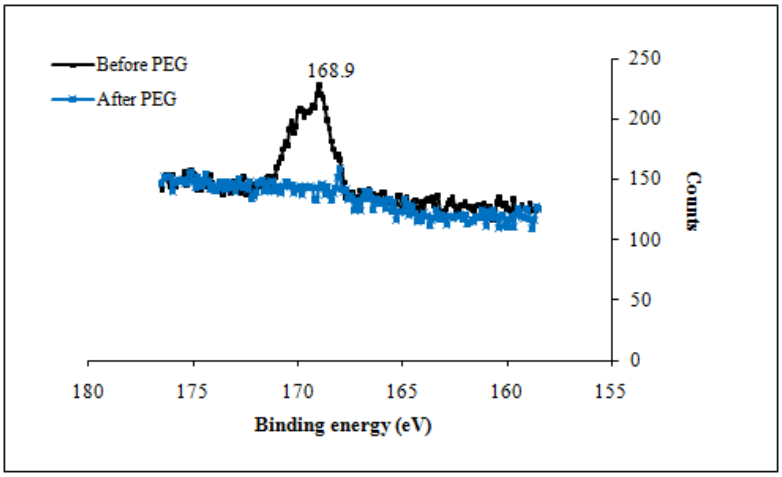


**Figure 12.** High resolution S 2p XPS spectra before and after PEG modification. (Before PEG - PAX NPs encapsulated with 3 bilayers CS/DEX polyelectrolyte; after PEG- PAX NPs with 3 bilayers CS/DEX in conjugation with $H_2N$-PEG-COOH).

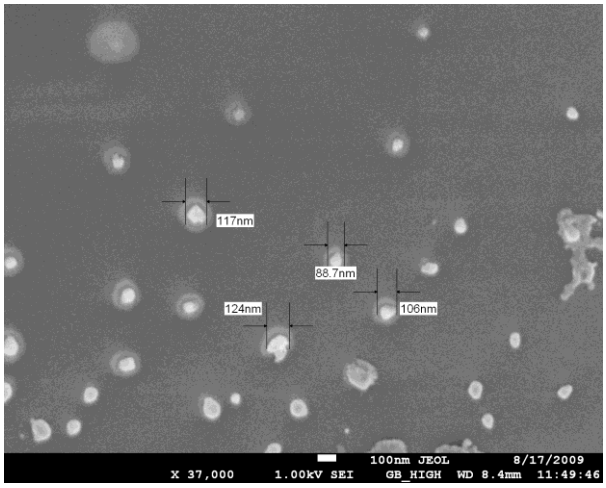


a)

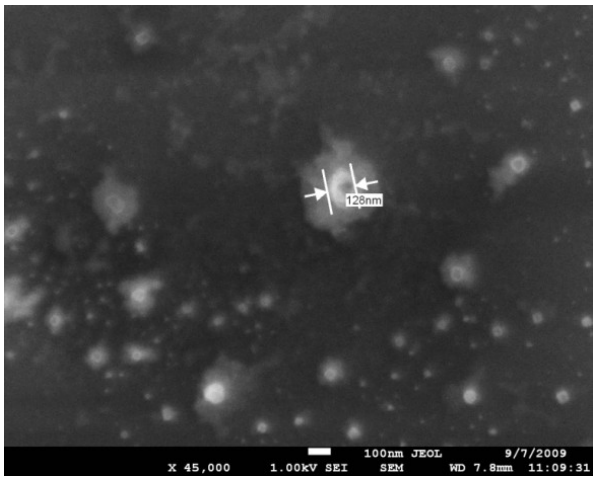


b)

**Figure 13.** SEM images of polyelectrolytes encapsulated PAX NPs. a) PAX-NP with 2 bilayers of PAH/PSSCMA conjugated with PEG; b) PAX-NP with 2 bilayers of CS/DEX conjugated with PEG. Fresh prepared samples were well sonicated to break down possible aggregates. 10 μL of the suspended nanoparticles were dropped onto a TEM grid and dried at ambient conditions. All samples were stored in vacuum oven one day before imaging (room temperature).

Figure 13 showed SEM images of 2 bilayers of PAH/PSSCMA and CS/DEX polyelectrolytes encapsulated PAX NPs. Samples were well dispersed by sonication to avoid aggregates, dropped onto a TEM grid and dried in a vacuum oven (room temperature). After PEG conjugation, particles were easily suspended and zeta potential

showed a value around -28 mV (with less than 5 % standard deviation), indicating highly charged particle surfaces, and therefore fairly stable particle dispersion. PEG with the good hydrophilic property and flexible chains in the solution could promote the repulsion effect between particles. It was found that the functions of PEG were to stabilize particles when covalently modified onto their surfaces and to reduce nonspecific protein adhesion.[66]

3.3.3.2 Modification with F-WGA

An effective antitumor drug therapy must be able to make its way into the blood vessels of the tumor, across the vessel wall, and finally migrate through the interstitium.[67] Thus a tumor targeting system is necessary to deliver the reactive agent efficiently. Lectin is a protein that can recognize and bind to sugar complexes due to its high specificity for the chemical structure of the glycans. Transformed or cancerous cells often express different amounts of glycans compared with their normal counterparts.[68] It has been proved that PAX NPs, which were conjugated with the lectin WGA, allowed efficient targeting to cancer cells.[28,69,70] Fluorescence labeled WGA was used as the targeting moiety, and polystyrene sulfate nanoparticles were used as the model core in this experiment to study the feasibility of conjugating this lectin onto nanoparticle surfaces.

First, the time of incubating the PAH/PSSCMA assembled particles with F-WGA was optimized. (Figure 14) Negative control suggested nonspecific adhesion of fluorescence lectin onto LbL assembled PAX NPs. It was increased as the exposing time to F-WGA was extended. There was no obvious difference between the blank samples and negative controls when incubating the particles with F-WGA for 20 min and 2 h. The fluorescence intensity of tagged particles reacted with F-WGA for 20 h had been increased significantly as compared to those reacted for shorter times. Tagged nanoparticles (20 h reaction) showed an almost seven fold increase in fluorescence intensity over its negative control sample, suggesting conjugation of this lectin onto the particles was successful.

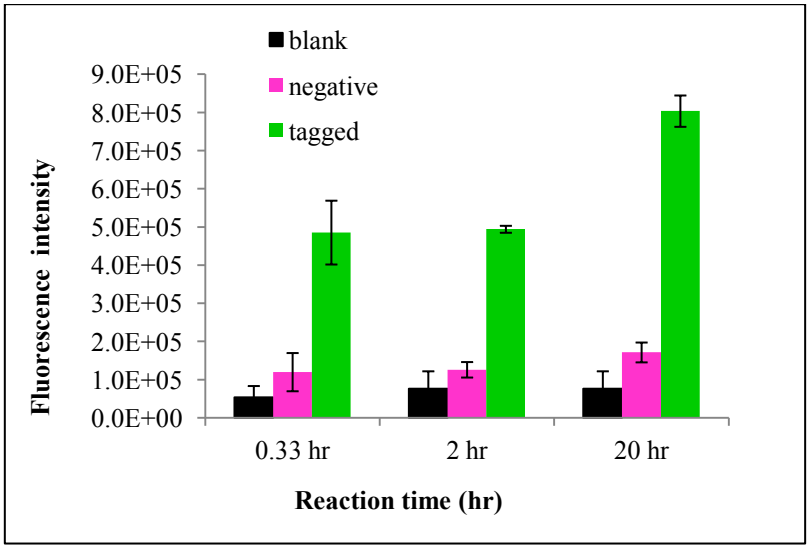


**Figure 14.** Effect of reaction time on fluorescence intensity of F-WGA conjugated LbL assembled nanoparticles. [b]

[b] Blank: control, particles treated with the LbL procedure (P.E.:PAH/PSSCMA). Negative control: LbL self-assembled nanoparticles exposed to F-WGA but not EDAC. Tagged particles: LbL self-assembled nanoparticles conjugated with F-WGA using reagents EDAC and s-NHS. (All samples were treated with PEs: PAH/PSSCMA 5 bilayers).

After conjugating F-WGA onto LbL assembled nanoparticles, the wavelength of maximum fluorescence intensity shifted. Tagged particles showed the highest level of fluorescence intensity within the emission scanning range (Figure 15).

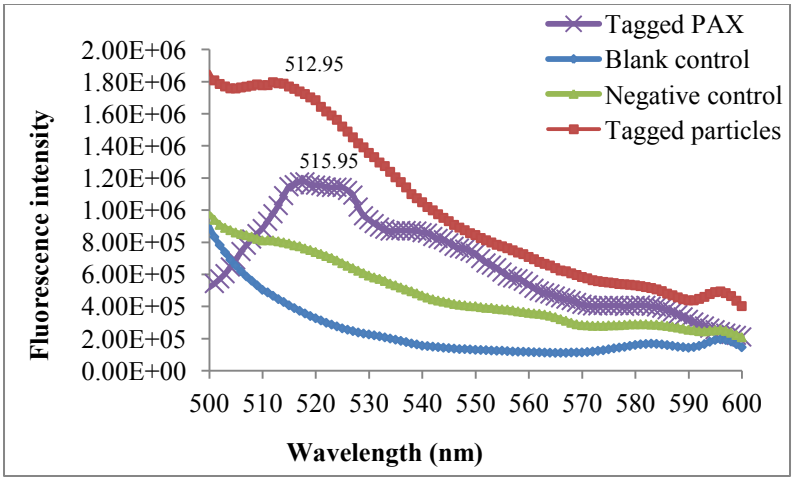


**Figure 15.** Fluorescence level of Bio-PEs encapsulated PS NPs and PAX NPs (3 bilayers) in conjugation with F-WGA. Fluorescence intensity corresponding to F-WGA concentration indicated lectin F-WGA successfully conjugated onto nanoparticles' surfaces.

### 3.4 Conclusion

A nanoparticle based system consisting of a paclitaxel drug based core encapsulated with a nanometer thick synthetic / biomacromolecule shell using the LbL assembly technique was successfully fabricated and characterized. The nanoshell provided reactive groups on the surface which could be further modified with functional moieties such as the hydrophilic polymer PEG and ligand to build a biocompatible and tumor specific targeting system. The thickness and density of the shell could be varied by controlling the experimental conditions, such as buffer pH, ionic strength (salt concentration), and polyelectrolyte composition.[7] This biocompatible drug delivery system, which combined the EPR effect with active targeting property, might possibly provide an alternative to more efficiently deliver hydrophobic drugs to tumors, as compared to our previous work. [57]

# 4. *IN VITRO* STUDY OF PACLITAXEL RELEASE FROM NANOPARTICLES*

Core shell structured PAX NPs were prepared by encapsulating biomacromolecules chitosan and dextran using the LbL self-assembly technique. The poly (ethylene glycol) was conjugated onto the outermost layer of the drug nanoparticles for this release study. Adjustable release profiles may be obtained by tuning the layer number and buffer ionic strength.[18]

## 4.1 Introduction

For different types of cancer, (e.g. undetectable cancer, metastatic cancer, or cancer that is not confined in a solid tumor, etc), chemotherapy has been proved to be a necessary and effective treatment.[4] However, for most anti-cancer drugs, the poor solubility causes low bioavailability, and the properties of the drugs themselves are usually unfavorable. Therefore, novel engineering formulations for increasing cellular uptake and cell targeting were developed, and drug release profiles from these delivery systems were studied.[4, 71]

Nanoparticles made of biodegradable polymer poly(lactic-co-glycolic acid) (PLGA) is one promising system that may promote a controlled and targeted delivery of the drug with desired released kinetics, high cell uptake and high cytotoxicity.[4] Poorly soluble drugs can also be incorporated in the inner core of a micelle system by physical entrapment through hydrophobic interaction between the drug and the copolymers.[72]

---

*Parts of this section are reproduced with the permission of (Yu, X.; Pishko, M. V., *Biomacromolecules* **2011,** *12* (9), 3205-3212.). Copyright (2011) American Chemical Society.

*In vitro* study of the paclitaxel release from nanoparticles could be conducted by suspending the nanoparticles in buffer solution (pH 7.4) and then placing them in a tube in the shaking water bath, which was maintained at 37 ºC. Samples were withdrawn at particular time intervals by centrifuging down the nanoparticles and extracted the supernatant with dichloromethane (DCM), which were analyzed later by HPLC. The nanoparticle residuals were re-suspended by fresh buffer, and the release study continued. Another way to perform the *in vitro* release study is to prepare the same paclitaxel nanoparticle suspension and dilute it with PBS in a pre-calculated number of flasks. Two flasks were withdrawn at predetermined intervals to identify the paclitaxel concentration in the nanoparticle residuals. The release part can then be calculated based on the difference between the initial paclitaxel mass amount and the paclitaxel in the residuals. [60]

The surfaces of PAX NPs were observed containing micro-caves and pores rather than being simply smooth.[4] This porous structure may be the reason paclitaxel can be released through diffusion. One possible mechanism could be: an initial burst release during the first 24 hr, followed by a slower and continuous diffusion release.[4, 60]

So far there were few references studying the paclitaxel release from LbL self-assembly. Core-shell structured PAX NPs were formed by encapsulating polyelectrolyte layers onto the PAX NPs. The release of the drug from the self-assembly is related to the stability of the system, the interaction between the hydrophobic drug and the amphiphilic matrix. The process may be explained as follows: as the environmental condition changes, the LbL structure is disrupted. Foreign buffer diffuses in, which causes the erosion of the core nanoparticles, and then the diffusion of the drug out of the matrix started.

Paclitaxel and other taxanes have complex structures including the presence of numerous hydrolytically sensitive ester groups and a chiral center that readily undergoes epimerization. Degradation kinetics of paclitaxel have been intensively studied as a function of temperature, pH and buffer concentration, and degradation products were

identified by LC/MS.[73-74] This phenomena should be noticed during the *in vitro* release studies.

Synthetic polymers PAH/PSSCMA have been widely used as an example for microcapsule application and the layer permeability could be tuned to achieve controlled release of small molecules.[75] However, for further application, bio-polyelectrolytes are preferred because they are biodegradable and biocompatible. In this experiment, PAX NPs were encapsulated within bio PE nanofilms, and the release profiles of paclitaxel from LbL assembly with different layer numbers were investigated.

## 4.2 Materials and methods

Chitosan (low molecular weight), dextran-sulfate (average Mw > 500,000), poly (vinyl alcohol) (PVA, Mw 9000-12,000 g/mol and Mw 22,000 g/mol), sodium alginate (from brown algae, low viscosity) were purchased from Sigma-Aldrich, USA. Semisynthetic paclitaxel (from *Taxus* sp.), ≥ 97% was purchased from Sigma. Poly (ethylene glycol) ($NH_2$-PEG-Carboxymethyl, Mw~ 3400) was purchased from Laysan Bio, Inc. USA. EDC (ECDI; 1-Ethyl-3-(3-dimethylaminopropyl) carbodiimide, HCl), and s-NHS (Sulfo N-Hydroxysulfosuccinimide) were purchased from Fisher scientific, USA. Ultrapure water used for all experiments was obtained from a Millipore system with a specific resistance 18 MΩ/cm. Polyelectrolyte solutions were prepared in a 30 mM KCl solution or 0.15 M NaCl. Phosphate-buffered saline solution (PBS, pH 7.4) consisted of 1.1 mM potassium phosphate monobasic, 3 mM sodium phosphate dibasic heptahydrate, and 0.15 M NaCl.

**Paclitaxel release from LbL assembly.** The release profile of hydrophobic drug paclitaxel from LbL assembled core-shell nanoparticles was investigated. Studies were performed at the physiological pH condition in phosphate buffered saline solution (10 % DMSO) with magnetic stirring all the time. All 10 mL samples were withdrawn, and particles were ultracentrifuged down at a speed of 10,000 rpm/15 min. Supernatant was collected for further HPLC analysis, and particles were re-suspended by 10 mL of fresh PBS (10 % DMSO). Cumulative paclitaxel release as measured by HPLC was quantified

with time. The paclitaxel HPLC peak was integrated to calculate the area, with concentrations determined from the calibration curve.

**High performance liquid chromatography (HPLC).** The paclitaxel concentration was analyzed using Waters Breeze HPLC System with a refractive index detector. The drug release was monitored at predetermined times. The supernatant was extracted by dichloromethane (DCM) three times. DCM phase was then evaporated at low heat under air flow overnight until fully dried. The residue was then dissolved in the mobile phase of acetonitrile: water (70:30, v/v), and analyzed by HPLC at a flow rate of 1 mL/min, injection volume of 20 µL using a reverse phase column C 18 (Higgins Analytical, Inc., PROTO 200 C18 column 5 µm, 250 × 4.6 mm, CA, U.S.A.). Column temperature was set to 30 ºC, and the detector temperature was maintained at 35 ºC. This HPLC technique was analytically validated.[76] For all release studies, 10 % v/v DMSO was added to avoid paclitaxel saturation in the aqueous solution.[77] All HPLC measurements were at least duplicated with three parallel samples each time. A calibration curve was obtained by preparing standard paclitaxel (≥ 97%) solutions at different concentrations. The calibration concentration ranges from 5 µg/mL to 100 µg/mL.

## 4.3 Results

### 4.3.1 Fabrication of LbL assembled nanoparticles

PAX NPs were prepared by a modified emulsification evaporation method. The particle size was around 120-130 nm, and zeta potential was at -41 eV. The chitosan and dextran were encapsulated onto the PAX NPs alternatively until the desired layer number was obtained. To stabilize the nanoparticles in suspension, PEG was modified at last and the particles were ended up with a zeta potential at -32 eV. These PEG conjugated PAX NPs were then stored in 4 ºC fridge for further use. All release experiments were performed with fresh prepared PAX NPs (prepared within 3 days before use).

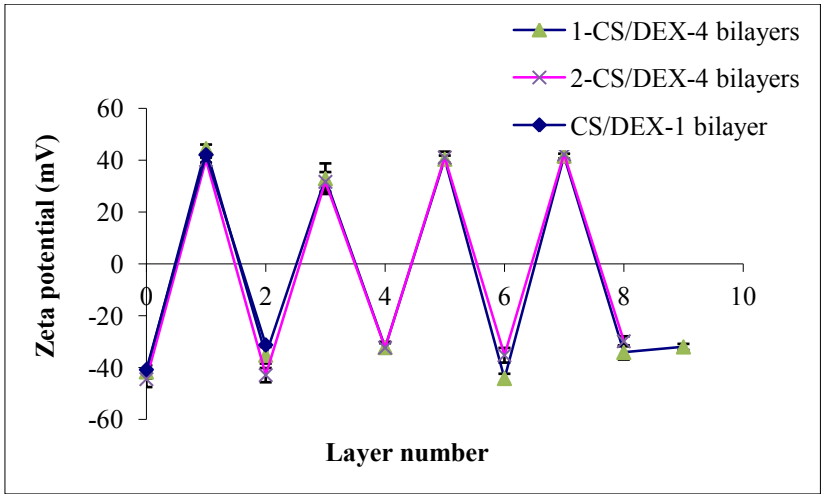


**Figure 16.** Zeta potential of chitosan and dextran encapsulated PAX NPs.

### 4.3.2 Release of paclitaxel from nanoparticles

4.3.2.1 HPLC calibration curve

Since a refractive index detector was used through the whole release studies. The calibration curve between paclitaxel concentration in standard samples and HPLC integrated area was obtained to validate the assay. Paclitaxel concentrations ranging from 5 µg/mL to 100 µg/mL were prepared and analyzed by HPLC. Retention time for the standard samples ranges from (4.432 ± 0.008) min to (4.648 ± 0.059) min. This may be caused by the degradation of paclitaxel in the aqueous solution over time.[73] So both standard and the test samples should be prepared and kept as fresh as possible for HPLC analysis, i.e. within 3 days after acquirement.

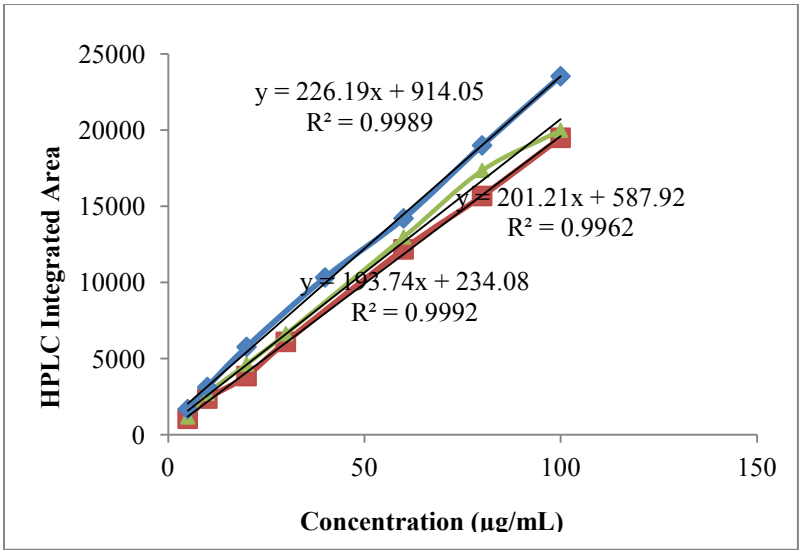


**Figure 17.** HPLC calibration curves of standard paclitaxel. Note: HPLC calibration curve should be measured every time before the experimental samples are analyzed.

4.3.2.2 SEM images of PAX NPs

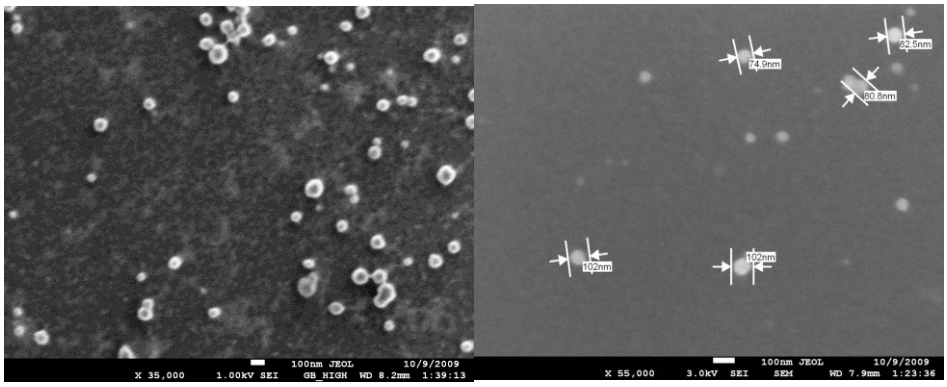


**Figure 18.** SEM images of bare PAX NPs (above two) and polyelectrolytes encapsulated PAX NPs (Figure 13). Fresh prepared samples were well sonicated to break down possible aggregates. 10 µL of the suspended nanoparticles were dropped onto a TEM grid and dried at ambient conditions. All samples were stored in vacuum oven one day before imaging (room temperature).

4.3.2.3 Paclitaxel release from bare and LbL assembled nanoparticles

Figure 19 shows the release profile of paclitaxel from bare nanoparticles and biomacromolecule LbL assembly. The accumulative release of paclitaxel from bare nanoparticles was used as a control in this experiment. Its release rate was the dissolution rate of the nanoparticles in PBS 7.4 at 37 ºC. It was observed that within 8 h, 86 % of PAX NPs were dissolved, and free drug paclitaxel was released in the buffer solution. A fast burst release of paclitaxel from the bare nanoparticles was observed as 20% of the drug was detected during the first hour. The kinetics of paclitaxel release from its bare nanoparticles may be influenced by its solubility, the polymorphic form, crystallinity, particles size and size distribution, the use of surfactant in the organic phase or not, and the drug encapsulation efficiency, etc.[60, 78]

Instability and disassembly of the layers were the main causes of paclitaxel's release from the self-assembly, which were induced by the environmental pH and ionic strength (salt concentration) changes.[79] It was found that high salt concentration weakened electrostatic interactions between adjacent layers of PEs and caused the destruction of PE multilayer nanofilms.[54] From Figure 18, after encapsulating these PAX particles with one bilayer of PEs CS/DEX, around 48.6 % of the self-assembled nanoparticles was released, and 32 % of four bilayers assembled nanoparticles was released during 8 h. (Both LbL assembled nanoparticles were conjugated with PEG.) [80]

A possible explanation for the release of free drug from the LbL assembly in this experiment could be: as the PBS buffer permeated through the polyelectrolyte layers, the nanoshell became unstable due to the presence of a less charged state of chitosan (in our case), which was caused by pH changes, resulting in the disassembly of PE layers. The DMSO (10% v/v) added into the aqueous phase may facilitate the dissolution of PAX NPs. The fewer the PE layers were, the easier the assembled structure would be destabilized. As the buffer went into the core, the process became the release and dissolution of the PAX NPs, and the drug molecules then diffused out of the disassembled PE layers.

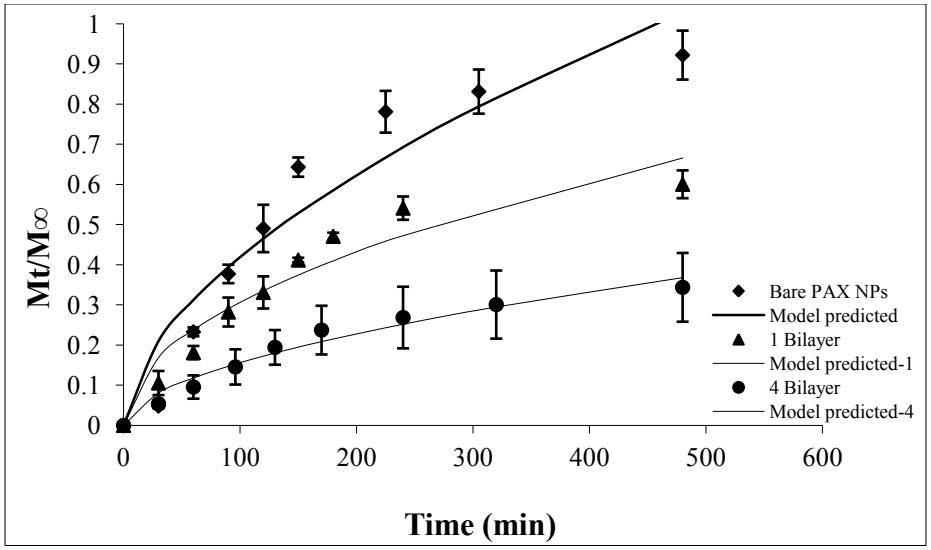


**Figure 19.** Accumulative release of paclitaxel from LbL assembled nanoparticles and bare PAX NPs (different layer number indicated in the graph).

4.3.2.4 Model fitting

Exponential approximation model was applied to the obtained experimental data. (Figure 18) This simple exponential relation $\frac{Mt}{M\infty} = kt^n$ , could be used to describe the general solute release behavior from different polymeric devices.[50] $\frac{Mt}{M\infty}$ is the fractional solute release, t is the release time, k is a constant, and n is the diffusion exponent, indicating the release mechanism. This equation can not only be used to describe the release of drug from slabs and cylinders, but also spherical particles. Different values of n can be obtained according to the geometry of the systems, suggesting different release behaviors of the drug from corresponding controlled release systems. Influence of device geometry on the release mechanism, showing that for pure Fickian release, the exponent n has a limiting value of 0.43 for spheres.[51] A value of n in the range from 0.43 to 1.00 indicated non-Fickian transport. In this release study, experimental data was fitted in the exponential model, and the diffusion exponent n and mechanism of the controlled release systems were analyzed as summed up in Table 6. The best fit curve is from the

experiment: the accumulative release of paclitaxel from 4 bilayer assembled nanoparticles.

**Table 7. Diffusion exponent and possible mechanism of paclitaxel release from the controlled release systems**

| Sample ID | Diffusion exponent n | Constant k | Possible drug release mechanism |
|---|---|---|---|
| Spherical sample [51] | 0.43 | _____ | Fickian diffusion |
| | 0.43<n<0.85 | _____ | Anomalous (non-Fickian) transport |
| Bare PAX NPs | 0.57 | 0.030 | Non-Fickian transport |
| 1 bilayer CS/DEX LbL assembled PAX NPs | 0.50 | 0.031 | Non-Fickian transport |
| 4 bilayers CS/DEX LbL assembled PAX NPs | 0.55 | 0.013 | Non-Fickian transport |

## 4.4 Conclusion

In recent research, polyelectrolyte capsules have been widely introduced as new vehicles which may release therapeutic reactive due to their permeability changes in response to environmental stimuli.[81] However, for further *in vivo* drug delivery, its application is limited by the requirement of extreme stimuli release mechanisms, which do not occur or are not applied *in vivo*.[79] Naturally PE shells would only be permeable to molecules with MW under 5 kDa.[82] While, in this study, PAX NPs with size under 200 nm might be passively accumulated to pathological areas.[52] In combination with the active targeting moiety, a more effective system may be formed. Stability of this nanoparticle based, LbL assembled drug delivery system was also expected to be better than that of capsules, which may be very sensitive to environmental pressure, leading to unexpected leakage or breakage. In all, this PAX NP based, bio-polyelectrolyte LbL assembled system might be a promising vehicle to deliver hydrophobic drugs or other macromolecules.

# 5. *IN VITRO* STUDY OF NANOPARTICLE RELEASES FROM PH SENSITIVE POLYSACCHARIDE BASED HYDROGELS*

Two different kinds of dextran based pH sensitive and enzyme degradable hydrogels: dextran maleic acid (Dex-MA), and glycidyl methacrylated dextran (Dex-GMA) were synthesized for oral delivery of nanoparticles. Hydrogels of both kinds were stable in simulated gastric fluid, but prone to swelling and degradation in the presence or absence of enzyme dextranase in simulated intestinal fluid. The release profiles of nanoparticles could be tuned under simulated human GI conditions. These two biodegradable hydrogels, which can release nanoparticles depending on pH changes, may be suitable as potential colon targeting vehicles for oral delivery of drug nanoparticles.[83]

## 5.1 Introduction

It is reported that 40 % or more of active substances are identified as poorly soluble in water, which has become an industry wide issue in drug discovery.[84] The limitation of this kind of drug relies on its inadequate ability to be wetted and dissolved into the fluid in the gastrointestinal (GI) tract; therefore they exhibit low bioavailability *in vivo*.[85]

Paclitaxel (PAX) is one of the best antineoplastic drugs found from nature in the past decades, and it is water insoluble. PAX NPs (PAX NPs) can be prepared by a solvent emulsification and evaporation method with controllable size and surface charges.[57] Surface coatings and modifications can then be performed onto particle

---

*Parts of this section are reproduced with the permission of the Royal Society of Chemistry, original link: http://pubs.rsc.org/en/content/articlelanding/2011/sm/c1sm05729d.

surfaces towards specific functions, such as material biocompatibility and cell targeting.[18]

Oral delivery of anticancer drugs has the advantages over current cancer chemotherapy, *e.g.* injection or infusion. Several advanced drug delivery systems have recently been developed for oral delivery of paclitaxel.[10-14] One promising way is to use hydrotropic polymers and their micelles as vehicles and copolymerize them with acrylic acid. The release of paclitaxel from these vehicles can be completed within 12 hr in simulated intestinal fluid.[86] Another way is to fabricate pH modulated polymeric microspheres containing ethyl cellulose and Eudragit® to deliver small actives by an oral route.[87] Biodegradable PLGA thin films were also synthesized, and the controlled release of paclitaxel from these films could be realized by adjusting its degradation rates.[77]

Due to the physiological characteristic, a controlled drug delivery system could be designed to potentially regulate the drug release through external physiological pH changes. Moreover, the intestinal micro flora are characterized by a complex and relatively stable community of microorganisms, some of which are responsible for a wide variety of metabolic processes.[38] Dextranases (systematic name: 1,6-α-D-glucan-6-glucanohydrolases (EC 3.2.1.11)), which were mainly produced by the bacteria in the human colon, can hydrolyze the 1,6-α-D-glucosidic linkages of dextrans.[88] The bacteria are gram negative intestinal bacteria, genus *Bacteroides*, which are the numerically predominant anaerobes in the colonic region of humans.[89] Dextran has been found to be degraded in human feces due to bacterial action.[90] Dextran pro-drugs were also shown to release the drug specifically in the colonic region of pigs.[91]

Therefore, the mechanism of successfully providing colonic drug release was proposed to be a result of the complete stability of the hydrogel matrix in the stomach and small intestine followed by its disintegration, in the colonic region with a subsequent release of the drug.[88]

In this study, controlled releases of the anticancer drug paclitaxel were realized by combining smart materials, *i.e.* pH sensitive polysaccharide based hydrogels, with

drug nanoparticles for oral administration. Dextran based pH sensitive hydrogels were chemically synthesized and used as the delivery vehicles to target specifically to the human colon (Figure 20).[41,44, 92] PAX NPs were prepared by an optimized method named solvent emulsification and evaporation.[57]

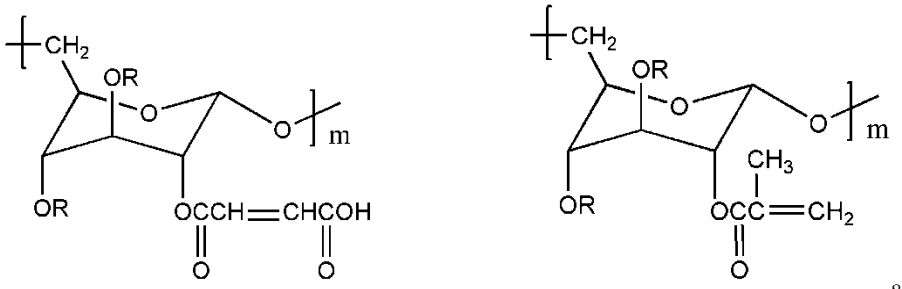

**Figure 20.** Chemical structures of dextran-maleic acid and methacrylated dextran.[83]

## 5.2 Materials and methods

Dextran from *Leuconostoc mesenteroides* (Mw 64,000-76,000), maleic anhydride, dimethyl formamide (DMF), triethylamine (TEA), lithium chloride (LiCl), isopropyl alcohol, glycidyl methacrylate, dimethylamino pyridine (DMAP), dimethyl sulfoxide (DMSO), 2,2-dimethoxy-2-phenyl-acetophenone (DMPA), *N*-Methyl-2-pyrrolidone (NMP), poly (ethylene glycol) diacrylate (PEG-DA 575), acrylic acid (AA), Sigmacote®, dextranase from *Penicillium sp.* (25.3 units/mg solid) were purchased from Sigma-Aldrich Co. (St. Louis, MO, USA). Semisynthetic paclitaxel (from *Taxus sp.,* ≥ 97%), was also purchased from Sigma. FluoSpheres® amine-modified microspheres (F-NPs, 0.2 μm) were purchased from Invitrogen (Oregon, USA). All reagents were of analytical grade, and used as received. Double deionized water used for all experiments was obtained from a Millipore system with a specific resistance 18 MΩ/cm.

**Synthesis of Dex-MA and Dex-GMA precursors.** Dextran maleic acid precursor (Dex-MA, degree of substitution (DS = 0.99)) was prepared by the reaction of dextran with maleic anhydride in the presence of the catalyst triethylamine. Briefly, dextran was dissolved in LiCl/DMF (10 wt %) solvent at 90 ºC under nitrogen. Then the

temperature was cooled to 60 ºC, and triethylamine was then added and stirred for 15 min. The proper amount of maleic anhydride was injected to obtain the dextran derivative and reacted for 20 hr.[44] The final product was precipitated, washed by isopropyl alcohol, and dried at room temperature in a vacuum oven. The purified product was stored at -20 ºC for further use. Proton nuclear magnetic resonance ($^1$H-NMR) spectrum was recorded to calculate DS of Dex-MA.

Methacrylated dextran (Dex-GMA) precursor was synthesized by a well established method.[43] In short, dextran was dissolved in DMSO at 60 ºC under nitrogen for 2 hr. After dissolving 1 g of the catalyst DMAP and stirring for 20 min at room temperature, a proper amount of glycidyl methacrylate was added and reacted for 48 hr. The reaction was stopped by injecting the equimolar amount of concentrated HCl to neutralize DMAP. The reaction mixture was then transferred to a dialysis membrane (MWCO=14,000) and dialyzed for 2 weeks against deionized water at 4 ºC.[43] Dex-GMA was then lyophilized, and white fluffy powder was obtained and stored at -20 ºC for further use. The DS of the synthesized dextran derivative was confirmed by $^1$H-NMR to be 6.2.

**Preparation of pH sensitive hydrogels by photocrosslinking.** All hydrogels were formed by UV irradiation using a long wave UV lamp (UVP®, Upland, CA, U.S.A.). Different UV irradiation times were studied for the F-NPs' release experiments and set to 20 min for further PAX NPs' release experiments. Figure 18 showed the chemical structures of both dextran derivatives Dex-MA and Dex-GMA. PEG-DA and AA were added to the precursor solution and copolymerized with the dextran derivative Dex-MA and Dex-GMA respectively. All hydrogels were prepared in a Ø50×35 mm glass dish (coated with Sigmacote®) with a height of 1.5 mm and cut into small disks at a dimension of Ø8×1.5 mm.

**Loading F-NPs and PAX NPs in hydrogels.** PAX NPs and F-NPs were well dispersed by sonication to remove any possible aggregates before they were added to the Dex-MA or Dex-GMA precursor solution. The sample was well mixed with 20 μL/mL of the photoinitiator DMPA, before being placed under the UV lamp. After a certain

time, semi-transparent hydrogels were formed with nanoparticles loaded within the networks. UV irradiation time was extended to consume all C=C bonds: 20 min or more for Dex-MA. The gelation time of Dex-GMA-co-AA depended on its composition. Double deionized water was used to wash the hydrogels three times.

**Swelling Ratio *(SR).*** Swelling ratio of dextran based hydrogel was calculated based on the equation (2) in the presence and absence of enzyme dextranase. *Wt* represents the weight of the hydrogel disk at time t; *Wi* represents the initial weight of the hydrogel disk.

$$SR = \frac{Wt}{Wi} \quad (2)$$

**pH sensitive swelling.** Hydrogel disks were placed in the buffers at different pH values or with pH gradient changes (from SGF 1.2 to 4.5 to SIF 6.8) to study the pH sensitive swelling behavior. Two buffers used were simulated gastric fluid (SGF, pH=1.2) and simulated intestinal fluid (SIF, pH=6.8). SGF was prepared without pepsin and consisted of 0.2 % (w/v) sodium chloride in 0.7 % (v/v) hydrochloric acid, the pH of which was adjusted to 1.2. SIF was prepared according to the USP, including 0.896 g of NaOH, 6.805 g of $KH_2PO_4$ in 1 L deionized water, with the pH adjusted to 6.8.

Swelling behavior of the copolymer Dex-GMA-co-AA in the presence and absence of the enzyme dextranase (1.0-2.5 units/mL) was studied with buffer pH changed from SGF (1.2) to SIF (6.8).[92,93]

***In vitro* release studies of nanoparticles from dextran based hydrogels.** The *in vitro* release of F-NPs was first studied in SGF and SIF separately and then with pH gradient changes from 1.2 to 6.8. For the first 0-2 hr, the hydrogel disk loaded with F-NPs was incubated in SGF; at 2 hr, NaOH and $KH_2PO4$ were added to adjust the pH to 4.5; after 4 hr, the buffer changed to SIF with the enzyme dextranase added (final enzyme concentration at 1.0-2.5 units/mL). The PAX NPs' release experiments were conducted with pH gradient changes from SGF to SIF (0-2 hr, SGF; 2 hr- total release, enzyme concentration at 1.0-2.5 units/mL added after 15 min incubation in SIF).

For the F-NPs' release experiments, one hydrogel disk (Ø8×1.5 mm) was placed in a 10/15 mL one-neck flask and incubated in a shaking water bath (50 rpm, 37 ºC). 50 μL of the samples were withdrawn at a predetermined time without disturbing the disk, and fresh SGF/SIF was added to maintain a constant volume. For the PAX NPs' release experiments, 5 disks were placed in a 10/15 mL flask and incubated in the water bath under the same condition. The entire 5 mL of SGF/SIF solution was withdrawn at a predetermined time without disturbing the disks, and the PAX NPs released were centrifuged down at a speed of 8500 rpm/15 min. The supernatant was restored to the flask and a proper amount of SGF/SIF buffer was added to maintain a constant volume. The particles centrifuged down were dissolved in acetonitrile/water (70/30, v/v) with sonication under low heat and filtered through a 0.22 μm membrane for HPLC analysis.

**Measurement of fluorescent nanoparticles' concentration.** Fluorescence intensity of nanoparticles was measured by a PTI QuantaMaster series spectrofluorometer. A calibration curve was acquired by measuring the fluorescence intensity of nanoparticles at different concentrations. The linear correlation parameter was 0.9903 with concentration ranging from 0.1 to 25 μg/mL.

**Measurement of paclitaxel concentration by HPLC.** The paclitaxel concentration was analyzed using Waters Breeze HPLC System with a refractive index detector. All samples withdrawn were dissolved in the mobile phase of acetonitrile: water (70:30, v/v), filtered and analyzed by HPLC at a flow rate of 1 mL/min, injection volume of 20 μL using a reverse phase column C 18 (Nest Group. Inc., 250×4.6 mm, particle size 5 μm). The column temperature was set to 30 ºC, and the detector temperature was maintained at 35 ºC. All HPLC measurements were duplicated or triplicated with three parallel samples each time. A calibration curve was obtained by preparing standard paclitaxel (≥ 97%) and PAX NP solutions at different concentrations. The calibration concentration of paclitaxel in the mobile phase ranges from 5 μg/mL to 100 μg/mL with a linear correlation parameter at 0.9984. The volume of PAX NP suspension dissolved ranges from 5 μL to 100 μL with a linear correlation at 0.9986.

**SEM observation of dextran based hydrogels in different pH medium.** The samples of dextran based hydrogels for SEM were prepared by a method named cryofixation.[94] Briefly, Dex-GMA-co-AA hydrogels were incubated in PBS (pH 1.4 vs. 7.4) for 72 hr until they reached swelling equilibrium and quickly frozen below their freezing points using liquid nitrogen. Both samples were then transferred to a freeze-dryer until all water sublimed, and light-weight dry gels were obtained. Dry gels were stored in a vacuum oven at room temperature before SEM imaging.[94] Samples were fractured during the freeze-drying process so that the surface and interior structures of the gel could be studied. Samples were mounted onto a stud, fixed with double-sided carbon tape and sputter-coated with platinum for 240 s. The surface and interior morphology of the hydrogels were recorded by a field emission scanning electron microscope JEOL JSM-7500F.

## 5.3 Results

One of the main obstacles present in oral delivery is the harsh environment in the stomach. To overcome this difficulty, pH sensitive hydrogels were developed as drug delivery vehicles, which could protect the nanoparticles before they reach the targeted location. The enzyme dextranase produced by micro flora in the human colon can degrade the hydrogels through an endo-hydrolysis process, and then release the nanospheres.[41]

### 5.3.1 Swelling properties of dextran based pH sensitive hydrogels

The dextran derivative, Dex-MA (DS = 0.99) may be sensitive to oxygen after precipitation from isopropanol. So it was suggested to dry the precipitates under inert gas before they were transferred to the vacuum oven. Dex-GMA was obtained as white fluffy powder after the lyophilization. Both dextran derivatives were stored at -20 ºC for further use. The synthesized dextran derivatives were characterized by $^{1}$H-NMR with a factor determined to be 0.99 for Dex-MA, 6.2 for Dex-GMA. (Figure 21)

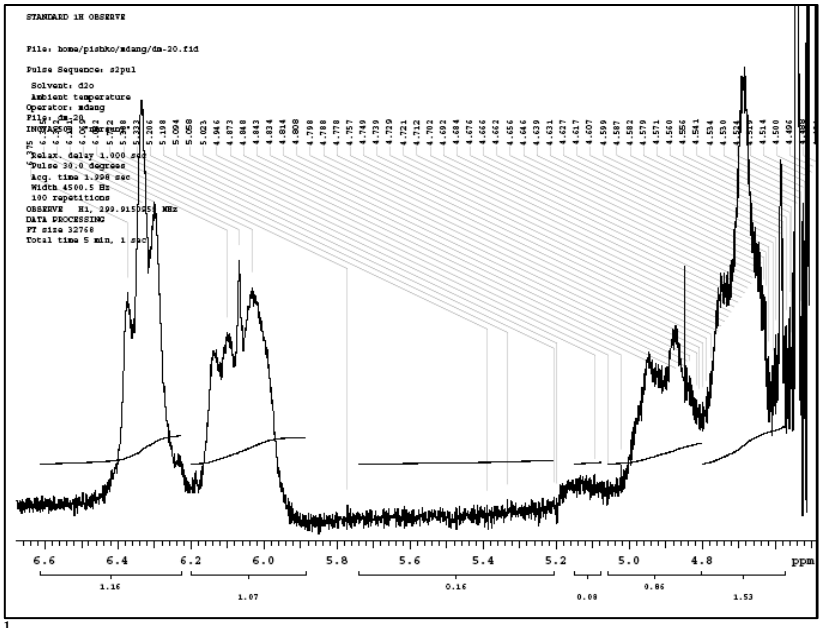


$^{1}$H-NMR spectra for precursor dextran-maleic acid

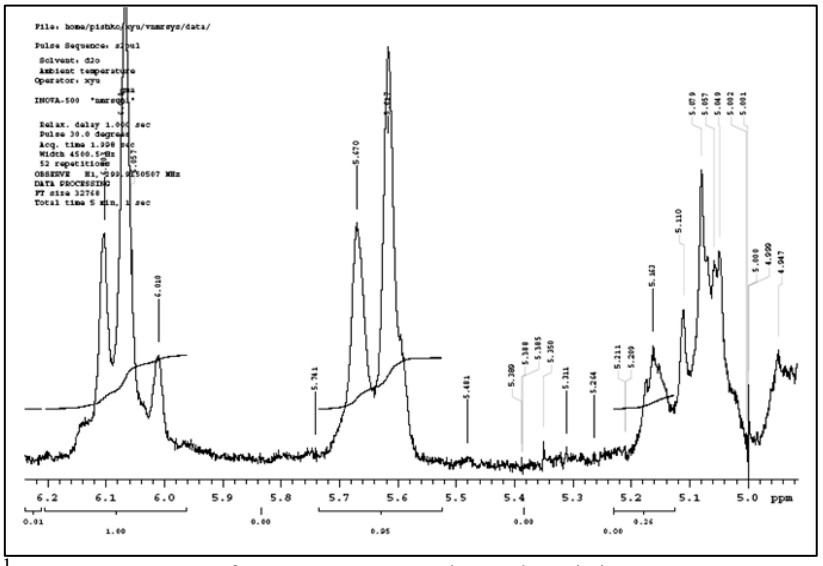


$^{1}$H-NMR spectra for precursor methacrylated dextran

**Figure 21.** $^{1}$H-NMR spectra of dextran based precursors for synthesis of pH sensitive hydrogels.

The Dex-MA based hydrogel was transparent with yellow color when newly formed by UV irradiation. The gelation time took 4 min under a long wave UV lamp, which was much faster than what was reported (40 min).[44] Prolonged UV irradiation of

the hydrogel was preferred to be at least 20 min. Further washing by deionized water was performed three times to clean the gel and removed any unreacted chemicals. The Dex-MA disk, cut at a dimension of Ø8×1.5 mm, shrunk immediately when being placed in SGF, while gradually swelled until equilibrium within 5-6 hr in SIF (Figure 22). Swelling ratio (SR) was calculated based on the initial weight of the disk. Hydrogels were also dried at ambient conditions until no weight changes were observed and then re-swelled till they reached equilibrium in SGF/SIF with the SR at 4.8 in SGF and 29.2 in SIF (based on dry-weight). The swelling ratio depended upon medium pH, degree of substitution and the crosslinking density of the Dex-MA hydrogel.

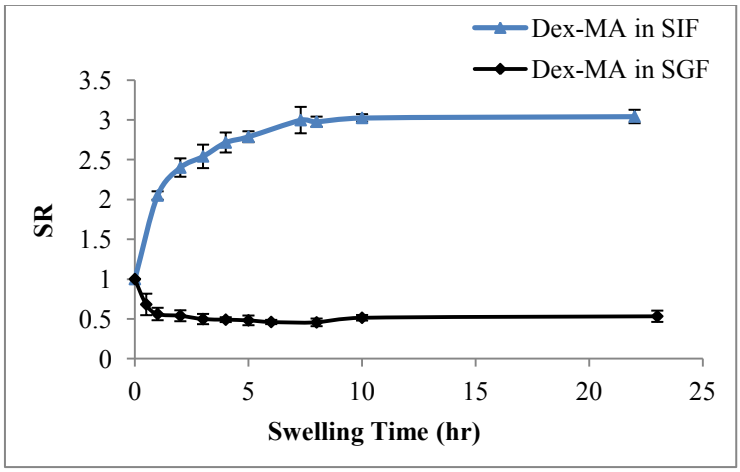


**Figure 22.** pH sensitive Swelling of Dex-MA hydrogel in SGF vs. SIF. (hydrogels were loaded with 300 µL of 1.6 mg/mL F-NPs; polymerization time 30 min; data obtained from triplicate of three independent experiments).

White fluffy powder of Dex-GMA was obtained by lyophilization, and the final product was stored at -20 ºC. With acrylic acid (AA) used as a modulator and copolymerized within the hydrogel, pH sensitive property was obtained. Different compositions between Dex-GMA and AA were tested to acquire hydrogels with desirable swelling and mechanical property. (The AA composition was varied from 28 % to 90 % in mass percentage, Table 8)

**Table 8. Different compositions of Dex-GMA based copolymers**

| | Dextran-GMA (mg) (characterization factor=6.2) | Acrylic acid (μl) | UV time (min) |
|---|---|---|---|
| 1 | 10 | 20 | 30 |
| 2 | 10 | 30 | 30 |
| 3 | 10 | 50 | 25 |
| 4 | 10 | 60 | 15 |
| 5 | 10 | 70 | 10 |
| 6 | 10 | 87 | 60 |
| 7 | 30 | 25 | 20 |
| 8 | 30 | 50 | 20 |
| 9 | 40 | 25 | 20 |
| **10** | **40** | **50** | **20** |
| 11 | 50 | 25 | 20 |
| 12 | 50 | 50 | 20 |
| 13 | 80 | 30 | 20 |

It is known that copolymerization of acrylic acid within the hydrogel was to promote its pH sensitivity for resisting the gastric fluid. However, too much of this small monomer may jeopardize the gel's mechanical property. With more acrylic acid copolymerized within the hydrogel network, it became highly water absorbent (SR could reach as high as 12.24, Figure 23), and ended in a fluid-like form, which may not be considered as a good delivery candidate. With more dextran derivative present in the hydrogel, the rigidness of the hydrogel increased, and the degradation behavior became more sensitive to the presence of enzyme dextranase. The final optimized composition of the Dex-GMA-co-AA hydrogel in the PAX NPs' release experiment was 40 mg/mL of Dex-GMA and 52.5 mg/mL of AA.

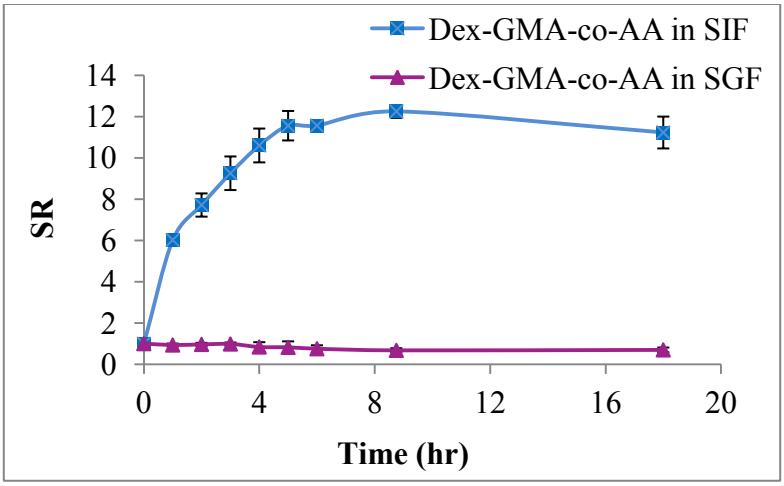


**Figure 23.** pH sensitive swelling of Dex-GMA-co-AA hydrogel in SGF vs. SIF. (Composition of Dex-GMA-co-AA hydrogel: Dex-GMA 10 mg/mL, AA 87 µL/mL, UV irradiation time 1 hr; 300 µL of 1.6 mg/mL F-NPs loaded within the hydrogels; data obtained from triplicate of three independent experiments).

To better simulate *in vivo* conditions, the swelling behavior of the hydrogels with pH gradient change from SGF (pH 1.2) to SIF (pH 6.8) was studied (Figure 24). At 0-2 hr in SGF, the Dex-MA gel shrank, became compact and resisted to acidic fluid due to the formation of hydrogen bonds. Water trapped within the network was expelled, so the SR decreased. At 2 hr, as the medium switched to SIF, both kinds of hydrogels started swelling and reached equilibrium until 5 hr. Dex-GMA-co-AA with the enzyme added in the medium showed obviously extended swelling equilibrium time till 10 hr and higher SRs. The explanation could be: enzyme dextranase needs time to diffuse in and degrade the hydrogel, so the time required to reach swelling equilibrium was prolonged; after the component Dex-GMA in the hydrogel Dex-GMA-co-AA was degraded, a relatively loose network was left, leading to absorption of more water and thus a higher SR. UV polymerization time did not affect SR much. The Dex-MA copolymerized with PEG also showed similar swelling behaviors to Dex-MA hydrogel.

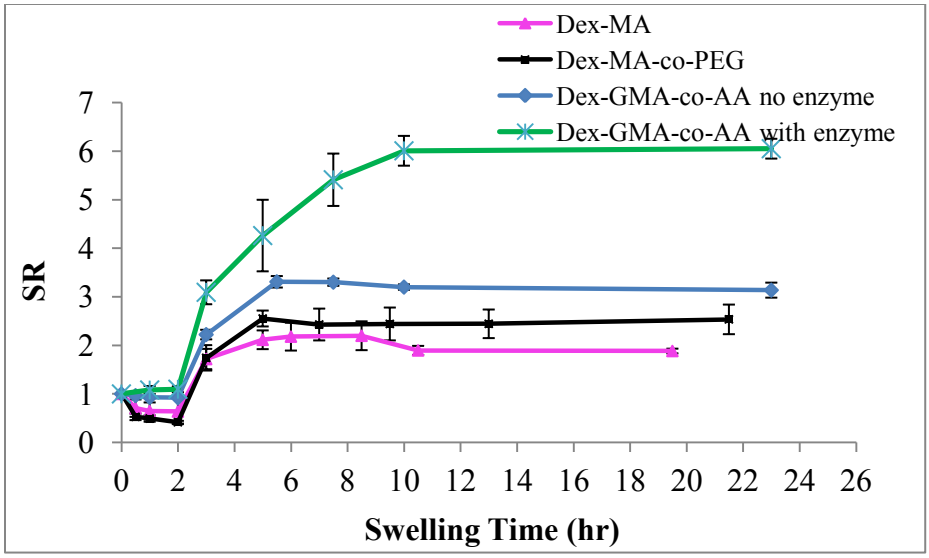


**Figure 24.** pH sensitive swelling of dextran based hydrogels with pH gradient change. (500 µL of 1 mg/mL well sonicated PAX NPs were loaded within the hydrogel networks; UV irradiation time was 20 min; Dex-GMA-co-AA composition at 40 mg/mL of Dex-GMA and 50 µL/mL of AA. Data was obtained from at least duplicate of two independent experiments).

### 5.3.2 *In vitro* release studies of fluorescent nanoparticles (F-NPs) from dextran based hydrogels

#### 5.3.2.1 Release studies of F-NPs from dextran based hydrogels in simulated gastric fluid vs. simulated intestinal fluid (SGF vs. SIF)

The release studies of F-NPs from different hydrogels were performed in SGF/SIF in the presence and absence of dextranase (1.0-2.5 units/mL) in a shaking water bath (50 rpm, 37 ºC). The release profiles were obtained by measuring the mass percentage of released F-NPs (*i.e.* Mt/M∞) at specific times.

From Figure 25, it is suggested that both dextran based hydrogels were stable in SGF with less than 10 % of F-NPs released within the first 24 hr; while, in SIF, both hydrogels were degraded totally within 8-10 hr and released all the fluorescent nanoparticles loaded.

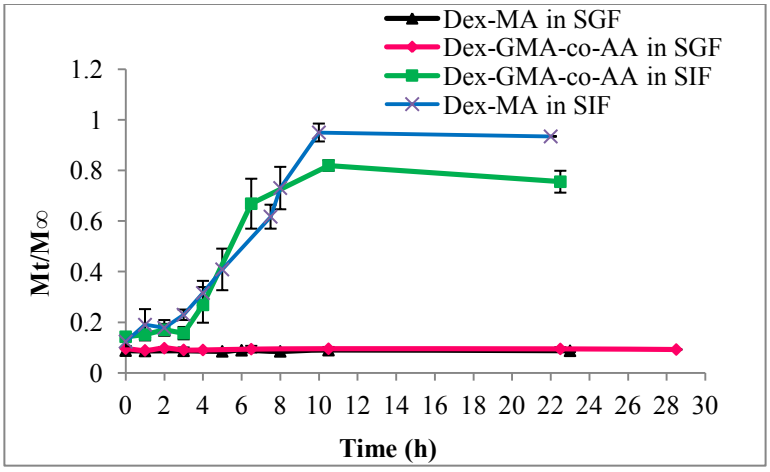


**Figure 25.** Different release profiles of F-NPs from dextran based hydrogels in SGF vs. SIF. (Dex-MA: 30 min UV irradiation, Dex-GMA-co-AA 1 hr UV; all hydrogels were loaded with well-sonicated 300 μL of 1.6 mg/mL F-NPs; data obtained from the triplicate of three independent experiments).

For the hydrophobic drugs' release from thin polymer films, a three – stage release model was proposed to describe the underlying release mechanisms and kinetics: burst release, relaxation induced release and diffusion release.[77] This model may also apply in our case with some modifications. In the beginning, the burst release of nanoparticles occurred with less than 15 % observed in SIF, probably caused by the F-NPs loosely staying on the hydrogel surfaces. As the SIF solution (with dextranase at 1.0-2.5 units/mL) diffused in the hydrogel, polymer chains were hydrated and the network expanded. This took about 2-3 hr; during this time, nanoparticles were still trapped. With sufficient swelling and enzyme induced degradation, the hydrogels broke down with nanoparticles leaking out of the gel, or the hydrogel pores reached a certain size at which the nanoparticles (size of the F-NPs: 200 nm or less) could diffuse out freely, and thus the release started. Due to the circuitous internal structure of the gels, nanoparticles diffused through paths of different hindrance. This would take as long as 10 hr for both kinds of dextran based pH sensitive hydrogels to totally release all the F-NPs. The final release reached over 80% of the initial amount of nanoparticles; the rest may have been lost during centrifugation or deviation when taking the sample. The

significant difference between nanoparticles' release profiles in different pH medium, *i.e.* SGF/SIF, suggested that these dextran based hydrogels could be regarded as promising vehicles for colon targeting delivery of nanoparticles through the oral route.

5.3.2.2 Release study of F-NPs in SIF in the absence of enzyme dextranase

The Dex-MA hydrogel was also used to study the release of F-NPs in the absence of the enzyme. (Figure 26) As a result, this dextran based hydrogel could be degraded through the polymer chain hydration, but it is suggested to be a very slow process as compared with enzyme induced degradation. In the first 6 days, only less than 10 % of F-NPs were released, possibly due to the burst effect. More F-NPs were gradually released from day 7 till day 12 with the gel totally broken and dissolved, and then all the particles were released after 12 days. Since the retention time for oral drug formulation in the gastrointestinal (GI) tract is known to be 14-16 hr, and it is desirable for the delivery vehicle to release all the PAX NPs within 20 hr.[87] The enzyme dextranase was added in the following release experiments.

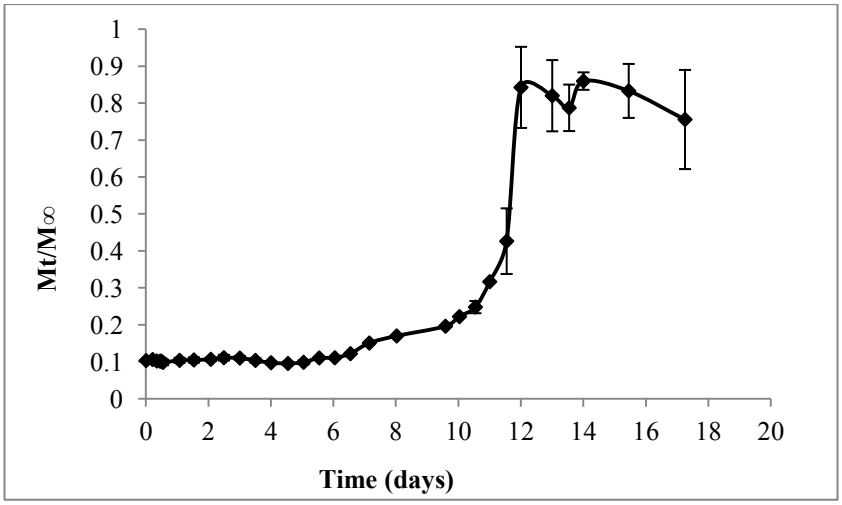


**Figure 26.** Release of F-NPs from Dex-MA hydrogel in SIF without dextranase. (Sodium azide added at a concentration of 0.025 % w/v, and results were based on 2 independent experimental data with three parallel samples in each experiment.)

5.3.2.3 Tunable release profiles of F-NPs from different dextran based hydrogels

To better simulate *in vivo* situation, the pH of the medium used to study the F-NPs' release from the hydrogels was changed gradually from SGF (pH 1.2), SGF/SIF (pH 4.5), to SIF (pH 6.8). Four different dextran based hydrogels were prepared under different UV irradiation times and varied compositions.

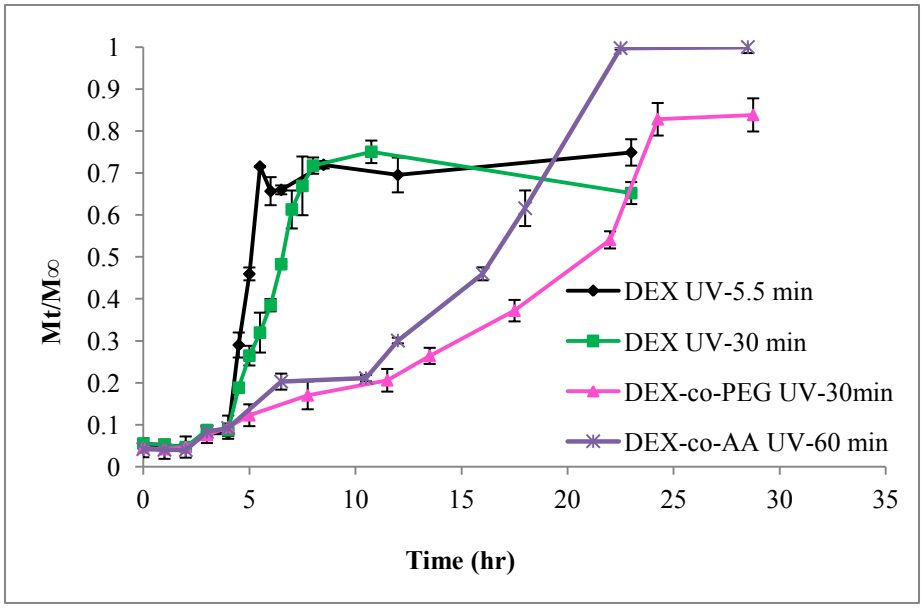


**Figure 27.** Tunable release profiles of F-NPs from dextran based hydrogels under different conditions. (Results were triplicated with three parallel samples each time; 0.025 % w/v of sodium azide was added in the solution when necessary).

Gelation time for the Dex-MA hydrogel was 4-5 min, which was shorter than that reported.[44, 47] The Dex-MA hydrogel prepared by 5.5 min UV irradiation was not as strong as gels prepared by the longer UV time, e.g. 20-30 min. After switching from SGF to SIF, the hydrogel edge became blurred, and an immediate release of F-NPs was observed with a total release at 6 hr (Figure 27). A longer UV irradiation time was desirable for this Dex-MA based hydrogel, because the double bonds, which participated in the crosslinking reaction, were present in the middle of the MA segment in Dex-MA, and polymerization might be hindered by the adjacent carboxylic acid and dextran

macromolecules.[44] Non-uniform and less cross-linked hydrogel networks may be formed by insufficient UV irradiation. When the polymerization time was extended to 30 min, all active double bonds were expected to be consumed, and a better cross-linked hydrogel was obtained. A steadily increased release of nanoparticles from the Dex-MA hydrogel was observed from 4 hr to 11 hr (Figure 27). Tunable release profiles could be obtained by copolymerizing Dex-MA with enzyme non-degradable component PEG-DA. In our case, as 5 μL/mL of PEG-DA was added in the Dex-MA precursor solution to form the gel, a slower release profile of F-NPs was obtained with the complete release extended up to 24 hr. PEG was not degraded by dextranase, so it was left as white precipitates in the end. Another kind of dextran based hydrogel was copolymer Dex-GMA-co-AA. Methacrylated dextran has been widely used as a vehicle for delivering small drug molecules.[11, 93, 95] For oral delivery of nanoparticles, copolymerization with AA could help the gel to resist gastric fluid. The AA composition was examined in a range from 28 % to 90 % (mass percentage), and the hydrogel Dex-GMA-co-AA formed with a higher amount of AA was soft, super water absorbent, and released all the F-NPs within 23 hr. Considering that the mechanical property may not be suitable as a delivery vehicle, the composition was optimized to 40 mg/mL of Dex-GMA and 50 μL/mL of AA for further experiments.

### 5.3.3 Release of PAX NPs from Dextran Based Hydrogels

PAX NPs (PAX NPs) were prepared by a modified solvent emulsification evaporation method with the size at 110 ± 10 nm and zeta potential at -42 ± 2.6 mV. PAX NPs were loaded within three different dextran based hydrogels, and the release behaviors of these particles were studied with the hydrogel property adjusted and the buffer pH changed from SGF (pH 1.2) to SIF (pH 6.8 with dextranase 1.0-2.5 units/mL).

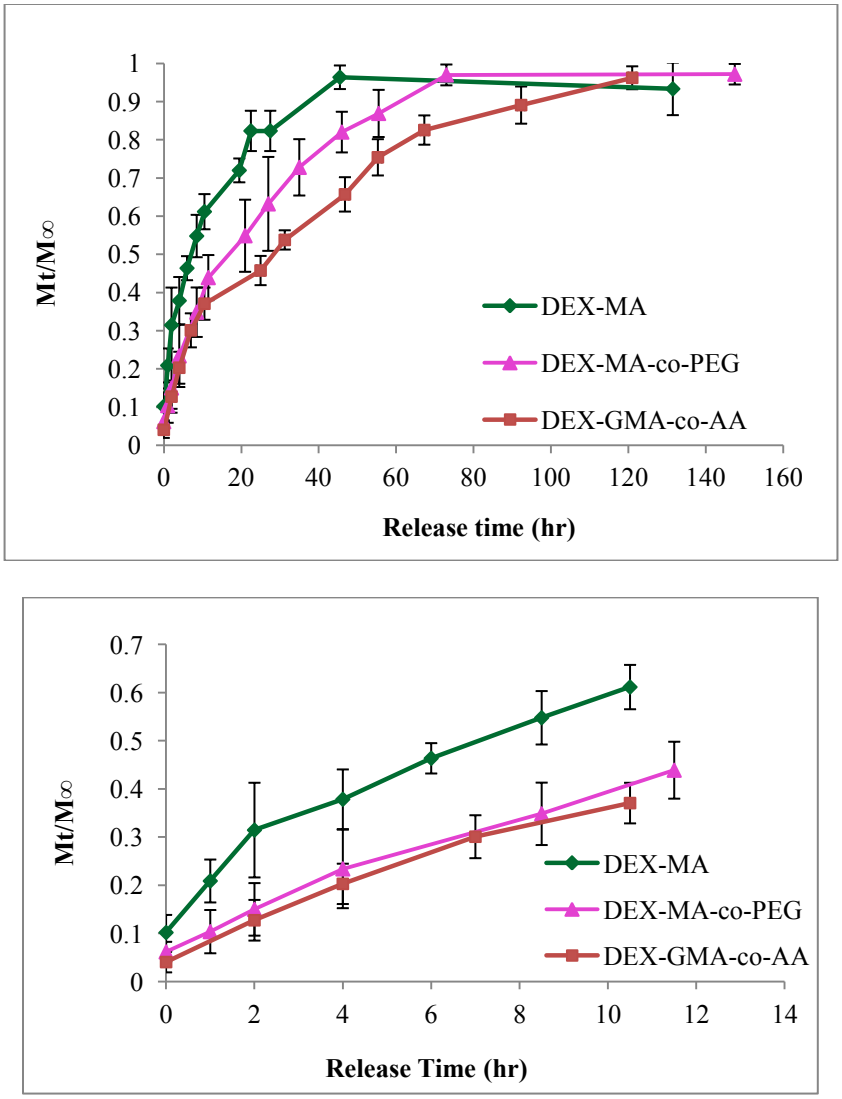


**Figure 28.** Tunable release of PAX NPs from dextran based pH sensitive hydrogels with adjusted properties (top); first 12 hrs of PAX NPs' release from different dextran based hydrogels (bottom). (Dex-GMA-co-AA composition at 40 mg/mL of Dex-GMA and 50 μL/mL of AA) (Results were at least duplicated with three parallel samples each time, 0.025 % w/v of sodium azide added in the solution.)

Figure 28 showed the release profiles of PAX NPs from different dextran based hydrogels and the detailed information in the first 12 hr. For the hydrogel Dex-MA, it first shrank in SGF with a burst release of PAX NPs up to 30 % observed. Particles

loosely adhered onto the hydrogels were possibly released at this time. The releases of PAX NPs from the Dex-MA hydrogels took a much longer time than those of the F-NPs did. This may be due to the different conditions between F-NPs (300 μL of 1.6 mg/mL solid spheres) and PAX NPs (500 μL of 1.0 mg/mL, paclitaxel loaded in the particles with E.E. at (31 ± 0.08) %). The Dex-MA hydrogel could be totally hydrolyzed by the enzyme dextranase with no residues left in the end. For the Dex-MA-co-PEG hydrogel, at the same concentration of Dex-MA, PEG was copolymerized within the network, and a denser hydrogel was formed with a slower release profile obtained. For both Dex-MA-co-PEG and Dex-GMA-co-AA hydrogels, only 12 % of PAX NPs was released in SGF during the first 2 hr, less than that from the hydrogel Dex-MA itself. In the next 8 hr, only 37 % of PAX NPs was released from both copolymers, as compared to over 60 % of PAX NPs released from the Dex-MA. Total release of PAX NPs was 72 hr from the hydrogel Dex-MA-co-PEG with non-degradable white precipitates observed in the end. For the Dex-GMA-co-AA hydrogels, sustained release profiles of PAX NPs were also obtained with the total release time of PAX NPs extended over 100 hr. The composition between Dex-GMA and AA could be adjusted to achieve desired release profiles of PAX NPs.

The release of nanoparticles from the Dex-MA based hydrogels was proposed as a degradation-controlled process. The release mechanism of PAX NPs could be described: in SGF, the gel could trap most drug nanoparticles within the first two hours. As the medium switched to SIF (pH 6.8), carboxylic acid group in the MA section was ionized and the hydrogel started swelling and degrading, resulted in gradual breakdown of the networks and PAX NPs' release. While, for the Dex-GMA-co-AA based copolymer, in the presence of enzyme dextranase in SIF, a higher SR was observed and the diffusion-controlled drug release would be dominant. Since only the dextran based component could be degraded, a soft and loosely cross-linked hydrogel was formed after 3-4 hr incubation in SIF. This degradation induced higher swelling created pores large enough for drug particles to diffuse out. A higher AA composition was used for the F-

NPs' release experiment, and no gel was left after the dextran degradation since the AA based hydrogel was totally dissolved.

### 5.3.4 SEM images of dextran based hydrogels

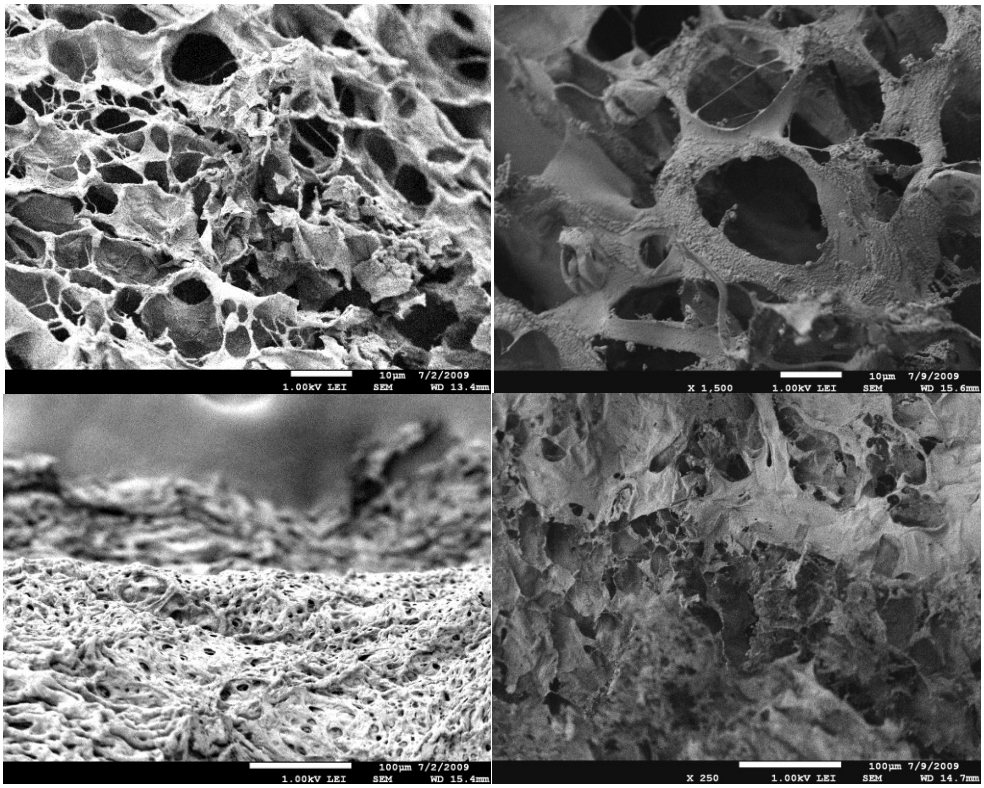


**Figure 29.** SEM images of cryo-fixed hydrogels Dex-GMA-co-AA (10 mg/mL of Dex-GMA and 85 µL of AA) in PBS 1.4 (left) vs. PBS 7.4 (right). Top images showed characteristic internal pore structures; bottom images showed surface structures of the gels. Samples were prepared by swelling the gel until equilibrium and quickly transferred into a chamber filled with liquid nitrogen; a three-day freeze-drying process was followed, and then stored in a vacuum oven at room temperature before SEM imaging.

Figure 29 showed the SEM observation of internal and surface morphology of the dextran based hydrogels after they reached swelling equilibrium in PBS at different pH values (7.4 vs. 1.4). This could be considered as a reference to understand the

particles' diffusion-controlled release from the Dex-GMA-co-AA hydrogel. Highly swollen hydrogels in PBS pH 7.4 exhibited pores large enough for particles to diffuse, while the hydrogels in pH 1.4 shrunk with a tightly packed network and more tortuous interior structures formed, trapping the nanoparticles within the hydrogels.

## 5.4 Conclusions

Two polysaccharide dextran based pH sensitive hydrogels Dex-MA and Dex-GMA-co-AA have been produced by the photocrosslinking reaction with both fluorescent NPs (F-NPs) and hydrophobic drug PAX NPs loaded within the networks. Adjustable release profiles of both F-NPs and PAX NPs were obtained by copolymerizing with PEG-DA (575) or optimizing the composition ratio between Dex-GMA and AA. The resulted two hydrogels showed good pH responsive swelling property. A higher SR was observed for Dex-GMA-co-AA hydrogel at a composition of 40 mg/mL of Dex-GMA and 50 μL/mL of AA in the presence of the enzyme dextranase. A fragile Dex-MA hydrogel was synthesized with a faster release of the F-NPs observed under a shorter UV photocrosslinking time. The sustained release profiles of F-NPs were obtained for both Dex-MA-co-PEG and Dex-GMA-co-AA hydrogels. Two release mechanisms were proposed: degradation controlled and diffusion controlled. Considering the more complicated environment *in vivo*, stronger hydrogels with extended release profiles would be desirable. The two Dex-MA-co-PEG and Dex-GMA-co-AA hydrogels developed here, could release PAX NPs up to 5 days with 40 % of the PAX NPs released during the first 12 hr. Based on these results, it is suggested that both the Dex-MA and Dex-GMA-co-AA hydrogels could be considered as potential colon targeting vehicles for delivering nanoparticles orally.

# 6. *IN VITRO* EVALUATION OF MODIFIED NANOPARICLES

In this study, polystyrene nanoparticles were first modified by both synthetic polymers and biomacromolecule chitosan and dextran. The anticancer drug paclitaxel core was replaced temporarily so as to characterize the surface morphology nanoparticles encapsulated by different types of polyelectrolytes, optimize conjugation conditions for the surface functional groups, and evaluate *in vitro* material biocompatibility and targeting group functionality with cells. A preliminary study on the stability of the nanoparticles in simulated intestinal fluid (SIF) was also investigated in this section.

## 6.1 Introduction

Tumor cells are abnormal cells that grow uncontrollably, and tumor blood vessels possess a number of different properties from those in normal tissue.[96] Especially in the rapidly growing and large solid tumors, new blood vessels are often deficient in interrupted or absent membranes, leading to unstable blood flow.[97] This phenomenon together with a poorly developed lymphatic network results in an effect called "passive targeting".[98] Sufficient concentration, traversing through the tumor microcirculation, diffusing into the interstitium, and remaining at the site for the duration to induce a therapeutic effect are requirements for an antitumor drug therapy to be effective.[99] A solid hydrophobic anti-cancer drug core, coated with different hydrophilic polymer thin films, and modified by a biocompatible group and a cell targeting group, therefore may offer a promising solution to meet all the requirements. Of these characteristics, the efficient binding and uptake capability with specific tumor cells is the key.

Transformed or cancerous cells often express different amount of glycans compared with their normal counterparts. Lectin is a protein that can recognize and bind to sugar complexes due to its high specificity for the chemical structure of the glycans. It has been suggested that the lectin wheat germ agglutinin (WGA) conjugated

nanoparticles will allow efficiently targeting to cancer cells.[28] Recently it has also been demonstrated *in vitro* that it may be possible to exploit the increased WGA binding capacity exhibited by Caco-2 cells compared to that of non-cancerous human colonocytes to build a more efficient tumor-specific drug delivery system for colon cancer chemotherapy.[29]

For the nanoparticle based cancer chemotherapy, there are two aspects that have attracted our close attention: the size and the surface modification of the drug loaded nanoparticles. It has been found that the size of the particles plays a key role in their adhesion to and interaction with the biological cells.[100] The possible mechanisms for the particles to pass through the gastrointestinal and other barriers could be: paracellular passage – particles "kneading" between intestinal epithelial cells due to their extremely small size (<50 nm); endocytotic uptake – particles adsorbed by intestinal enterocytes through endocytosis (particles size < 500 nm); lymphatic uptake – particles adsorbed by M cells of the Peyer's patches (particle size < 5 microns).[6] Lectin mediated cell binding and uptake of the nanoparticles with the size below 500 nm combines the passive accumulation with active targeting, which belongs to the second mechanism as described above.

The monolayer of Caco-2 cells, which are derived from human colorectal adenocarcinoma, has been widely used as an *in vitro* model of the gastrointestinal epithelium for a number of years.[101] It is considered as a valuable source for investigating the interaction between active compounds and the lining of the small intestine before initiating animal studies.[102] In this research, it will be used as the tumor cell model to investigate the material compatibility and cell uptake efficacy of the lectin mediated nanoparticles.

## 6.2 Material and Methods

Poly (allylamine) hydrochloride (PAH, Mw~70 000 g/mol), Poly(4-styrenesulfonic acid-co-maleic acid) sodium salt (PSSCMA, Mw~20,000 g/mol), chitosan (low molecular weight), carboxyl methyl dextran (average Mw > 500,000),

poly (vinyl alcohol) (PVA, Mw 9000-12,000 g/mol and Mw 22,000 g/mol), sodium alginate (from brown algae, low viscosity) were purchased from Sigma-Aldrich, USA. Semisynthetic paclitaxel (from Taxus sp.), ≥ 97% was purchased from Sigma. Poly (ethylene glycol) ($NH_2$-PEG-CM, Mw ~ 3400) was purchased from Laysan Bio, Inc. USA. FITC labeled wheat germ agglutinin (F-WGA) was purchased from Sigma, USA. Caco-2 cells and EMEM (Eagle's minimum essential medium) were purchased American type culture collection (ATCC, USA). Fetal bovine serum (FBS) was purchased from Fisher scientific, USA. Live/dead® cell viability assay, Alexa Fluor® 647 hydrazide, polystyrene latex (PS NPs, 0.2 μm), and FluoSpheres® sulfate-modified microspheres (F-NPs, 0.2 μm) were purchased from Invitrogen (Oregon, USA). Ultrapure water used for all experiments and cleaning steps was obtained from a Millipore system with a specific resistance 18 MΩ/cm. Polyelectrolyte solutions were prepared in 0.15 M NaCl. Phosphate-buffered saline solution (PBS, pH 7.4) consisted of 1.1 mM potassium phosphate monobasic, 3 mM sodium phosphate dibasic heptahydrate, and 0.15 M NaCl.

**Preparation of PS LbL self-assembled nanoparticles.** Core-shell structured nanoparticles were built by a well-established method named LbL self-assembly (section 2). Polystyrene nanoparticles were used first to test the feasibility of building a core-shell system and conjugating with functional groups PEG and F-WGA. Fluorescent nanoparticles were used to study the stability of LbL assembly on spheres.

**Characterization of self-assembled nanoparticles.** Particles before and after the LbL assembly and modifications were characterized by transmission electron microscopy (TEM) and scanning electron microscopy (SEM).

**Caco-2 cell cultivation.** Caco-2 cells were routinely cultured in EMEM, supplemented with 20% (v/v) of fetal bovine serum (FBS) and 1% (v/v) of streptomycin-penicillin solution, at 37 ºC in a 5% CO2 incubator. For the F-WGA binding and uptake experiment, cells were trypsinized and washed by PBS before use.

***In vitro* Caco-2 biocompatibility studies.** Cell compatibility of CS/DEX and PEG encapsulated nanoparticles was evaluated *in vitro* using Caco-2 cells. Viability of

cells were studied by fluorescence microscopy using a standard protocol of live/dead® cell viability assay. Percentage ratio between viable cells and total cell number was calculated using a cell counter for all parallel samples (n = 4).

**Confocal laser scanning microscopy.** This microscope utilizes an inverted DMI 6000 microscope which is equipped with three excitation laser lines 488, 543 and 633 nm and 10x, 40x, 63x objectives. The particles prepared by the self-assembly method at different F-WGA concentrations interacted with Caco-2 cells for 20 h at 4 ºC and suspended in the sterile PBS for confocal microscope imaging. Both bright field and fluorescent images were recorded by the 63x objective.

**Fluorescence microscopy.** LIVE/DEAD® viability/cytotoxicity assay kit is a two-color fluorescence cell viability assay that can determine live and dead cells by recognizing the intracellular esterase activity and plasma membrane integrity. Concentrations of the two dyes were optimized first to reduce the interference. Fluorescence microscopy with green and red excitation laser lines was used to study the live/dead states of cells. Polystyrene nanoparticles (PS NPs) were used as the blank control, and self-assembled PS NPs (3 bilayers of CS/DEX, CS/DEX: 1 bilayer of particles' encapsulation with chitosan and carboxyl methyl dextran/dextran-sulfate) with and without PEG modification were tested.

**Fluorescence activated cell sorting (FACS).** A number of fluorescent labeled cells was analyzed by FACS. Caco-2 cells were cultivated at a density of $4 \times 10^5$ cells/mL. Three different kinds of particles (fluorescent nanoparticles, fluorescent particles encapsulated with CS/DEX-PEG, particles encapsulated with CS/DEX-PEG in conjugation with F-WGA) were prepared and then contacted directly with suspended cells for 20 h at 4 ºC. A low temperature was used to facilitate surface binding of nanoparticles and the analysis by FACS. Caco-2 cells were used as the reference before analyzing all samples. 20,000 – 40,000 cells were counted for each sample (n = 3) and the experiments were triplicated.

## 6.3 Results

### 6.3.1 TEM and SEM images of chitosan/dextran encapsulated PS NPs

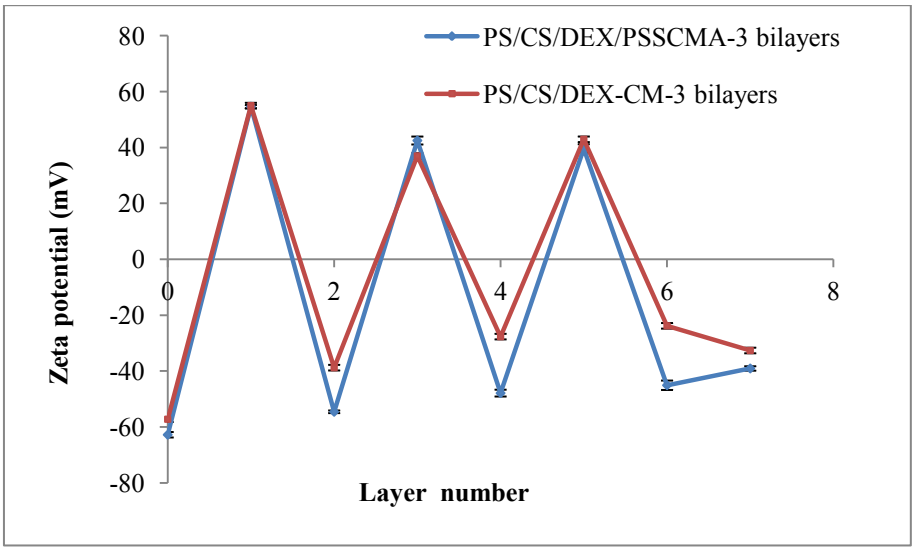


**Figure 30.** Zeta potential of chitosan/dextran encapsulated PS NPs (3 bilayers).

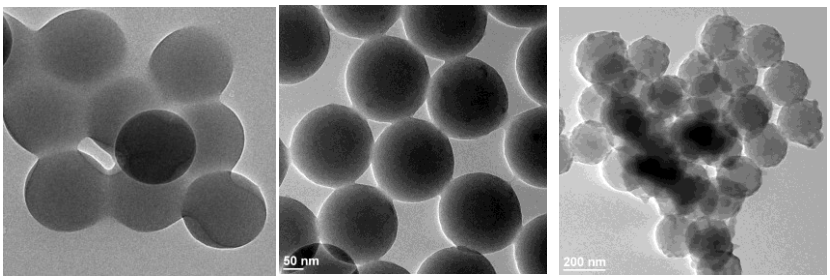


**Figure 31.** TEM images of CS/DEX LbL assembled PS NPs. (3 bilayers). From left to right: 1) PS NPs; 2) 5 bilayers of PAH/PSSCMA encapsulated PS NPs (each layer 2nm); 3, 4) 3 bilayers of CS/DEX encapsulated PS NPs (each layer 5nm). Fresh prepared samples were well sonicated to break down possible aggregates. 10 µL of the suspended nanoparticles were dropped onto a TEM grid and dried at ambient conditions. All samples were stored in the vacuum oven one day before imaging (room temperature).

Two different kinds of dextran polyelectrolytes were used in this experiment: dextran-sulfate and carboxymethyl dextran (Dex-CM). Dextran-sulfate is a strong anion, and usually easily adsorbed onto the cationic surfaces. But for further modification with

PEG ($H_2N$-PEG-COOH) using the carbodiimide chemistry, a polyelectrolyte with carboxyl group is adsorbed onto the outermost layer of the nanoparticles. Dex-CM is a weak anion with a carboxyl group modified on the dextran branches. It was used here to replace the dextran-sulfate. For weak ions, the pH was adjusted to be 6.5 for Dex-CM and 4.0 for chitosan, and they were both encapsulated onto PS NPs (3 bilayers). (Figure 30)

TEM images showed the size and morphology of LbL assembled PS NPs (Figure 31). 3 bilayers of biomacromolecules chitosan and dextran were encapsulated onto PS NPs (two images on the right), showing a rougher surface as compared with those of bare PS NPs (left) and PS NPs encapsulated with 5 bilayers of synthetic polymers ($2^{nd}$ from the left). This may be due to the glucose ring that exists in the structure of these polysaccharides. Smooth surfaces with fine textures were observed after adsorbing synthetic polyelectrolytes onto the particles. These results were consistent with the literature, which used biomacromolecules chitosan and heparin as the polyelectrolytes.[13] The pH and ionic strength/salt concentration are two factors that affect the charge state and conformation of the polyelectrolyte chains, which further influence the layer thickness of the polyelectrolyte.[13] Chitosan layer with lower molecular weight was able to grow faster, and the pH of the medium affected the charge state of chitosan (pKa of chitosan is 6.5-7.3).[64] Different ionic strengths of the incubating medium were used for synthetic and bio-polyelectrolytes, and the obtained nanofilms were different in thickness. Biomacromolecules chitosan and hyaluronan were observed to form a uniform film after only a few depositions at a high salt concentration (*e.g.* 0.15 M), while it is very difficult to buildup the film at a low salt concentration, *e.g.* $10^{-4}$ M NaCl.[64] The thickness of one polyelectrolyte layer was around 5 nm for each bio-macromolecule CS/DEX layer, and 2 nm for the synthetic polymer PAH/PSSCMA layer under the experimental ionic strength and the pH of the buffers. (i.e. concentration: 20 mg/mL for PAH/PSSCMA in 30 mM KCl; 2 mg/mL for CS/DEX in 0.15 M NaCl; Data were obtained from analysis of the SEM/TEM images.)

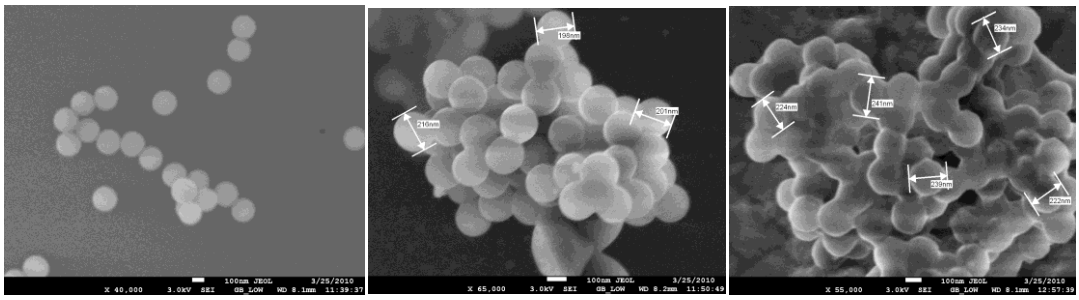

**Figure 32.** SEM images of PS NPs (left), CS/DEX layer-by-layer assembled PS NPs (middle image, 3 bilayers) and self-assembled PS NPs conjugated with PEG and F-WGA (right image, 3 bilayers of CS/DEX). Fresh prepared samples were well sonicated to break down possible aggregates. 10 μL of the suspended nanoparticles were dropped onto a TEM grid and dried at ambient conditions. All samples were stored in vacuum oven one day before imaging (room temperature).

SEM images may provide more information about the surface morphology of the nanoparticles. Figure 32 showed the images of PS NPs, CS/DEX self-assembled nanoparticles and their further modification with PEG and WGA. The original PS NPs were white spheres, and after being coated with CS/DEX layers, the color turned darker, possibly due to the presence of high atomic number element S in the DEX layer. Surface scanning of the particles with CS/DEX layers (middle image) showed sticky surfaces as compared with the original polystyrene particles (left image). Further covalently binding with PEG ($NH_2$-PEG-CM, Mw~ 3400), particles tended to stabilize themselves in suspension and could be easily re-dispersed, possibly under the repulsion effect among the flexible PEG chains (carboxymethyl group present in the PEG). The particles were further conjugated with F-WGA; it was shown that they became agglomerated and sonication could help to reduce the particles' aggregation at this time.

### 6.3.2 Stability of LbL assembled nanoparticles

Methods to study the stability of polyelectrolyte assembled nanospheres were still under development, and it is difficult to find a proper way to quantify the disruption of layered structure and disassembly of the shell. However, measurements of the

particles' zeta potential could provide one possible way for studying the stability of particles in suspension.

In this section, chitosan/dextran polyelectrolyte layer was encapsulated onto fluorescent nanoparticles (F-NPs). Zeta potential was monitored after incubating the LbL assembled nanoparticles in SIF for certain times, and fluorescence intensity before and after polyelectrolytes' adsorption onto the particles was also measured.

6.3.2.1 Measurement of zeta potential

Figure 33 showed the zeta potential of different modified PS nanoparticles incubated in SIF. The PS nanoparticles as a control showed a zeta potential at -35 mV. The particles with DEX-CM as the outmost layer (1 bilayer) were not as stable as particles with PEG surface modification, based on the relatively smaller zeta potential (absolute value) of PS-1bilayer (PS-1bi) without PEG. It seemed that the 1 bilayer assembled particles could maintain the same surface charge within 22 h in SIF at 37 ºC. During the first 2 h, the particles with PEG conjugation still showed zeta potential below -25 mV, and the standard errors were small, suggesting they were still stable in the suspension. The particles encapsulated with 5 bilayers of P.E. were easily disturbed by the SIF, even after conjugating the surface with PEG. T test was performed to study the statistical significance of the above data. (Table 9, tails=2, type=2)

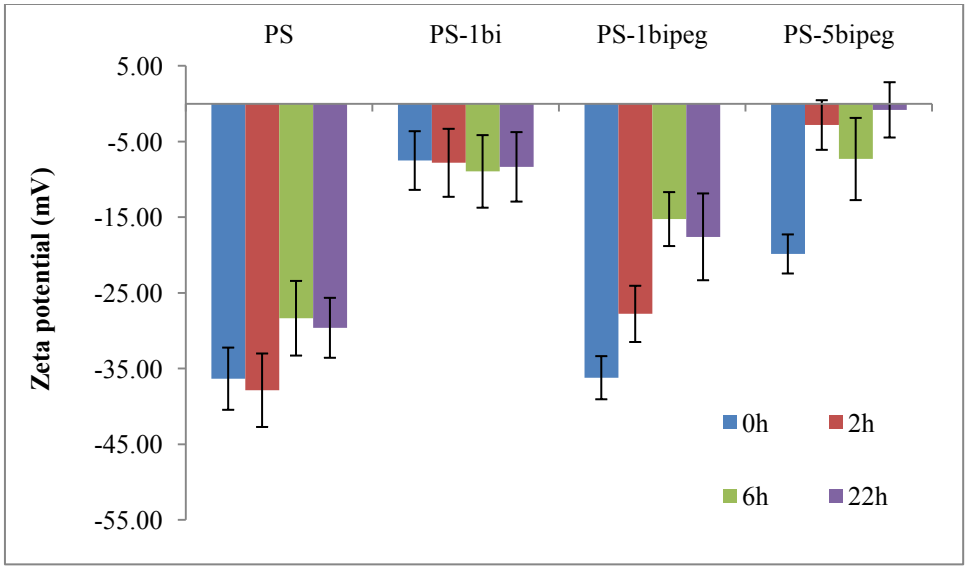


**Figure 33.** Zeta potential of particles with different CS/DEX layer numbers incubated in SIF. PS: polystyrene nanoparticles as a control; PS–1bi: particles with 1 bilayer of CS/DEX; PS-1bipeg: 1 bilayer of CS/DEX encapsulated particles in conjugation with PEG; PS-5bipeg: 5 bilayers of CS/DEX built onto particles modified with PEG. All measurements of zeta potential were done 3 times for each of the three parallel samples. Independent experiments were at least duplicated.

**Table 9. p values from t-test of the zeta potential data under different conditions**

| p value | 0-2h | 0-6h | 0h-22h | Difference |
|---|---|---|---|---|
| PS vs. PS-1bi | 6.97E-04 | 9.40E-04 | 4.70E-05 | Significant |
| PS vs. PS-1BIPEG | **3.55E-01** | **3.14E-01** | **1.52E-01** | Not significant |
| PS vs. PS-5BIPEG | **9.48E-02** | **1.48E-02** | 2.05E-03 | Depends |

6.3.2.2 Measurement of fluorescence intensity

At time t = 0 h (Figure 34), the fluorescence intensity of particles with CS/DEX or CS/DEX-PEG layers were reduced to less than 40% of the original intensity of bare F-PS nanoparticles. The fluorescence intensity of particles with 5 bilayers of the polyelectrolyte layers and PEG modification was decreased to 16.6 %. This is due to the coverage of the polyelectrolyte layers on the particles' surfaces that masked the

fluorescence. (There may also be some particles lost during the washing and centrifugation steps during the LbL procedure).

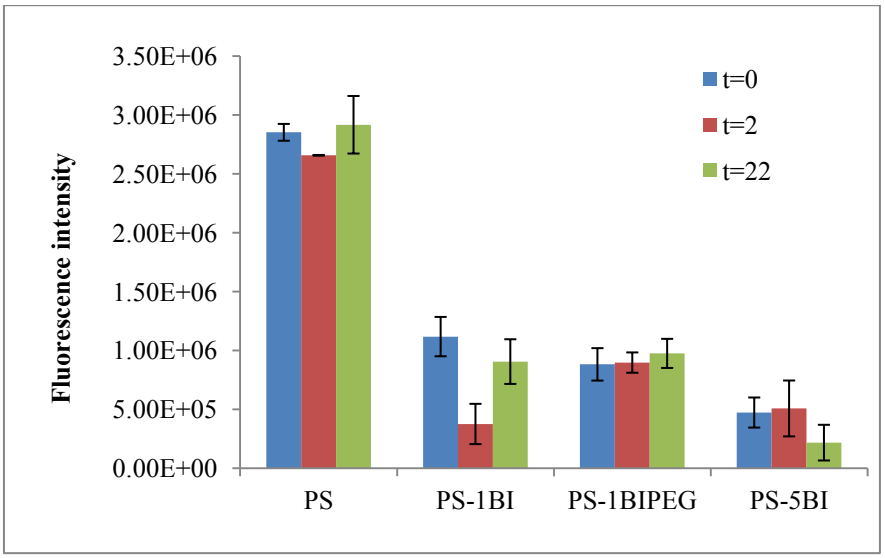


**Figure 34.** Fluorescence intensity of particles with different polyelectrolyte layers incubated in SIF under different time intervals. (PS at concentration 1.6 mg/mL).

After incubating the particles in SIF under different conditions for some time, the fluorescence intensity of particles with 1 bilayer coating and PEG surface modification were maintained over time; while, without the PEG conjugation, particles may have a disrupted structure, and fluctuated fluorescence intensity over time. Particles with higher polyelectrolyte layer number may be more easily interrupted on their surfaces.

From Figure 34, 1 bilayer CS/DEX encapsulated nanoparticles conjugated with PEG was also observed showing similar fluorescence intensity as compared with the nanoparticles without PEG modification. This may be attributed to the fact that PEG layer was not covering onto the particles' surfaces, but extended as flexible chains into the solution.(Samples were nanoparticles in suspension)

### 6.3.3 F-WGA conjugation onto nanoparticles

WGA can selectively bind to N-acetyl glucosamine and N-acetylneuraminic acid residues. Nonspecific adhesion during the carbodiimide chemical reaction was studied first at different polyelectrolyte layer numbers and types.

#### 6.3.3.1 Nonspecific adhesion – polyelectrolyte layer number

Nonspecific adhesion is usually caused by undesired reactions. Alexa Fluor® 647 hydrazide was used first to test the feasibility of conjugating F-WGA onto layer-by-layer self-assembled nanoparticles and study the effect of different assembled layer numbers on nonspecific adhesion. This fluorescence reagent has an active amine group, so it can react with the carboxylic acid group through the carbodiimide reaction. EDAC (1-ethyl-3-(3-(dimethylamino) propyl) carbodiimide) was used as the carbodiimide to promote the formation of the amide bond. S-NHS (N-hydroxysulfo succinimide) was added to form a more stable intermediate product. The nonspecific adhesion study of Alexa Fluor® 647 on the nanoparticles was performed by mixing both the dye and particles without adding carbodiimide and s-NHS.

Figure 35 shows that, as the layer number increased, the fluorescence intensity of Alexa Fluor® 647 conjugated nanoparticles decreased. The reason might be: the higher coverage of particles with more polyelectrolyte layers, the less frequently nonspecific adhesion of Alexa Fluor® 647 occurred.

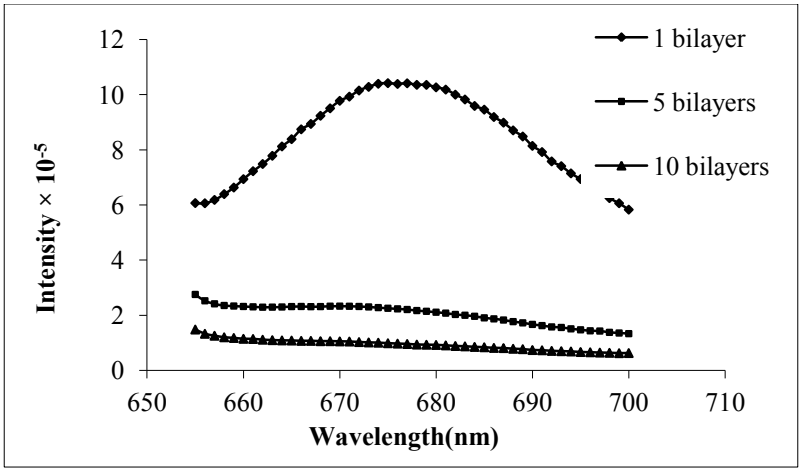


**Figure 35.** Effect of different layer number assembled PS NPs on non-specific adhesion of Alexa Fluor® 647 hydrazide (polyelectrolyte layer PAH/PSSCMA).

6.3.3.2 Nonspecific adhesion – polyelectrolyte type

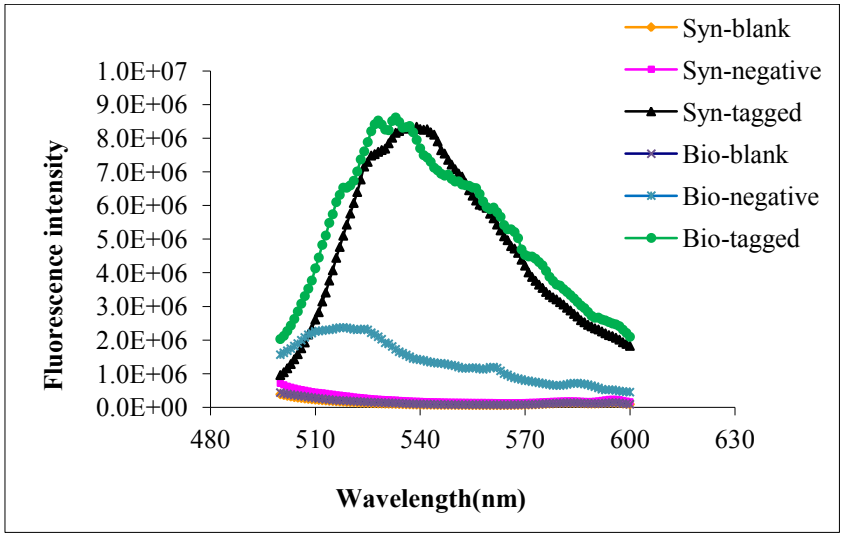


**Figure 36.** Effect of the polyelectrolyte type (bio vs. synthetic) on nonspecific adhesion of F-WGA conjugated onto LbL assembled nanoparticles. Blank – layer-by-layer treated polystyrene nanoparticles (LbL PS NPs); Negative – nonspecific adhesion of F-WGA on LbL treated PS NPs; Tagged – LbL treated PS NPs reacted with F-WGA in the presence of EDC and s-NHS; Syn-synthetic polyelectrolytes.

Here fluorescence labeled WGA was used as a targeting moiety to Caco-2 cells. Both synthetic PAH/PSSCMA and bio-polyelectrolytes CS/DEX were encapsulated onto the particles with PEG modification, and WGA were then conjugated to the outmost layer.

From Figure 36, the highest fluorescence intensity was observed when conjugating the LbL assembled particles with F-WGA in the presence of EDC/s-NHS, as compared with blank and negative controls. This is due to the successful formation of the covalent amide bonds between F-WGA and the particles' outmost layer. Nonspecific adhesion of bio-polyelectrolyte CS/DEX was higher than that of synthetic polyelectrolyte PAH/PSSCMA. (PEG was conjugated to all the particles' surfaces after LbL self-assembly) In solution, wheat germ agglutinin exists as a heterodimer with a molecular weight of approximately 38,000 Daltons and is normally cationic under physiological conditions. This may cause higher affinity of the F-WGA to biomacromolecule CS/DEX than that of synthetic PAH/PSSCMA.

The wavelength corresponding to the maximum fluorescence intensity shifted after conjugating F-WGA onto the particles' surfaces, 528 nm and 535 nm for biomacromolecules and synthetic polymers respectively. (For F-WGA itself, the maximum fluorescence is at 519 nm wavelength.) Conjugation efficiency was calculated according to the F-WGA concentration at the maximum fluorescence intensity over the initial amount of F-WGA added in the reaction, which was 36.7% (after 3 bilayers of CS/DEX encapsulated PS NPs and PEG conjugated). The average F-WGA concentration (at max. intensity) on particles' surfaces was 102 μg/mL, as obtained from the standard curve of WGA concentration versus fluorescence intensity (n=3).

### 6.3.4 Interaction between F-WGA modified polyelectrolyte assembled nanoparticles and Caco-2 cells

#### 6.3.4.1 Effect of WGA/nanoparticle concentration on Caco-2 cell binding/uptake capability

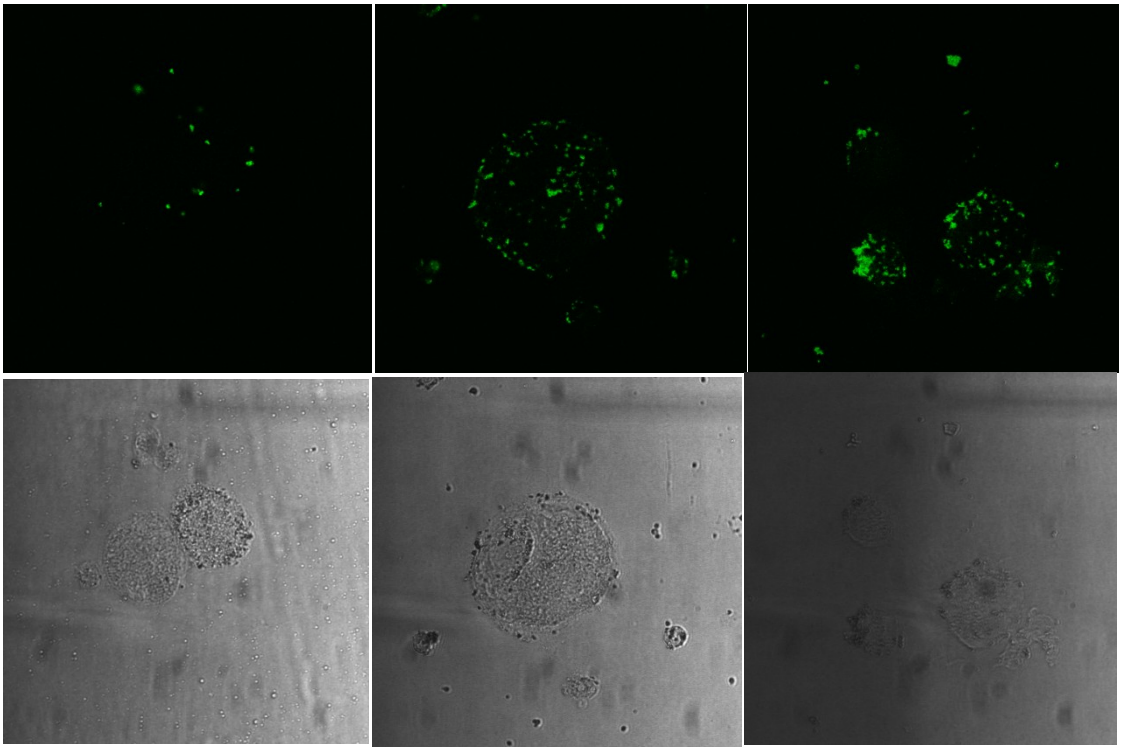

**Figure 37.** F-WGA conjugated, LbL assembled nanoparticles at different F-WGA concentrations in contact with Caco-2 cells. (20 h at 4 ºC) (Left to right, 1.5, 7.5, 15 µg/mL of F-WGA on the nanoparticle surfaces; 3 bilayers of CS/DEX assembled) Images are based on the same settings of the confocal microscope at the magnification 63×.

Confocal microscopy was used first to study the interaction between F-WGA conjugated, LbL assembled nanoparticles with suspended Caco-2 cells. The concentration of F-WGA on LbL nanoparticles was calculated according to the fluorescence intensity of the particles from F-WGA after conjugation. Three concentrations of F-WGA on particle surfaces were used, 1.5, 7.5 and 15 µg/mL (Figure 37). Particles contacted with cells for 20 h at 4 ºC. This temperature was set to avoid

energy dependent particle uptake behavior. So the particles were expected to bind only on the cell surfaces.

FACS stands for fluorescence associated cell sorting, which can differentiate fluorescent labeled cells from non-labeled ones and separate cells with fluorescence at different wavelengths. Cells were washed three times with PBS after the incubation. Caco-2 cells were used as a blank control, and all the gating results were based on this sample. The concentration of WGA on particles' surfaces ranged from 1.5 to 15 μg/mL. 20,000 cells were counted for each sample (n = 3), and the experiments were triplicated (Figure 38).

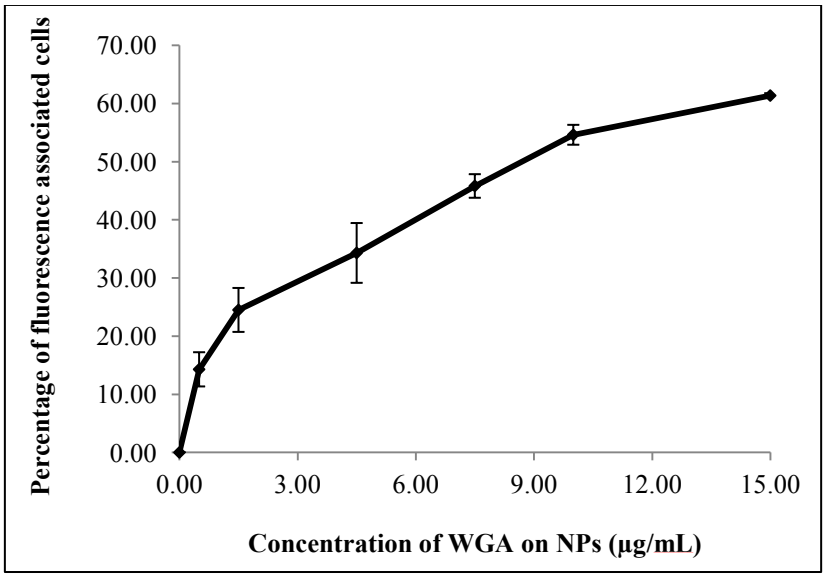


**Figure 38.** Effect of WGA/nanoparticle concentration on Caco-2 cell binding capability.

The percentage of fluorescence associated cells was calculated from the cells being bound with fluorescent WGA, which was conjugated onto the LbL assembled PS NPs. These results indicated the capability of Caco-2 cells binding with F-WGA modified NPs at different concentrations. The concentration of the F-WGA on particles' surfaces at 7.5 μg/mL showed more than 40% of the cells were bound with the particles. Further increase of the F-WGA concentration to 15μg/mL, the percentage of the labeled cells could reach 60%. At a higher temperature, *e.g.* 37 ºC, the binding and uptake of

nanoparticles by the cells may be more efficient than at 4 ºC, at which certain enzyme activity related to this process might be suppressed.

6.3.4.2 Effect of F-WGA as a targeting group to Caco-2 cells

The effectiveness of F-WGA as a targeting group to Caco-2 cells was also investigated by FACS (Figure 38). Three different kinds of particles (fluorescent nanoparticles, fluorescent particles encapsulated with CS/DEX-PEG, particles encapsulated with CS/DEX-PEG in conjugation with F-WGA) were prepared and then incubated with cells for 20 h at 4 ºC. The fluorescence of the cells counted by flow cytometry was directly associated with the particles which were bound onto the cells (blank control: Caco-2 cells only). A significant increase in the percentage of fluorescent labeled cells was detected after the cells were incubated with the lectin F-WGA conjugated particles, as compared with two other samples, *i.e.* fluorescent nanoparticles and particles without F-WGA modification. The different percentage of fluorescent cells between this experiment and the previous one (Figure 38) might be caused by the non-uniform mixing of cells with particles during the incubation. The experiment was repeated twice and the percentage of fluorescent cells for the F-WGA conjugated NPs was 36% to 42% (three parallel samples for each independent experiment).

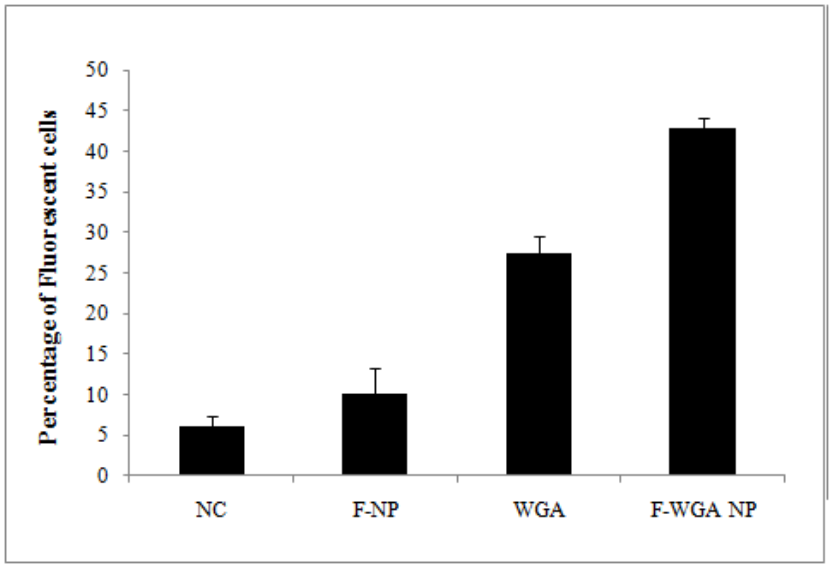


**Figure 39.** Function of lectin F-WGA as a targeting group as evaluated by flow cytometry. Caco-2 cells were incubated for 20 h with WGA or WGA conjugated CS/DEX (3 bilayers encapsulated nanoparticles (FWGA-NP)) at the WGA concentration 1.5 μg/mL at 4 ºC (different batches from Figure 32). Cell fluorescence was caused by fluorescence of particles binding with the cells. NC – negative control, fluorescent nanoparticles; F-NP fluorescent nanoparticles encapsulated with 3 bilayers of CS/DEX and conjugated with PEG without WGA; WGA – F-WGA molecule only, positive control.

### 6.3.5 Preliminary study on material biocompatibility

PEG as a functional group was chemisorbed onto the nanoparticles' surfaces so as to stabilize nanoparticles in suspension and increase the material biocompatibility. This molecule has been suggested to avoid adsorption of different proteins and increase the circulating time in the human body.[103] This study was to test if these materials, including the polyelectrolytes, nanoparticles (polystyrene as the model core) and PEG, would be regarded to be safe to the human colon cells. As we know, paclitaxel was an anti-cancer drug, so it will show a therapeutic effect on the cells; therefore polystyrene nanoparticles were used temporarily here as the test core.

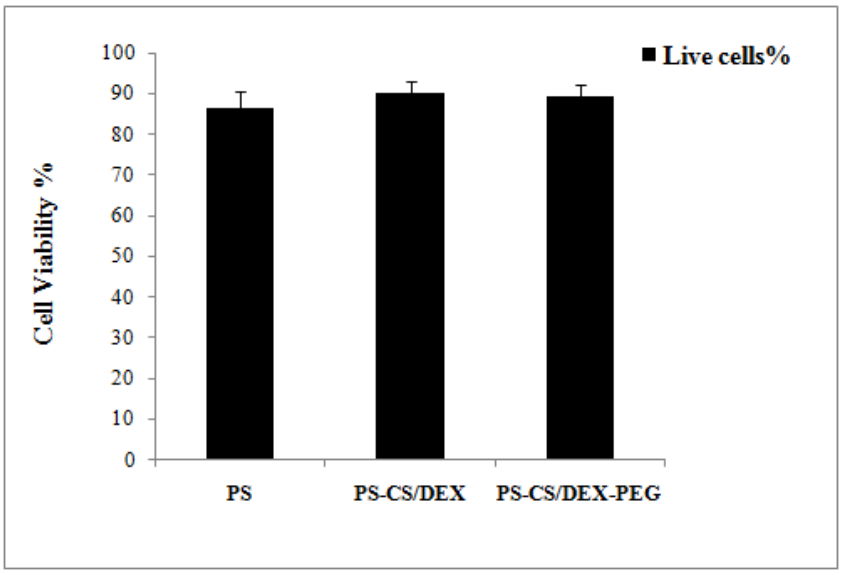


**Figure 40.** Cell viability as evaluated by the live/dead® cell viability assay (Invitrogen, USA) on Caco-2 cells after 20 h of incubation at 37ºC in direct contact with PEG conjugated CS/DEX encapsulated polystyrene nanoparticles (i.e. PS-CS/DEX-PEG). Cell viability data are reported as percentage ratio between viable cell number and total cell number. Control was used to incubate cells with polystyrene nanoparticles (PS) only. Negative control was CS/DEX encapsulated PS NPs before PEG conjugation (i.e. PS-CS/DEX).

Figure 40 shows the results obtained from the particles' direct contact with Caco-2 cells, and the cell viability was tested using the live/dead® cell viability assay. It was found that there was no significant difference of the cell viability among fluorescent particles, particles encapsulated with CS/DEX, and particles with CS/DEX layers conjugated with PEG after incubating them with cells. The data suggested that materials, *i.e.* particles, CS/DEX polyelectrolytes and PEG used in this drug delivery system did not release any substance that would significantly interfere with the cell viability for 20 h.

## 6.4 Conclusion

In this section, the morphology of different polyelectrolyte encapsulated PS NPs was first studied by TEM and SEM. Bio-polyelectrolytes chitosan and dextran have large glucose rings, so the LbL assembly showed rough surfaces as observed from the TEM images. LbL assembled particles modified with PEG were confirmed to be more stable than those without the PEG conjugation. The polyelectrolyte type and encapsulated layer number on the nanoparticles were found to be two factors that would influence the non specific adhesion of F-WGA. F-WGA was confirmed as an effective targeting group after it was conjugated onto the LbL assembled nanoparticles. The fluorescence associated cells reached 60% when the F-WGA concentration on the particles' surfaces was 15μg/mL. The preliminary biocompatibility study of the PEG modified nanoparticles showed: CS/DEX and PEG did not release any obvious toxic substances that would influence the cell viability.

# 7. SUMMARY AND CONCLUSIONS

## 7.1 Summary

This project mainly includes three parts: fabrication, encapsulation and modifications of paclitaxel based nanoparticles, synthesis, characterization and *in vitro* drug release study of the dextran based hydrogels, and *in vitro* evaluation of the modified nanoparticles with Caco-2 cells.

PAX NPs were first fabricated at 100 nm by the modified emulsification evaporation method. Core-shell structured PAX NPs were prepared by encapsulating biomacromolecules chitosan and dextran using the LbL self-assembly technique. Surface modifications were then performed by conjugating with poly (ethylene glycol) and wheat germ agglutinin, so as to build a biocompatible and targeting drug delivery system. Adjustable release profiles could be obtained by tuning the layer number and buffer ionic strength.

Two different dextran based pH sensitive and enzyme degradable hydrogels: dextran maleic acid (Dex-MA), and glycidyl methacrylated dextran (Dex-GMA) were synthesized for oral delivery of nanoparticles. Hydrogels of both kinds were stable in simulated gastric fluid, but prone to swelling and degrading in the presence or absence of enzyme dextranase in simulated intestinal fluid. The release profiles of nanoparticles were tuned by copolymerizing with other components under simulated human GI conditions. Two possible release mechanisms were discussed for Dex-MA and Dex-GMA-co-AA hydrogels respectively: degradation controlled, and diffusion controlled. These two biodegradable hydrogels were considered as potential colon targeting vehicles for oral delivery of the drug nanoparticles.

The stability test is important in developing a good nanoparticle based formulation. Particle instability may induce aggregation in suspension, which is undesirable for storage. The stability of LbL assembled fluorescent nanoparticles was investigated by measuring the zeta potential and the fluorescence intensity of the suspension after incubating the nanoparticles in SIF over certain time periods. *In vitro*

study of these WGA conjugated nanoparticles' binding and uptake by Caco-2 cell line was performed at different WGA/nanoparticle concentrations. The efficacy of WGA as a targeting group to Caco-2 cells was studied by comparing particles with different surfaces, confirming that WGA was an effective group that promoted the particles' binding capability to Caco-2 cells. Material biocompatibility was studied by incubating PEG conjugated nanoparticles with Caco-2 cells for 20 h at 37 ºC.

### 7.2 Conclusions

A nanoparticle based system consisting of a paclitaxel drug based core encapsulated with a nanometer thick biomacromolecule shell using the LbL assembly technique was successfully fabricated and characterized. The nanoshell provided specific sites on the surface which had been further modified with functional moieties, such as hydrophilic polymer PEG and ligand. This biocompatible drug delivery system, which combined passive accumulation with the active targeting moiety, could provide a potential alternative to more efficiently deliver hydrophobic drug to tumors.

Two newly formed hydrogels developed in this project showed a good pH responsive swelling property. A much higher SR was observed for the Dex-GMA-co-AA hydrogel at a composition of 40 mg/mL of Dex-GMA and 50 μL/mL of AA in the presence of enzyme dextranase. Adjustable release profiles could be obtained with the time window from 5 hr to 22 hr. The two Dex-MA-co-PEG and Dex-GMA-co-AA hydrogels, could promote dissolution of PAX NPs up to 5 days with 40 % of the PAX NPs released during the first 12 hr. It is suggested that both Dex-MA based and Dex-GMA-co-AA hydrogels could be used as potential colon targeting vehicles for delivering nanoparticles orally.

The key word of this colon targeting nanoparticle based drug delivery system is biocompatibility. Polysaccharides have been widely used in both building the nanoparticles' polyelectrolyte shell and developing the new functional excipients for oral drug delivery. In the near future, it will become quite obvious that polysaccharide and

their derivatives will play a very important, if not the most important role, in developing novel formulations, especially functional excipients.

# 8. FUTURE WORK

Further development of a potential nanoparticle based formulation is one of the next goals in this research. During the preparation of drug nanoparticles, different emulsifiers, instead of PVA, can be investigated to optimize the particle size and drug encapsulation efficiency. Other characterization tools such as differential scanning calorimetry (DSC) can be used to understand the physical state of the drug in the nanoparticles. *In vitro* kinetic models can be further explored to explain the drug nanoparticles' releasing mechanism from the hydrogels. Using the microfluidic device to make the micro sized pH sensitive hydrogels is a potential way to obtain novel drug delivery vehicles for oral administration of nanoparticles.

## 8.1 Development of paclitaxel nanoparticle based formulation

### 8.1.1 Emulsifiers during the preparation of nanoparticles

The enhanced activity of paclitaxel when incorporating it into nanoparticles can be explained: this system can act as a reservoir for paclitaxel, protecting the drug from epimerization and hydrolysis.[104] Also it can provide sustained drug release and enhancement of its anti-tumor activity.[60] Emulsifiers used in preparing these PAX NPs are critical to the particle encapsulation efficiency (EE) and particle size. A small amount of emulsifier would result in large particles, while a large amount of emulsifier would result in reduced drug EE. There is thus an optimal value of the emulsifier amount, at which nanoparticles of desired size and high EE can be obtained.

The further study can start to explore natural emulsifiers, instead of just using the often-used surfactant PVA. PVA has the disadvantages of low emulsifying efficiency, low drug encapsulation efficiency, difficulty in removal and possibly being harmful to the human body.[105, 106] D-α -tocopheryl polyethylene glycol 1000 succinate (vitamin E TPGS or TPGS) has recently been discovered as a good candidate in the paclitaxel based nanoparticle formulations.[107] It was used in the paclitaxel-PLGA nanoparticle based drug

delivery system, which can be treated either as the surfactant stabilizer added in the water phase or as a matrix component material added in the oil phase in the process.[107-108] The drug encapsulation efficiency can be achieved as high as 100 %.[4]

### 8.1.2 Further characterization of the nanoparticles

In the process of manufacturing nanoparticles, several parameters are important, which can determine the physiochemical and pharmaceutical properties of the PAX NPs. These factors include the emulsifier used and its concentration in the aqueous phase, drug loading ratio, the oil to water phase ratio, the pH, homogenization speed and the temperature, etc.

Various state-of-the-art techniques have been used in this research study to characterize the particles: dynamic light scattering (DLS) for size and size distribution, scanning electron microscopy (SEM), and transmission electron microscopy (TEM) for morphology, zeta-potential measurement for particle charge, X-ray photoelectron spectroscopy (XPS) for surface chemistry, and high performance liquid chromatography (HPLC) for drug EE and *in vitro* drug release studies.

Other than the above techniques, the physical status of paclitaxel in the nanoparticles can also be analyzed by differential scanning calorimetry (DSC). This is to study the thermal characteristics of drug loaded nanoparticles.[107] It was found that paclitaxel formulated in the nanoparticles was in an amorphous or disordered-crystalline phase of a molecular dispersion or a solid solution state in the polymer matrix.[109]

For the LbL assembled nanoparticles, the XPS and zeta potential were used to confirm the success of building self-assembled polyelectrolyte layers on drug nanoparticles. The thickness of the polyelectrolyte layer built onto drug nanoparticles have been only estimated in this research from the TEM and SEM images. A more accurate measurement can be done by using fluorescent labeled polyelectrolyte, e.g. chitosan-FITC.[64] The conformational state of a multilayer surface can be explored indirectly via the measurements of the surface roughness of dried films. For particles' surfaces comprised of a significant population of loops and tails, upon drying, a

molecularly rough surface will be produced; smoother surfaces will be created if it is dominated by flat, trainlike segments.[20] The layer thickness of weak polyelectrolytes may be greatly influenced by the pH in the buffer and the charge density. If the weak polyelectrolyte charge density is increased, the transition from thick adsorbed layers (~ 8nm) to very thin adsorbed layers (0.4nm) can be observed, even over a very narrow pH range.[20]

### 8.1.3 Development of the nanoparticle based formulation

More than 40% of compounds have been identified as poorly soluble in water through a combinatorial screening program. The conventional method of formulating these drugs will not be appropriate. Nanoparticle based formulations for poorly soluble drugs have shown promising results regarding drug circulating time in the human body, bioavailability, drug exposure and feasibility of being postprocessed into other solid dosage forms.[110]

The properties of nanoparticles which will determine their *in-vitro* and *in-vivo* performance include: particle size and size distribution, surface morphology and charge, surface chemistry, surface erosion and adhesion, drug diffusivity and encapsulation efficiency, drug stability and release kinetics, and the hemodynamic property of the nanoparticles.[61] Stability of particles in the suspension is very important and it is ideal to maintain a good dispersion of these nanoparticles. An unstable nanoparticle suspension may change the above properties and thus the particles' performance. Since this is the direct form obtained from the study, the stability of nanoparticles in suspension and storage of the suspension should be investigated first. A more stable formulation may be prepared using the freeze-thaw and then lyophilization/freeze- drying method.

Freeze-drying has been considered as a good technique to improve the long-term stability of colloidal nanoparticles. The poor stability in an aqueous medium of these systems forms a real barrier against the clinical use of nanoparticles.[111] The instability of nanoparticles may be caused by the polymer type used in preparing the nanoparticles,

pH in the aqueous dispersion, chemical stability of the entrapped drug, and storage temperature.[111]

**8.2 Release study**

*In vitro* release kinetic study is one important way to understand and possibly predict the drug release behavior in the human body. The release of poorly soluble drug from the nanoparticles in the aqueous suspension is dominated by self-erosion and dissolution of the matrix.[112] Some factors may influence the release behavior of the drug from bare nanoparticles. It was found that based on different emulsifiers used, the release rates of paclitaxel from nanoparticles may be differed based on the ratio of hydrophobicity and hydrophilicity of the nanoparticle matrix.[4]

Some factors that will influence the release rate of paclitaxel from bare nanoparticles are listed below:

a. Surfactants that are used
b. The property of the surfactants/emulsifier, more hydrophobic or hydrophilic
c. The polymer/surfactant concentration
d. The part where the surfactants are added. In the matrix formed materials or dissolved in the aqueous solution
e. The organic/aqueous phase ratio, which influences the particle size.

During the solvent extraction/evaporation process for preparing drug nanoparticles, natural emulsifiers, such as phospholipids, cholesterol, and vitamin E TPGS were applied to improve the drug encapsulation efficiency, desired drug release kinetics and higher cell uptake capacity.[4] It was found that these natural emulsifiers have great advantages for the paclitaxel nanoparticle formulation over the traditional macromolecular emulsifiers, such as polyvinyl alcohol (PVA).[105] The drug release profile can be controlled by using a specific emulsifier and optimizing its amount added. For example, with an increased amount of TPGS, the paclitaxel release rate increases

accordingly. This is because as more TPGS is used, the nanoparticle matrix becomes more hydrophilic.[4]

The *In vitro* release of paclitaxel from different formulations can be performed in the presence and absence of human serum albumin by using a membrane dialysis system in phosphate buffered saline at 37 ºC and pH 7.0.[113]

### 8.3 Dextran based pH sensitive microgels

It was found that agarose droplets in the range of 50-110 µm can be produced by utilizing a microfluidic device with hydrodynamic flow focusing geometry.[114] It has also been demonstrated that yeast cells can be encapsulated successfully into these agarose capsules.[114]

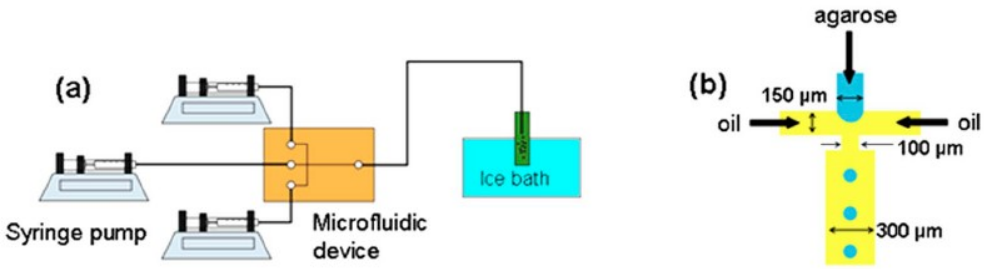


**Figure 41.** a) Experimental setup for generating agarose gelled droplets. (Ice bath is to initiate the gelation of agarose.) b) Schematic of the microfluidic device with flow focusing geometry producing agarose droplets.[114] Agarose solution is introduced into the center channel and two streams of oil are flowed into two side channels. The droplet size can be adjusted by changing the orifice size.

Based on the above technology, dextran based microgels may also be produced by simply preparing the precursor as the aqueous phase and placing a UV lamp in the end to form the gels. The dextran based precursor Dex-GMA synthesized by our group was used first with the microfluidic device. Micro sized hydrogels were successfully

polymerized by UV irradiation. (Figure 42) The size of these microgels was homogeneous and could be further adjusted by changing the orifice size.

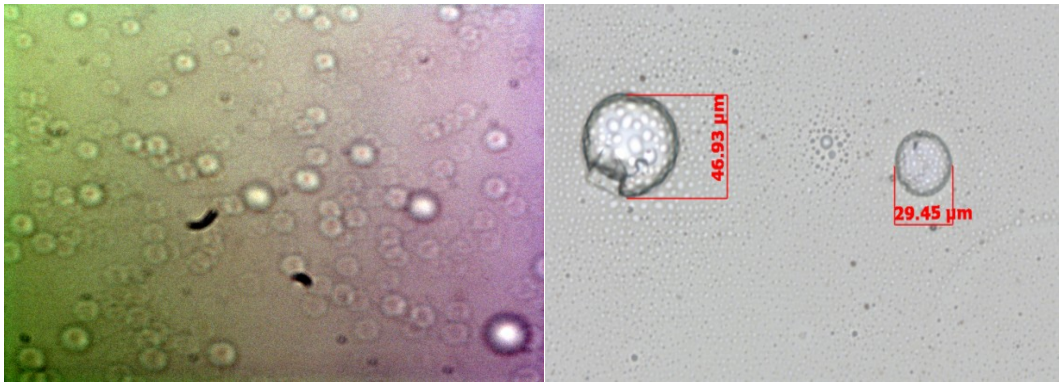


**Figure 42.** Dextran-GMA based microgels prepared by microfluidic device.

Fluorescent nanoparticles were added to the precursor solution and then encapsulated into the microgels. The encapsulation efficiency of nanoparticles into these microgels needs to be further studied. Some fluorescent nanoparticles might have been leaking out of the microgels during the centrifugation and washing process. There were still some fluorescent nanoparticles successfully trapped inside the microgels, as shown in the image obtained by fluorescence microscopy (Figure 43, right).

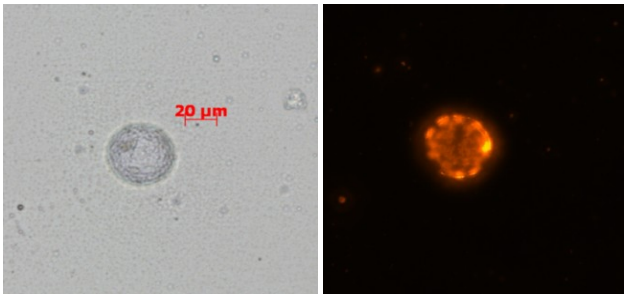


**Figure 43.** Dextran-GMA-co-AA based microgels encapsulated with fluorescent nanoparticles. Bright field image (left); fluorescent image (right).

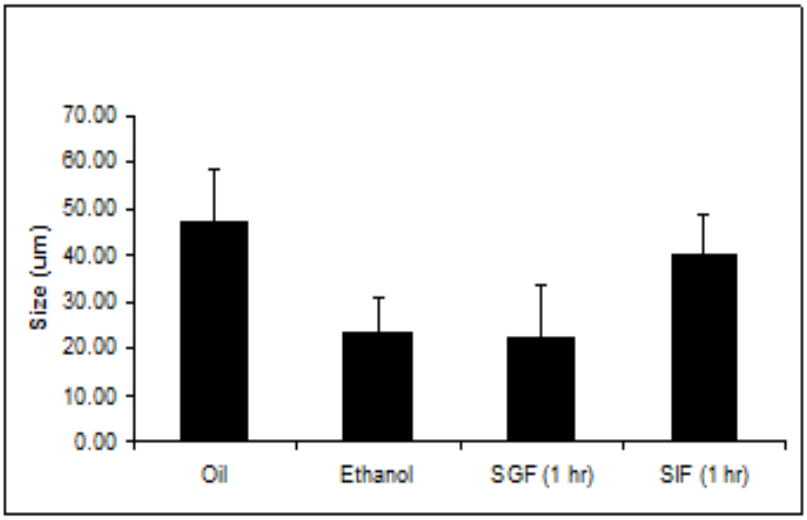


**Figure 44.** Size of dextran-GMA-co-AA microgels in different solvents.

Interestingly, these dextran-GMA-co-AA based microgels showed different sizes in different solvents. Light mineral oil is the original solvent where the droplets gelled under UV irradiation, and the microgels showed around 50 μm in size, which was consistent with the orifice size. Ethanol was followed to wash the microgels and remove the surfactant span 80 (5% w/w); the microgels shrunk in the ethanol. Different pH buffers were also used to test if these microgels were pH sensitive. The size of these dextran based microgels in SIF was bigger than that in SGF, indicating that they were pH sensitive.

Further experiments can be performed to study the release of fluorescent nanoparticles and drug nanoparticles from these microgels. Possible problems may be: since these microgels will be transparent in the aqueous solution, separation of nanoparticles from these microgels will be difficult. An appropriate centrifugation speed may be applied to sediment the microgels, and the concentration of the fluorescent nanoparticles released in the supernatant may then be measured.

### 8.4 *In vitro* cell uptake study and *in vivo* animal studies

The efficacy of the paclitaxel nanoparticle based system can be tested through incubating these particles with a colon adenocarcinoma cell line. Particles with and without drug encapsulation can be used, and the cell viability after the treatment with different nanoparticles can be analyzed by using the live/dead cell viability assay. The targeting group F-WGA can be conjugated onto the nanoparticles, and its efficiency can be measured by comparing the cell uptake capabilities.

HT-29 is another typical human colon adenocarcinoma cell line, and can be maintained by serial passages in McCoy's 5A medium supplemented with 10% fetal bovine serum (FBS), 2.2 g/L of sodium bicarbonate and 1% penicillin-streptomycin solution.[115] These cells can be harvested and mixed with Caco-2 cells to test if F-WGA conjugated nanoparticles can also bind with and uptaken by these cells.

NCM356 and NCM425 represent the first successful *in vitro* culture of human colonocytes derived from the normal mucosa. These cell lines are important resources for studying colon cancer and the physiology of intestinal cells.[116] These colon normal cells can be mix-cultivated with the human colon adenocarcinoma cells, and the *in vitro* targeting functionality of nanoparticles with the cancer cells can be studied.

*In vivo* animal testing can be further performed by using non-human vertebrate animals to understand the drug metabolic profile, material toxicology, and the drug delivery system.[117] Metabolic tests aim to investigate the drug pharmacokinetics, i.e. how a drug can be absorbed, distributed, metabolized and excreted.[117] The major obstacle for oral administration of poorly soluble drugs is low bioavailability and thus poor absorption by the body. Drug metabolic and efficacy tests between different formulations can provide valuable information to understand if the new formulation is superior on absorption. Since the colon targeting drug delivery system is pH dependent, and the small intestine shared similar pH with the colon, the small intestine transit time is therefore an important parameter for colon targeting drug delivery.[41] One major limitation for this drug delivery system is the *in vivo* variation of the small intestinal transit time, which may result in undesirable releases of the bioactive in the small

intestine or the terminal part of the colon.[41] The colon specific enzyme induced degradation of the hydrogels can possibly address the issue. Dextranase was found to indeed present in a human colonic fermentation model, and dextran based hydrogels had been investigated using the *in vivo* rats model. It was found *in vivo* that these dextran based pH sensitive hydrogels were degraded in the caecum of the rats, not in the stomach.[118] Still, the goal during early development of an efficient drug delivery system is to obtain a formulation that is simple, flexible and fit for its intended purpose.[117]

## REFERENCES

(1) Hanahan, D.; Weinberg, R. A.. *Cell* **2000,** *100* (1), 57-70.

(2) Foulds, L.. *Cancer Res.* **1954,** *14* (5), 327-339.

(3) American Cancer Society. *Cancer Statistics 2011 slide presentation.* **2011**.Online available:http://www.cancer.org/Research/CancerFactsFigures/CancerFactsFigures/cancer-facts-figures-2011.

(4) Feng, S. S.; Mu, L.; Win, K. Y.; Huang, G. F.. *Curr. Med .Chem.* **2004,** *11* (4), 413 424.

(5) Müller, R. H.. *Colloidal carriers for controlled drug delivery and targeting*. CRS Press, Inc.:Boca Raton, Florida, 1991.

(6) Win, K. Y.; Feng, S. S.. *Biomaterials* **2005,** *26* (15), 2713-2722.

(7) Ferrante, K.; Winograd, B.; Canetta, R.. *Cancer Chemoth. Pharm.* **1999,** *43*, S61-S68.

(8) Shin, B. S.; Kim, H. J.; Hong, S. H.; Lee, J. B.; Hwang, S. W.; Lee, M. H.; Yoo, S. D.. *Cancer Chemoth. Pharm.* **2009,** *64* (1), 87-94.

(9) Sparreboom, A.; Scripture, C. D.; Trieu, V.; Williams, P. J.; De, T. P.; Yang, A.; Beals, B.; Figg, W. D.; Hawkins, M.; Desai, N.. *Clin. Cancer Res.* **2005,** *11* (11), 4136-4143.

(10) Gelderblom, H.; Verweij, J.; Nooter, K.; Sparreboom, A.. *Eur. J. Cancer* **2001,** *37* (13), 1590-1598.

(11) Decher, G.. *Science* **1997,** *277* (5330), 1232-1237.

(12) Lynn, D. M.. *Adv. Mater.* **2007,** *19* (23), 4118-4130.

(13) Boddohi, S.; Killingsworth, C. E.; Kipper, M. J.. *Biomacromolecules* **2008,** *9* (7), 2021-2028.

(14) Hoogeveen, N. G.; Stuart, M. A. C.; Fleer, G. J.; Bohmer, M. R.. *Langmuir* **1996,** *12* (15), 3675-3681.

(15) Kato, N.; Schuetz, P.; Fery, A.; Caruso, F.. *Macromolecules* **2002,** *35* (26), 9780-9787.

(16) Clark, S. L.; Hammond, P. T.. *Langmuir* **2000,** *16* (26), 10206-10214.

(17) Il'ina, A. V.; Varlamov, V. P.; Ermakov, Y. A.; Orlov, V. N.; Skryabin, K. G.. *Dokl Chem.* **2008,** *421*, 165-167.

(18) Yu, X.; Pishko, M. V.. *Biomacromolecules* **2011,** *12* (9), 3205-3212.

(19) Schatz, C.; Viton, C.; Delair, T.; Pichot, C.; Domard, A.. *Biomacromolecules* **2003,** *4* (3), 641-648.

(20) Shiratori, S. S.; Rubner, M. F.. *Macromolecules* **2000,** *33* (11), 4213-4219.

(21) Pavinatto, F. J.; Caseli, L.; Oliveira, O. N.. *Biomacromolecules* **2010,** *11* (8), 1897-1908.

(22) Serizawa, T.; Yamaguchi, M.; Akashi, M.. *Macromolecules* **2002,** *35* (23), 8656-8658.

(23) Serizawa, T.; Yamaguchi, M.; Matsuyama, T.; Akashi, M.. *Biomacromolecules* **2000,** *1* (3), 306-309.

(24) Tobio, M.; Gref, R.; Sanchez, A.; Langer, R.; Alonso, M. J.. *Pharm. Res.***1998,** *15* (2), 270-275.

(25) Yoo, J. W.; Chambers, E.; Mitragotri, S.. *Curr. Pharm. Design* **2010,** *16* (21), 2298-2307.

(26) Veronese, F. M.. *Biomaterials* **2001,** *22* (5), 405-417.

(27) Roberts MJ, B. M., Harris JM.. *Adv. Drug Delivery Rev.* **2002,** *54* (4), 459-76.

(28) Bies, C.; Lehr, C. M.; Woodley, J. F.. *Adv. Drug Deliv Rev.* **2004,** *56* (4), 425-35.

(29) Padma V Devarajan, G. S. S.. *Express Pharma Pulse* [Online], 2003.

(30) Liu, Q. F.; Shao, X. Y.; Chen, J.; Shen, Y. H.; Feng, C. C.; Gao, X. L.; Zhao, Y.; Li, J. W.; Zhang, Q. Z.; Jiang, X. G.. *Toxicol Appl Pharm.* **2011,** *251* (1), 79-84.

(31) Stinchcombe, T. E.. *Nanomedicine-Uk* **2007,** *2* (4), 415-423.

(32) Ibrahim, N. K.; Desai, N.; Legha, S.; Soon-Shiong, P.; Theriault, R. L.; Rivera, E.; Esmaeli, B.; Ring, S. E.; Bedikian, A.; Hortobagyi, G. N.; Ellerhorst, J. A.. *Clin. Cancer Res.* **2002,** *8* (5), 1038-1044.

(33) Trickler, W. J.; Nagvekar, A. A.; Dash, A. K.. *AAPS PharmSciTech* **2008,** *9* (2), 486-493.

(34) Al-Ghananeem, A. M.; Malkawi, A. H.; Muammer, Y. M.; Balko, J. M.; Black, E. P.; Mourad, W.; Romond, E.. *AAPS PharmSciTech* **2009,** *10* (2), 410-417.

(35) Feng, Z. L.; Zhao, G.; Yu, L.; Gough, D.; Howell, S. B.. *Cancer Chemoth. Pharm.* **2010,** *65* (5), 923-930.

(36) Ravi, V.; Kumar, S. T. M. P.. *J. Mater. Sci-Mater. M* **2008,** *19* (5), 2131-2136.

(37) Kitano, S.; Kataoka, K.; Koyama, Y.; Okano, T.; Sakurai, Y.. *Makromol Chem-Rapid* **1991,** *12* (4), 227-233.

(38) Chourasia, M. K.; Jain, S. K.. *J. Pharm. Pharm. Sci.* **2003,** *6* (1), 33-66.

(39) Stubbe, B.; Maris, B.; Van den Mooter, G.; De Smedt, S. C.; Demeester, J.. *J. Controlled Release* **2001,** *75* (1-2), 103-114.

(40) Wikipedia, Colon (anatomy). *http://en.wikipedia.org/wiki/Colon_(anatomy)* **2012**.

(41) Jain, A.; Gupta, Y.; Jain, S. K... *J. Pharm. Pharm. Sci.* **2007,** *10* (1), 86-128.

(42) Sinha, V. R.; Kumria, R.. *Int. J. Pharm.* **2001,** *224* (1-2), 19-38.

(43) Van Dijk-Wolthuis, W. N. E., Franssen, O., Talsma, H., van Steenbergen, M. J., Kettenes-van den Bosch, J. J., and Hennink, W. E.. *Macromolecules* **1995,** *28*, 5.

(44) Kim, S. H.; Won, C. Y.; Chu, C. C.. *J. Biomed. Mater. Res.* **1999,** *46* (2), 160-170.

(45) Vandijkwolthuis, W. N. E.; Franssen, O.; Talsma, H.; Vansteenbergen, M. J.; Vandenbosch, J. J. K.; Hennink, W. E.. *Macromolecules* **1995,** *28* (18), 6317-6322.

(46) Giannuzzo, M.; Feeney, M.; Paolicelli, P.; Casadei, M. A.. *J.Drug Delivery Sci. and Technol.* **2006,** *16* (1), 49-54.

(47) Zhang, X. Z.; Wu, D. Q.; Chu, C. C.. *Biomaterials* **2004,** *25* (19), 4719-4730.

(48) Tripodo, G.; Pitarresi, G.; Palumbo, F. S.; Craparo, E. F.; Giammona, G.. *Macromol. Biosci.* **2005,** *5* (11), 1074-1084.

(49) Gautam Singhvi, M. S..*Inter.J. Pharm. Studies and Res.***2011,** *2* (1), 77-84.

(50) Philip R., Peppas N. A.. *J. Controlled Release* **1987,** *5*, 23-36.

(51) Siepmann, J.; Peppas, N. A.. *Adv. drug delivery Rev.* **2001,** *48* (2-3), 139-157.

(52) Torchilin, V. P.. *Adv. drug delivery Rev.* **2006,** *58* (14), 1532-1555.

(53) Wang, X.; Li, J.; Wang, Y. Q.; Cho, K. J.; Kim, G.; Gjyrezi, A.; Koenig, L.; Giannakakou, P.; Shin, H. J. C.; Tighiouart, M.; Nie, S. M.; Chen, Z.; Shin, D. M. *ACS Nano* **2009,** *3* (10), 3165-3174.

(54) Jiang, B.; Barnett, J.B.; Li., B..*Nanotechnol., Sci. Appl.* **2009,** *2*, 21-27.

(55) Xiao, K.; Luo, J. T.; Fowler, W. L.; Li, Y. P.; Lee, J. S.; Xing, L.; Cheng, R. H.; Wang, L.; Lam, K. S.. Biomaterials 2009, 30 (30), 6006-6016.

(56) ODonnell, P. B.; McGinity, J. W.. *Adv. drug delivery Rev.* **1997,** *28* (1), 25-42.

(57) Zahr, A. S.; Pishko, M. V.. *Biomacromolecules* **2007,** *8* (6), 2004-2010.

(58) Nakajima, N.; Ikada, Y.. *Bioconjugate Chem.***1995,** *6* (1), 123-130.

(59) Vauthier, C.; Bouchemal, K., Methods for the Preparation and Manufacture of Polymeric Nanoparticles. *Pharm. Res.***2009,** *26* (5), 1025-1058.

(60) Fonseca, C.; Simoes, S.; Gaspar, R.. *J. Controlled Release* **2002,** *83* (2), 273-286.

(61) Feng, S. S.. *Expert Rev Med Devices* **2004,** *1* (1), 115-25.

(62) Zahr, A. S.; De Villiers, M.; Pishko, M. V..*Langmuir* **2005,** *21* (1), 403-410.

(63) Decher, G.; Hong, J. D.; Schmitt, J..*Thin Solid Films* **1992,** *210* (1-2), 831-835.

(64) Richert, L.; Lavalle, P.; Payan, E.; Shu, X. Z.; Prestwich, G. D.; Stoltz, J. F.; Schaaf, P.; Voegel, J. C.; Picart, C.. *Langmuir* **2004,** *20* (2), 448-458.

(65) Moulder, J.F.; W. F. S.; Sobol, P.E.; Bomben, K.D.. *Physical Electronics, Inc. Minnesota* **1995**.

(66) Torchilin, V.. *Eur. J. Pharm. Biopharm.* **2009,** *71* (3), 431-444.

(67) Jain, R. K.. *Adv. Drug Delivery Rev.* **2001,** *46* (1-3), 149-168.

(68) Dalla Pellegrina, C.; Rizzi, C.; Mosconi, S.; Zoccatelli, G.; Peruffo, A.; Chignola, R.. *Toxicol. Appl.Pharm* .**2005,** *207* (2), 170-178.

(69) Mo, Y.; Lim, L. Y.. *J. Controlled Release* **2005,** *108* (2-3), 244-262.

(70) Mo, Y.; Lim, L. Y.. *J. Controlled Release* **2005,** *107* (1), 30-42.

(71) Feng, S. S..*Nanomedicine (Lond)* **2006,** *1* (3), 297-309.

(72) Hamaguchi, T.; Matsumura, Y.; Suzuki, M.; Shimizu, K.; Goda, R.; Nakamura, I.; Nakatomi, I.; Yokoyama, M.; Kataoka, K.; Kakizoe, T.. *Brit J Cancer* **2005,** *92* (7), 1240-1246.

(73) Tian, J. H.; Stella, V. J.. *J. Pharm. Sci.* **2008,** *97* (3), 1224-1235.

(74) Tian, J. H.; Stella, V. J.. *J. Pharm. Sci.* **2010,** *99* (3), 1288-1298.

(75) Antipov, A. A.; Sukhorukov, G. B.. *Adv. Colloid Interfac.* **2004,** *111* (1-2), 49-61.

(76) Bilensoy, E.; Gurkaynak, O.; Ertan, M.; Sen, M.; Hincal, A. A.. *J. Pharm. Sci.s* **2008,** *97* (4), 1519-1529.

(77) Lao, L. L.; Venkatraman, S. S.; Peppas, N. A.. *J. Biomed. Mater. Res. Part A* **2009,** *90A* (4), 1054-1065.

(78) Gautam S.; M. S.. *Inter. J. Pharm. Studies and Res.***2011,** *2* (1).

(79) De Geest, B. G.; Sanders, N. N.; Sukhorukov, G. B.; Demeester, J.; De Smedt, S. C.. *Chem. Soc. Rev.* **2007,** *36* (4), 636-649.

(80) Agarwal, A.; Lvov, Y.; Sawant, R.; Torchilin, V.. *J. Controlled Release* **2008,** *128* (3), 255-260.

(81) Del Mercato, L. L.; Rivera-Gil, P.; Abbasi, A. Z.; Ochs, M.; Ganas, C.; Zins, I.; Sonnichsen, C.; Parak, W. J.. *Nanoscale* **2010,** *2* (4), 458-467.

(82) Sukhorukov, G. B.; Brumen, M.; Donath, E.; Mohwald, H.. *J. Phys. Chem. B* **1999,** *103* (31), 6434-6440.

(83) Yu, X.; Pishko, M. V.. *Soft Matter* **2011,** *7* (19), 8898-8904.

(84) Lipinski, C.. *Am. Pharm. Rev.* **2002,** *5*, 82-85.

(85) Hu, J. H.; Johnston, K. P.; Williams, R. O.. *Drug Dev. Ind. Pharm.* **2004,** *30* (3), 233-245.

(86) Kim, S.; Kim, J. Y.; Huh, K. M.; Acharya, G.; Park, K.. *J. Controlled Release* **2008,** *132* (3), 222-229.

(87) Chandran, S.; Sanjay, K. S.; Asghar, L. F. A.. *J. Microencapsul* **2009,** *26* (5), 420-431.

(88) Simonsen, L.; Hovgaard, L.; Mortensen, P. B.; Brondsted, H.. *European J. Pharm. Sci.* **1995,** *3* (6), 329-337.

(89) Hehre, E. J.; Sery, T. W.. *J. Bacteriol* **1952,** *63* (3), 424-426.

(90) Aberg, B.. *Scand. J. Clin. Lab. Inv.* **1953,** *5* (1), 37-38.

(91) Larsen, C.; Harboe, E.; Johansen, M.; Olesen, H. P.. *Pharm. Res.* **1989,** *6* (12), 995-999.

(92) Casadei, M. A.; Pitarresi, G.; Calabrese, R.; Paolicelli, P.; Giammona, G.. *Biomacromolecules* **2008,** *9* (1), 43-49.

(93) Kim, I. S.; Oh, I. J.. *Arch. Pharm. Res.* **2005,** *28* (8), 983-987.

(94) Kim, S. H.; Chu, C. C.. *J. Biomed.Mater. Res.* **2000,** *53* (3), 258-266.

(95) Matricardi, P.; Pontoriero, M.; Coviello, T.; Casadei, M. A.; Alhaique, F.. *Biomacromolecules* **2008,** *9* (7), 2014-2020.

(96) Dubowchik, G. M.; Walker, M. A.. *Pharmacol. Therapeut.* **1999,** *83* (2), 67-123.

(97) Eskey, C. J.; Wolmark, N.; Mcdowell, C. L.; Domach, M. M.; Jain, R. K.. *J. Natl. Cancer I* **1994,** *86* (4), 293-299.

(98) Maeda, H.; Seymour, L. W.; Miyamoto, Y.. *Bioconjugate Chem.* **1992,** *3* (5), 351-362.

(99) Potineni, A.; Lynn, D. M.; Langer, R.; Amiji, M. M.. *J. Controlled Release* **2003,** *86* (2-3), 223-234.

(100) Braydich-Stolle, L.; Hussain, S.; Schlager, J. J.; Hofmann, M. C.. *Toxicol .Sci.* **2005,** *88* (2), 412-419.

(101) Yamashita, S.; Konishi, K.; Yamazaki, Y.; Taki, Y.; Sakane, T.; Sezaki, H.; Furuyama, Y., *J. Pharm.Sci.***2002,** *91* (3), 669-679.

(102) Blanchette, J.; Peppas, N. A.. J. Biomed. Mater. Res. Part A 2005, 72A (4), 381-388.

(103) Moghimi, S. M.; Hunter, A. C.; Murray, J. C.. *Pharmacol .Rev.* **2001,** *53* (2), 283-318.

(104) Slichenmyer, W. J.; Vonhoff, D. D.. *Anti-Cancer Drug* **1991,** *2* (6), 519-530.

(105) Mu, L.; Feng, S. S.. *Pharm. Res.* **2003,** *20* (11), 1864-1872.

(106) Feng, S. S.; Chien, S.. *Chem. Eng. Sci.* **2003,** *58* (18), 4087-4114.

(107) Mu, L.; Feng, S. S.. *J. Controlled Release* **2002,** *80* (1-3), 129-144.

(108) Mu, L.; Feng, S. S.. *J. Controlled Release* **2003,** *86* (1), 33-48.

(109) Dubernet, C.. *Thermochim. Acta.* **1995,** *248*, 259-269.

(110) Merisko-Liversidge, E. M.; Liversidge, G. G.. *Toxicol. Pathol.* **2008,** *36* (1), 43-48.

(111) Abdelwahed, W.; Degobert, G.; Stainmesse, S.; Fessi, H.. *Adv. drug delivery Rev.* **2006,** *58* (15), 1688-1713.

(112) Gautam Singhvi, M. S.. *Inter.J. Pharm. Studies and Res.* **2011,** *2* (1), 77-84.

(113) Cho, Y. W.; Lee, J.; Lee, S. C.; Huh, K. M.; Park, K.. *J. Controlled Release* **2004,** *97* (2), 249-257.

(114) Luo, D. W.; Pullela, S. R.; Marquez, M.; Cheng, Z. D.. *Biomicrofluidics* **2007,** *1* (3).

(115) Kelly, K. A.; Jones, D. A.. *Neoplasia* **2003,** *5* (5), 437-444.

(116) Stauffer, J. S.; Manzano, L. A.; Balch, G. C.; Merriman, R. L.; Tanzer, L. R.; Moyer, M. P.. *Am. J. Surg.* **1995,** *169* (2), 190-196.

(117) Mark H. Kleinman, B. L.. *John Wiley & Sons, Inc.* **2006,** 269.

(118) Hovgaard, L.; Brondsted, H.. *J. Controlled Release* **1995,** *36* (1-2), 159-166.

# APPENDIX A

# NANOPARTICLE BINDING WITH CELLS

**1. Influence of F-WGA concentration on nanoparticles binding with suspended Caco-2 cells**

1) Prepare the cells: cultivate for 5 days until 90% confluence. 18 mL 1.6*10^6 cells/mL.
2) Remove the old medium. Add PBS to wash the cells for 5 mins. Remove PBS, and add Trypsin/EDTA, incubate at 37 degree, 5% CO2 for 6 mins and check if cells are detached. Add fresh medium to deactivate the trypsin.
3) Centrifuge the cells down for 7 mins, 125g. Resuspend in PBS and wash the cells twice. Split the cells into 15mL falcon tubes (3) with each tube 6 mL. Centrifuge and the cells are collected.
4) Add the first tube with 6mL PBS and resuspend cells, this is negative control and used to calculate the autofluorescence. 2 ml in each well.
5) Add the second with 6mL F-WGA (12.5 μg/mL, dissolved in sterile PBS, better if filtered). Resuspend the cells well and split into 6 well plate with 2mL each well.
6) Add the third with 6mL NP/CS/DEX-PEG-FWGA with 2mL each well. Resuspend the particles and cells well. Well mixed.
7) Put in 4 degree, overnight, 20 hrs at 100 rpm shaking.
8) Before measuring the fluorescence with flow cytometer, stop the shaker and let the cell stay still for at least 30 mins. Wash the cells with PBS at least twice and resuspend them in PBS. Sample should be highly concentrated, estimated cell number (5*10^6) cells/ml, volume for FACS analysis could be 500 μl-1000 μl.

Appendix Table.1 F-WGA conjugated PS nanoparticles (4 batches), fluorescent intensity and corresponding WGA concentration (µg/mL)

| | 1 | 2 | 3 | 4 |
|---|---|---|---|---|
| F-WGA amount (mg) | 0.3 | 0.3 | 0.6 | 0.6 |
| MAX Intensity 10^(-6) at 512nm | 3.30 | 4.23 | 4.51 | 3.89 |
| Concentration (µg/mL) | 91.2 | 99.3 | 102 | 96.3 |

Average concentration of WGA conjugated onto PS nanoparticles: (97.1 ± 4.50) µg/mL

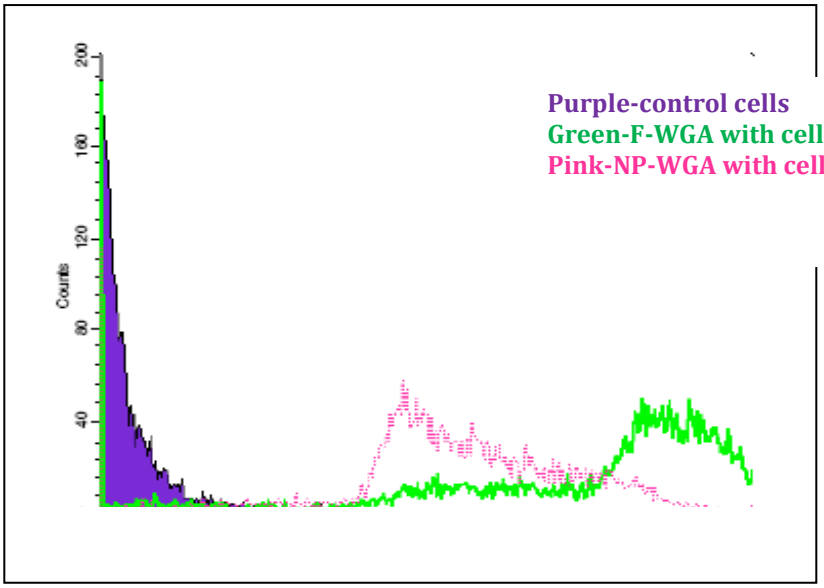


Appendix Figure.1 Fluorescence intensity of F-WGA lectin and nanoparticle-F-WGA interacting with Caco-2 cells by flow cytometer (number of cells counted: 10,000) FL1-H: gate one, wavelength at 510/21 nm.Cell density: 1.6 × 10^6 cells/mL, totally 18 mL, each 6 mL. Negative control: cells in PBS; positive control: F-WGA binding with cells; test sample: NP-WGA binding with cells. (For cells interact with lectin at concen. 13 µg/mL (the highest used)).

4 ºC, 20hr, 100 rpm shaking overnight (20 hrs)

| Sample number | 1 | 2 | 3 | 4 | 5 |
|---|---|---|---|---|---|
| F-WGA (µg/well) | 26 | 15 | 5 | 1 | 0.2 |
| F-WGA (µg/mL) | 13 | 7.5 | 2.5 | 0.5 | 0.1 |

4*2=8 flasks T-75 collect all cells, totally 42 mL cells in PBS/F-WGA/NP-WGA.

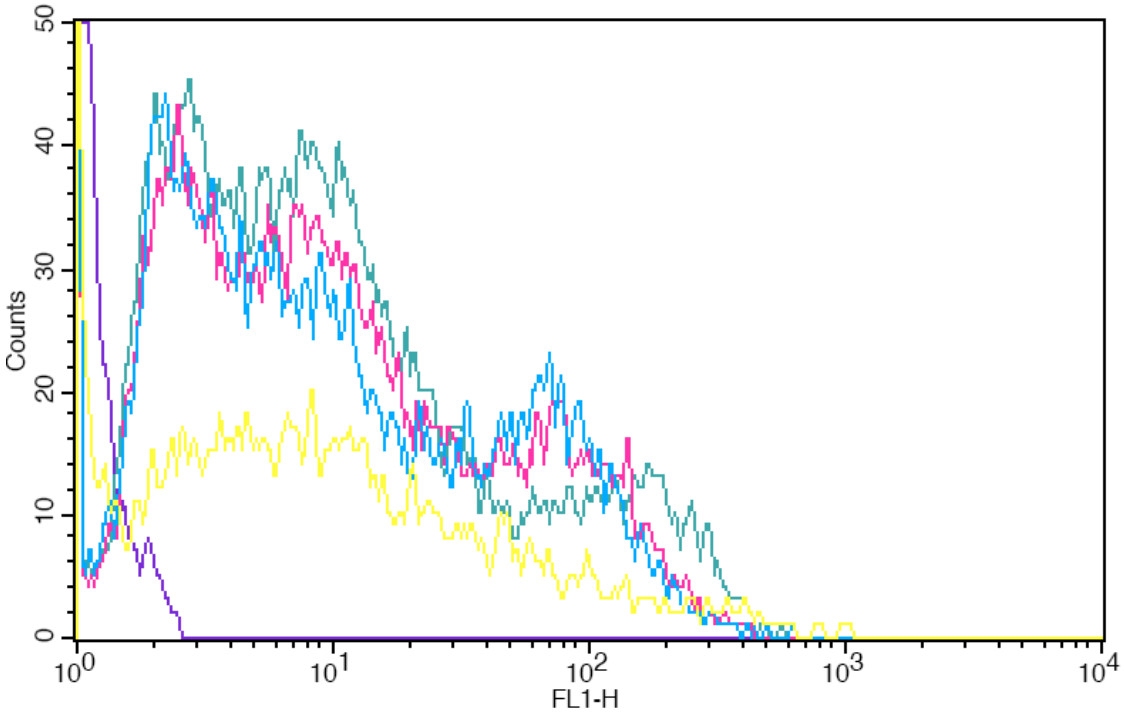


Appendix Figure.2 Histogram of different concentration of F-WGA conjugated nanoparticles binding with Caco-2 cells. Sample ID: purple- negative control; yellow: 0.5 µg/mL WGA conjugated nanoparticles; blue: 2.5 µg/mL WGA conjugated nanoparticles; pink: 7.5 µg/mL WGA conjugated nanoparticles; dark blue green:13 µg/mL WGA conjugated nanoparticles.

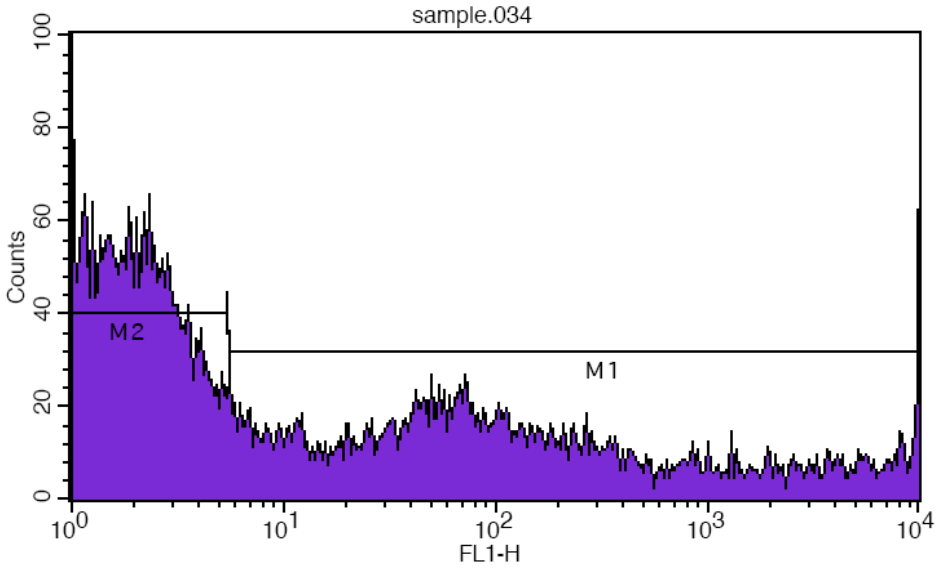


Histogram Statistics

File: sample.034
Sample ID: np7.5-3
Tube: Untitled
Acquisition Date: 26-Mar-10
Gated Events: 20000
X Parameter: FL1-H (Log)

Log Data Units: Linear Values
Patient ID:
Panel: Untitled Acquisition Tube List
Gate: No Gate
Total Events: 20000

| Marker | Left, Right | Events | % Gated | % Total | Mean | Geo Mean | CV | Median | Peak Ch |
|---|---|---|---|---|---|---|---|---|---|
| All | 1, 9910 | 20000 | 100.00 | 100.00 | 1319.66 | 18.71 | 238.11 | 4.03 | 1 |
| M1 | 6, 9910 | 9264 | 46.32 | 46.32 | 2846.81 | 313.53 | 144.71 | 176.24 | 9910 |
| M2 | 1, 5 | 10700 | 53.50 | 53.50 | 1.88 | 1.64 | 57.59 | 1.43 | 1 |

7.5 µg/mL WGA conjugated nanoparticles

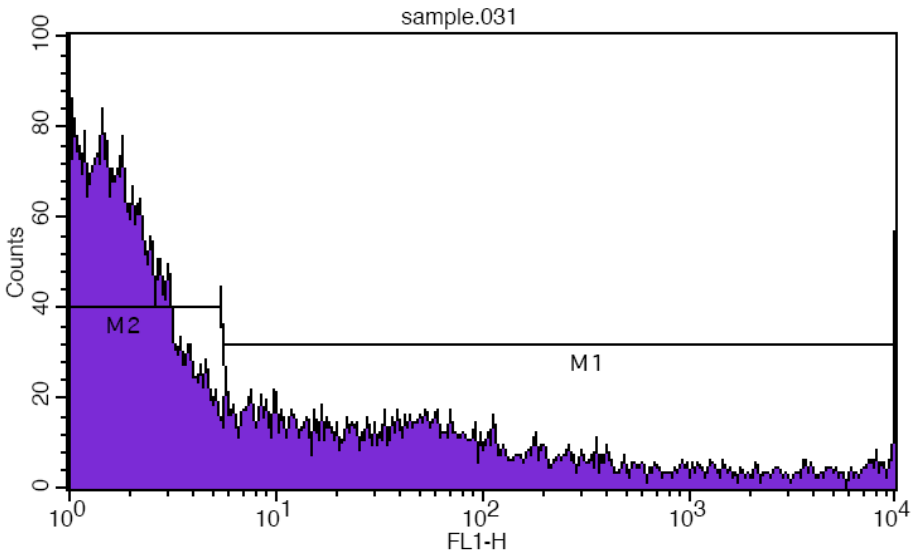


Histogram Statistics

File: sample.031
Sample ID: np4.5-3
Tube: Untitled
Acquisition Date: 26-Mar-10
Gated Events: 20000
X Parameter: FL1-H (Log)

Log Data Units: Linear Values
Patient ID:
Panel: Untitled Acquisition Tube List
Gate: No Gate
Total Events: 20000

| Marker | Left, Right | Events | % Gated | % Total | Mean | Geo Mean | CV | Median | Peak Ch |
|---|---|---|---|---|---|---|---|---|---|
| All | 1, 9910 | 20000 | 100.00 | 100.00 | 666.24 | 6.15 | 351.62 | 1.93 | 1 |
| M1 | 6, 9910 | 6128 | 30.64 | 30.64 | 2170.55 | 149.78 | 176.34 | 67.32 | 9910 |
| M2 | 1, 5 | 13849 | 69.25 | 69.25 | 1.69 | 1.50 | 57.06 | 1.25 | 1 |

4.5 µg/mL WGA conjugated nanoparticles

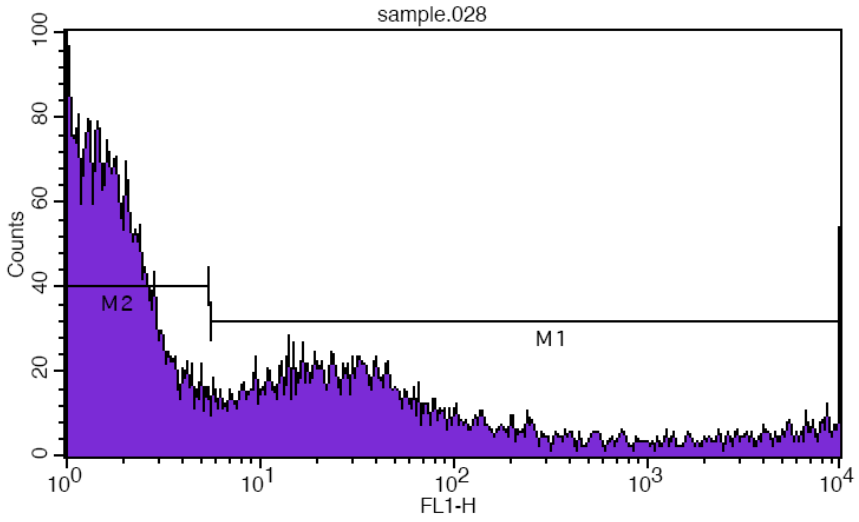


Histogram Statistics

File: sample.028
Sample ID: np1.5-3
Tube: Untitled
Acquisition Date: 26-Mar-10
Gated Events: 20000
X Parameter: FL1-H (Log)

Log Data Units: Linear Values
Patient ID:
Panel: Untitled Acquisition Tube List
Gate: No Gate
Total Events: 20000

| Marker | Left, Right | Events | % Gated | % Total | Mean | Geo Mean | CV | Median | Peak Ch |
|---|---|---|---|---|---|---|---|---|---|
| All | 1, 9910 | 20000 | 100.00 | 100.00 | 602.62 | 6.01 | 363.56 | 1.83 | 1 |
| M1 | 6, 9910 | 6554 | 32.77 | 32.77 | 1835.70 | 116.43 | 191.72 | 44.51 | 9910 |
| M2 | 1, 5 | 13423 | 67.12 | 67.12 | 1.58 | 1.41 | 55.60 | 1.14 | 1 |

1.5 µg/mL WGA conjugated nanoparticles

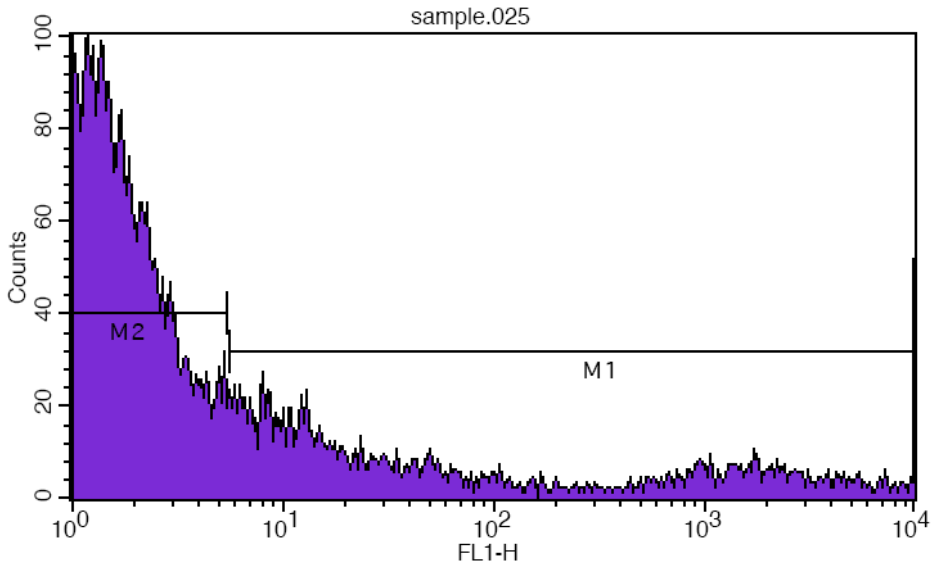


Histogram Statistics

File: sample.025
Sample ID: np0.5-3
Tube: Untitled
Acquisition Date: 26-Mar-10
Gated Events: 20000
X Parameter: FL1-H (Log)

Log Data Units: Linear Values
Patient ID:
Panel: Untitled Acquisition Tube List
Gate: No Gate
Total Events: 20000

| Marker | Left, Right | Events | % Gated | % Total | Mean | Geo Mean | CV | Median | Peak Ch |
|---|---|---|---|---|---|---|---|---|---|
| All | 1, 9910 | 20000 | 100.00 | 100.00 | 195.62 | 3.02 | 561.20 | 1.42 | 1 |
| M1 | 6, 9910 | 3861 | 19.30 | 19.30 | 1006.61 | 69.84 | 231.48 | 24.36 | 9910 |
| M2 | 1, 5 | 16103 | 80.52 | 80.52 | 1.60 | 1.42 | 57.88 | 1.14 | 1 |

0.5 µg/mL WGA conjugated nanoparticles

**2. WGA as a targeting group conjugated onto LbL assembled nanoparticles**

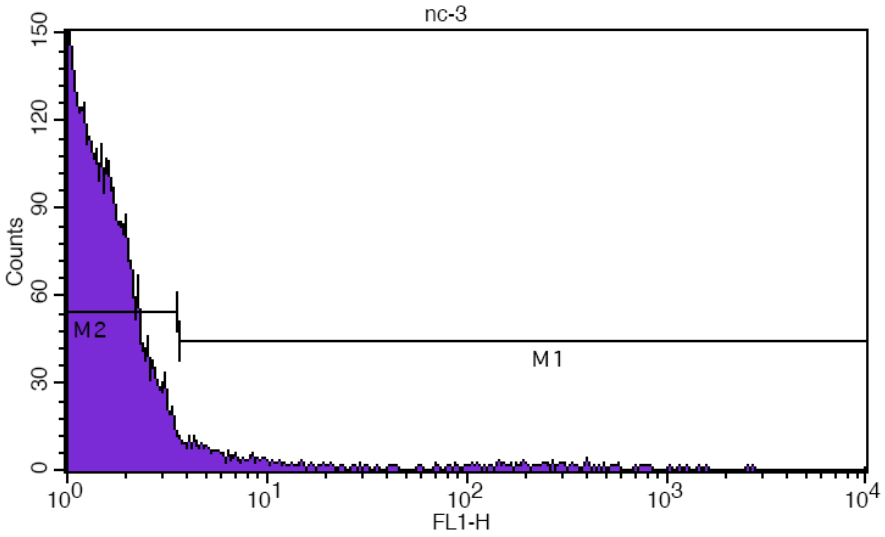


Histogram Statistics

File: nc-3
Sample ID: nc-3
Tube: Untitled
Acquisition Date: 09-May-10
Gated Events: 20000
X Parameter: FL1-H (Log)

Log Data Units: Linear Values
Patient ID:
Panel: Untitled Acquisition Tube List
Gate: No Gate
Total Events: 20000

| Marker | Left, Right | Events | % Gated | % Total | Mean | Geo Mean | CV | Median | Peak Ch |
|---|---|---|---|---|---|---|---|---|---|
| All | 1, 9910 | 20000 | 100.00 | 100.00 | 4.26 | 1.36 | 1903.19 | 1.03 | 1 |
| M1 | 4, 9910 | 664 | 3.32 | 3.32 | 89.81 | 13.83 | 486.33 | 6.61 | 3 |
| M2 | 1, 4 | 19318 | 96.59 | 96.59 | 1.32 | 1.25 | 38.19 | 1.01 | 1 |

Negative control: Caco-2 cells.

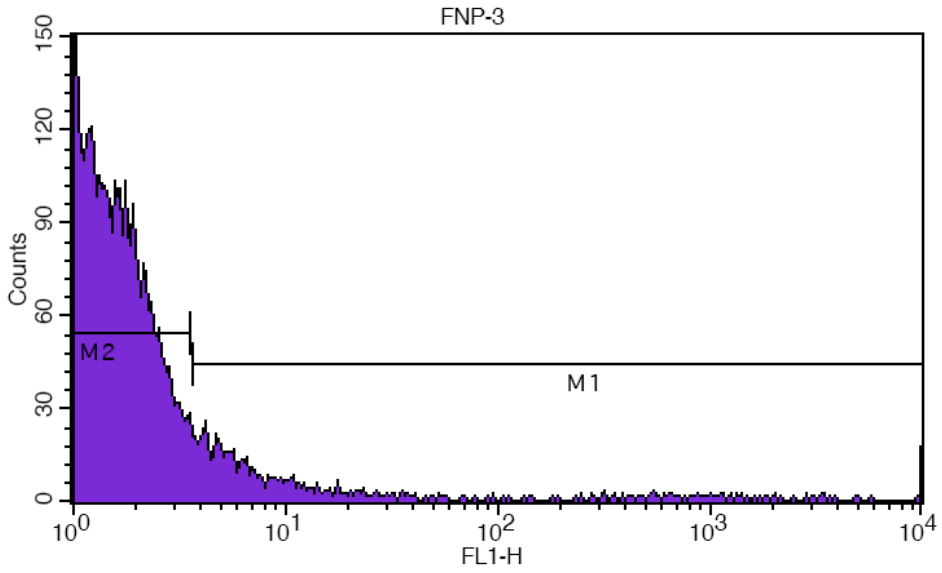


Histogram Statistics

File: FNP-3
Sample ID: f-3
Tube: Untitled
Acquisition Date: 09-May-10
Gated Events: 20000
X Parameter: FL1-H (Log)

Log Data Units: Linear Values
Patient ID:
Panel: Untitled Acquisition Tube List
Gate: No Gate
Total Events: 20000

| Marker | Left, Right | Events | % Gated | % Total | Mean | Geo Mean | CV | Median | Peak Ch |
|---|---|---|---|---|---|---|---|---|---|
| All | 1, 9910 | 20000 | 100.00 | 100.00 | 27.63 | 1.55 | 1589.85 | 1.14 | 1 |
| M1 | 4, 9910 | 1601 | 8.00 | 8.00 | 329.11 | 11.63 | 462.09 | 6.04 | 9910 |
| M2 | 1, 4 | 18356 | 91.78 | 91.78 | 1.39 | 1.30 | 41.08 | 1.06 | 1 |

Positive control: LbL assembled fluorescent PS nanoparticles with PEG conjugation. Fluorescence comes from the PS nanoparticles.

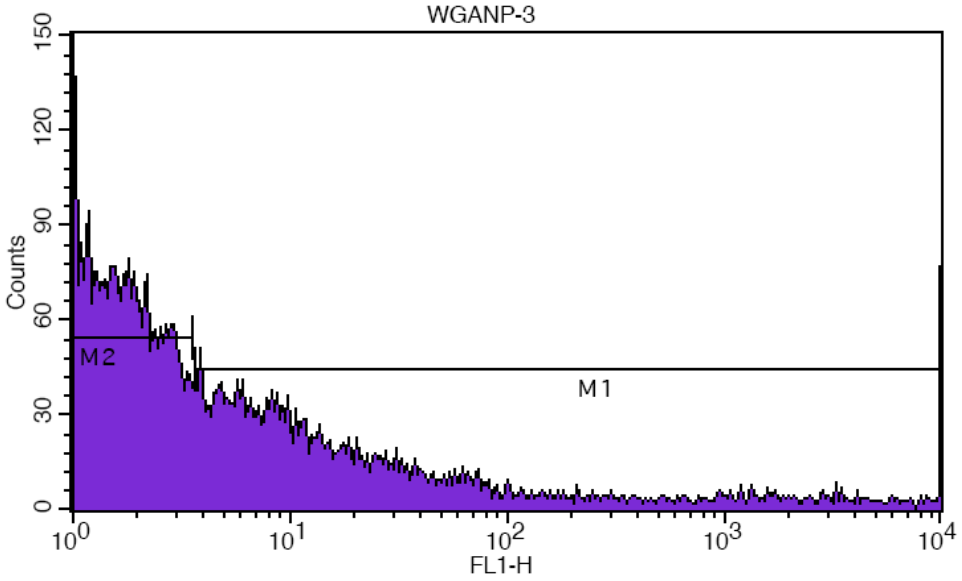


Histogram Statistics

File: WGANP-3
Log Data Units: Linear Values
Sample ID: NPWGA-3
Patient ID:
Tube: Untitled
Panel: Untitled Acquisition Tube List
Acquisition Date: 09-May-10
Gate: No Gate
Gated Events: 20000
Total Events: 20000
X Parameter: FL1-H (Log)

| Marker | Left, Right | Events | % Gated | % Total | Mean | Geo Mean | CV | Median | Peak Ch |
|---|---|---|---|---|---|---|---|---|---|
| All | 1, 9910 | 20000 | 100.00 | 100.00 | 256.18 | 4.20 | 549.98 | 2.13 | 1 |
| M1 | 4, 9910 | 7255 | 36.27 | 36.27 | 703.43 | 27.06 | 322.89 | 12.30 | 9910 |
| M2 | 1, 4 | 12676 | 63.38 | 63.38 | 1.57 | 1.44 | 44.38 | 1.26 | 1 |

Tagged nanoparticles: LbL assembled, PEG modified PS nanoparticles with F-WGA conjugation. Fluorescence comes from F-WGA.

# VITA

Email: asteryu@neo.tamu.edu

## EDUCATION

**Texas A&M University,** College Station, TX — May 2012
Ph.D., Chemical Engineering,

**Zhejiang University,** Hangzhou, China — Jul. 2007
M.Med., Microbial and Biochemical Pharmacy
Materials Science and Chemical Engineering

**Tianjin University,** Tianjin, China — Jun. 2005
B.S., Pharmaceutical Engineering, GPA 3.42